Developing a Space Shuttle Experiment for Hall and Pulsed Plasma Thrusters

by

Stephanie Thomas

S.B. Aeronautics and Astronautics
MIT, 1999

SUBMITTED TO THE DEPARTMENT OF AERONAUTICS AND ASTRONAUTICS IN PARTIAL FULFILLMENT OF THE REQUIREMENTS FOR THE DEGREE OF

MASTER OF SCIENCE IN AERONAUTICS AND ASTRONAUTICS
AT THE
MASSACHUSETTS INSTITUTE OF TECHNOLOGY

FEBRUARY, 2001

© Massachusetts Institute of Technology, 2001. All Rights Reserved.

Author .....
Aeronautics and Astronautics
February 1, 2001

Certified by .....
Manuel Martinez-Sanchez
Professor of Aeronautics and Astronautics
Thesis Supervisor

Accepted by .....
Wallace E. Vander Velde
Professor of Aeronautics and Astronautics
Chair, Committee on Graduate Students

MASSACHUSETTS INSTITUTE OF TECHNOLOGY
SEP 1 1 2001
AERO

Developing a Space Shuttle Experiment for Hall and Pulsed Plasma Thrusters

by

Stephanie Thomas

Submitted to the Department of Aeronautics and Astronautics on February 1, 2001, in partial fulfillment of the requirements for the degree of Master of Science in Aeronautics and Astronautics

Abstract

Very little data on Hall and Pulsed Plasma Thrusters has been taken in the hard vacuum of space. The Environment Effects Verifatication experiment is designed to take archival-quality data in space in the plume and far-field regions of these thrusters. Student involvement is a key element of the experiment, which is supported by the Massachusetts Space Grant and the Education branch of NASA. Design of the experiment is currently in the preliminary phase. A new facility at MIT, called the Micro Propulsion Lab, is available for testing related to this experiment, and some initial ground tests of a lab model Hall thruster have been completed.

Thesis Supervisor: Manuel Martinez-Sanchez
Title: Professor of Aeronautics and Astronautics

Table of Contents

List of Figures

List of Tables

Section 1.0. Introduction

1.1. The concept of a Hitchhiker experiment

The Hall Thruster and PPT Environmental Effects Verification experiment was conceived around 1995 as a joint university project to study low-power electric propulsion in space. Measurements would be taken in and around the thruster plumes in the Shuttle payload bay. The project would benefit students from Massachusetts universities by giving them valuable experience developing a space experiment, including design and construction of the flight hardware and reduction and interpretation of the data. A few students worked on the project sporadically, developing objectives and some idea of instrumentation, but the project never had committed funds and thus never advanced beyond the initial planning stages. However some discussions with NASA and Space Grant in 1996 suggested the possibility of a NASA-supported flight, in other words, at no cost to the experiment.

With the continued efforts of MIT Professor Martinez-Sanchez and the prospect of a "free" flight, Massachusetts Space Grant Consortium funding was obtained for fiscal year 2000. A graduate research assistant, myself, could now be maintained full-time on the project. However, so much time had passed from the initial conception of the project that the trail to the promised free flight had been lost. My first task was to recreate these links and get official NASA approval of the experiment, as the project was not feasible without a guaranteed flight berth. Re-networking took several months, but in June, 2000, a very positive teleconference took place with the Goddard Small Projects Payload office, and in August, 2000, NASA Form 1628 was signed. This brought project ETEEV (Electric Thruster Environmental Effects Verification) into official NASA existence in the queue for Hitchhiker payloads.

ETEEV is now waiting to be manifested on a shuttle flight. Integration leaders have been assigned at Goddard and Johnson. A part-time research engineer has been procured to assist the students with hardware development and ground lab tests, and a systems engineer to manage the heavy documentation, integration, and safety requirements of flying on the shuttle is forthcoming.

1.2. Motivation

The motivations and goals of this experiment have evolved over time, reflecting new work in the field of plume-spacecraft interaction studies and the interests of industry and others in the results of the work. Although when first conceived this project was to be the first experiment to fly these thrusters in space and return extensive diagnostic data, other projects have since come into existence. This reflects the growing interest in industry and government agencies in using electric propulsion on various missions for purposes from orbit transfer to attitude control and the lack of exhaustive knowledge of the spacecraft-thruster interactions involved.

Chemical engine plumes, their spacecraft interactions, and how to model them are well understood, but electric thrusters are newer and their behavior has not been investigated to

the same level. There are a number of areas in which electric thruster plume may affect the spacecraft on which they are used. First, there is erosion of surfaces by impingement of high energy ions. This may be the erosion of material inside the thruster body or the erosion of nearby spacecraft surfaces. Redeposition of these eroded materials could contaminate critical surfaces such as solar arrays, thermal control surfaces, optical sensors, and scientific instruments. Second, backflows of low-energy charge exchange ions could affect surface charging and the spacecraft potential. Third, the high plasma density of the plume may interfere with communications by attentuating or refracting incoming and outgoing electromagnetic signals. Fourth, radiant and conducted heat from the thruster must be accounted for in the thermal model of the spacecraft. Fifth, optical emissions from the plume could affect sensitive optical instruments. Both experiments and numerical models are required to predict these effects cumulatively over the spacecraft's lifetime.

Studies on the ground can effectively determine a number of the plume's characteristics, but uncertainties persist for some areas due to various facility effects. The following data can be confidently taken in ground facilities:

- Energy spectrum and angular dependence in the main plume
- Distortion of microwave beams through the plume
- General features of charge exchange ions in the near plume
- Thermal radiation from the thruster and plume
- Effect of imperfect vacuum on thrust and specific impulse measurements

There are a number of these facility effects which produce uncertainties in an extrapolation to true vacuum. They are:

1. Deposition of material from chamber walls

   Especially near the edges of the plume, material sputtered from the facility walls onto instruments may mask erosion products from thruster itself.

2. Recirculation of thruster plasma in the test facility

   Since the pumps in the chamber may not remove all of the xenon exiting the chamber immediately, xenon may recirculate in the chamber. The recirculated xenon in the plume area may be confused with charge exchange collision products.

3. Ingestion of facility background gas

   The thruster can ingest, ionize, and accelerate residual tank gases, which may artificially add to the measured thrust.

4. Background pressure interference

   The relatively high pressure in the chamber produces causes an artificially high flux of charge exchange ions and neutrals. The pressure may also have some effect on the thrust measurement itself - which raises the question that Hall thrusters may have lower performance on a spacecraft than on the ground.

5. Geomagnetic effects

   In the presence of the earth's magnetic field the plume is expected polarize and create a transverse electric field, but imperfectly. This will cause the plume to distort anisotropically due to preferential expansion along the geomagnetic field. The far-field evolution of the plume may affect microwave propagation near the thruster and optical contamination of sensitive instruments.

ETEEV will chiefly address the first four of these facility effects, as these most affect projections over the spacecraft's lifetime of surface contamination and environment quality. The fifth effect, the distortion of the far-field plume, may be addressed with photography, but it is a secondary objective.

In general, facility effects affect measurements the least near the center of the plume. Therefore, the ETEEV experiment was to have a focus on backplane measurements of the plume such as ion density, ion energy, material deposition and erosion rates, and ion temperature. As the experiment evolved, and especially after it was approved by NASA and had a higher chance of flying, other experts in the field suggested that the experiment focus should be on those measurements which characterize plume-spacecraft interactions in areas of interest. This practical need has pushed the objectives of ETEEV to focus additionally on the 30 to 45 degree range of the plume, where solar arrays are likely to be located (see Figure 1.1.), while continuing to look at larger angles as well.

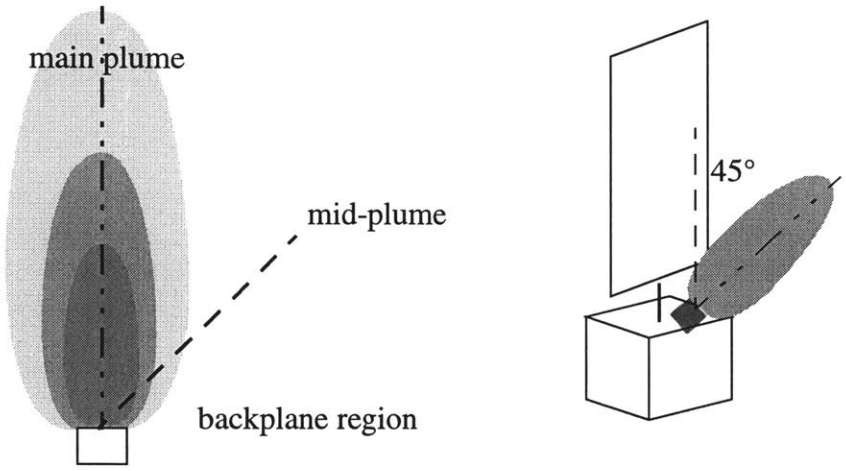

Figure 1.1. Plume Regions and Typical Cant Angle

Some experts have suggested that the experiment should focus on demonstrating new engines, such as a gas-fed PPT, rather than flying regular Hall thrusters and PPTs. However it has always been the intent of the experiment to conduct those measurements of mature and well-studied thrusters which are impossible to do on the ground, rather than test new thrusters or diagnostics. Therefore the experiment has not changed from its original structure of one 200 W Hall thruster and one low-power PPT.

The Shuttle bay is arguably not the best location for an experiment to solve all these problems, as the bay can be very contaminated with outgassing and water dumps. However, it is the best available short of the international space station, which won't be available for scientific slots for a few years. Also, every set of data taken in space will be valuable for comparison purposes as these thrusters are entering common use so quickly.

1.3. Outline of Thesis Work

My job as a research assistant was generally do some initial systems engineering on the flight experiment, to get the new vacuum facility working with the Busek Hall Thruster installed, and if possible to begin the ground baseline measurements of the thruster performance and plume characteristics. My systems-level studies were mostly limited to studying instruments and determining which were practical given the constraints of cost, a short operating time, the limits of student engineers, and the shuttle environment, as once the experiment was approved by NASA the need for a professional systems engineer to oversee the efforts at MIT and WPI was apparent. The next level of documentation required for NASA beyond Form 1628 is a detailed design of all the experiment subsystems that is beyond the capability and objectives of a student researcher.

Therefore, the thesis begins as I did, with an extensive review of recent research on thruster plumes and the plume diagnostics used, and an overview of other planned flight experiments. The next chapter discusses the design of ETEEV and the last chapter presents the work done to date at MIT's new ground vacuum facility. There are three appendices, one containing documentation for our thrust balance, one containing a spreadsheet which predicts the performance of a Langmuir probe, and one with a spreadsheet overview of some recent thruster plume research.

Section 2.0. State-of-the-Art in Electric Thruster Plumes

2.1. Introduction

This section reviews the scientific literature on Hall thruster plumes, with a focus on research since 1994. A brief overview of PPT plumes is given at the end.

The baseline operating conditions of some Hall thrusters, such as the SPT-100, are considered well-established. However understanding the interactions between the thruster and the spacecraft is often cited as research goal in recent work. Undesirable plume-spacecraft interactions include erosion of, or deposition on, solar arrays, thermal control surfaces, optical surfaces, and scientific instruments; interference with communications; and effects on surface conductivity and spacecraft charging. Understanding the physics and properties of the exhaust plume and how they change over the lifetime of the thruster is imperative to be able to predict the extent of these interactions over a spacecraft's lifetime. Plumes are also studied to understand fundamentally how a thruster is operating and performing, for example to learn where in the thruster body ionization takes place and what causes the oscillatory instabilities seen in Hall thrusters. Also, it is necessary to sweep the plume with a current detector to calculate the thruster's efficiency.

The exhaust plume of a Hall thruster consists of high-energy Xenon ions, eroded metal and ceramic from inside the thruster, and secondary ion products including slow Xenon ions and fast and slow neutrals. Fast neutrals and slow ions are created during charge exchange (CEX) processes when accelerated propellant ions strike ambient background gas or un-ionized propellant. Slow neutrals are either propellant which slipped through the thruster un-ionized or ambient background gas.

The ionized portion of the plume can be detected with traditional electrostatic probes such as Langmuir probes, Faraday probes, and retarding potential analyzers. The neutral portion is harder to detect but may be seen with adapted vacuum pressure gauges or measured indirectly. Deposited mass and erosion from the plume can be measured with witness plates and Quartz Crystal Microbalances. Optical spectrometers can be used to resolve the emission spectra of plume constituents. Other innovative probes include the Molecular Beam Mass Spectrometer and a heat flux probe, both developed at the University of Michigan.

Electromagnetic signal interference can be measured by sending a signal directly through the plume. The far-field shape of plumes in space has not been visually documented, but can be inferred from radio shadows or geomagnetic field perturbations, as was done on EPICURE for the cesium plasma generator.[23] This research suggests that the plume may be petal or pencil shaped past distances of 1-2 m from the thruster, depending on the orien-

tation of the geomagnetic field. The near-field plume is easily seen in a vacuum tank and has been frequently photographed.

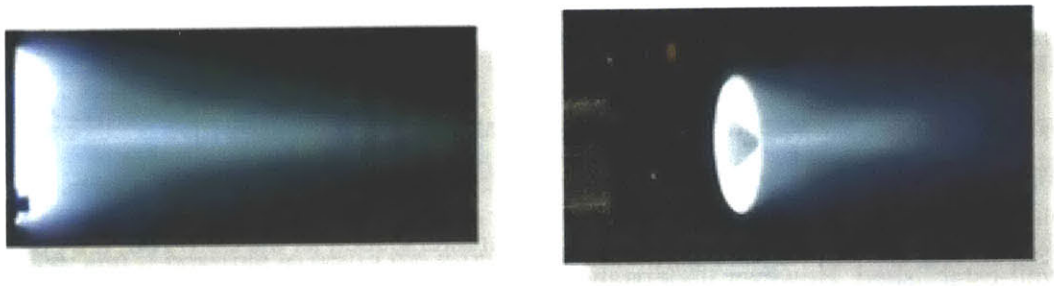

Figure 2.1. Hall thrusters firing at Busek, 600 W at left and 200 W at right

Many numerical studies have been done to predict thruster performance and plume properties, especially at MIT. This numerical work was not studied extensively for this project. A recent review of different modeling approaches can be found in Reference [3].

2.2. Basic Hall Thruster Characteristics

A Hall thruster is a high-efficiency gridless ion engine that uses a magnetic field to confine electrons for ionizing the propellant. Xenon is the most common propellant but Krypton and other materials have also been investigated.[24] Typical operating parameters are efficiencies of 40-50%, specific impulses between 1400 and 1800 sec, powers ranging from 50 W to 20 kW, and acceleration voltages usually of around 300 V (but newer designs have used voltages from 600 V up to 1800 V to produce a higher specific impulse). These parameters make Hall thrusters ideal for maneuvers like north-south stationkeeping and orbit raising.

The magnetic field strength is chosen so that the electron gyroradius is small compared to the thruster dimensions while the ion gyroradius is very large, allowing the ions to move basically unimpeded by the field while electrons are trapped orbiting the magnetic field lines. The direction of the magnetic field is radial while the applied electric field is axial, so electrons also have an azimuthal drift due to **E** x **B**, known as the Hall effect. The overall result is that the axial velocity of the electrons is greatly reduced, allowing time for inelastic collisions between electrons and propellant neutrals which produce ionized propellant. The ions are then accelerated out of the thruster at almost the full applied potential, with an exit velocity of

$$c \cong \sqrt{\frac{2qV}{m_i}} \tag{2.1}$$

The resulting plasma is quasi-neutral and the extracted ion current is not limited by space-charge effects. This gives Hall thrusters a higher thrust density than ion engines, where biased grids cause a space-charge issue. Hall thruster plumes have a relatively wider diver-

gence angle than ion engines due to a higher electron temperature, which produces greater sideways ion thermal velocities.

The construction of a Hall thruster can vary, producing various types such as BPT, TAL (Thrust Anode Layer), and SPT (Stationary Plasma Thruster). Usually there is a coaxial annular cavity, with magnetic poles in the center and circumference. An exterior cathode and an interior anode provide the electric field while a coil or permanent magnet may supply the magnetic field. The main fuel flow is introduced at the annular anode while about 10% of the overall propellant flow to the thruster runs through the external cathode.

The Busek 200 W "Tandem" Hall thruster and cathode, and Busek's 600 W thruster shown for comparison, are pictured below.

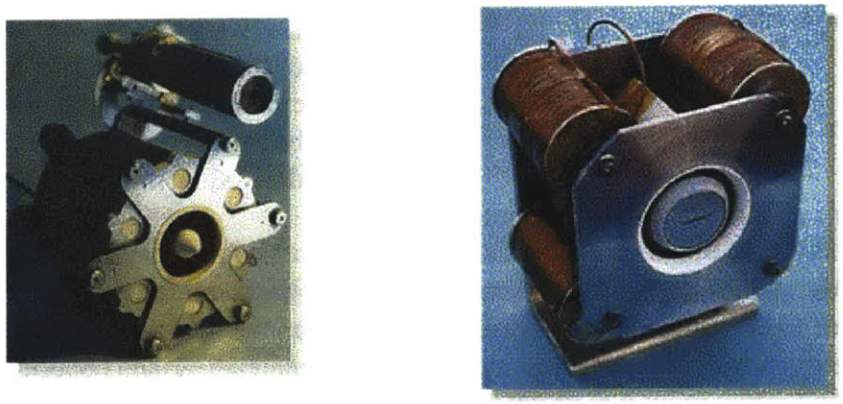

Figure 2.2. Busek 200 W tandem thruster at right, Busek 600 W thruster at left.

2.3. Overview of Hall thruster plumes

2.3.1 Density and composition of the plume

Hall thruster plumes are composed almost entirely of singly ionized Xenon, with some double and triply ionized Xenon and some neutrals. SPT-100 plasma has been found to consist of 89% Xe^{+}, 11% Xe^{2+}, 0.2% Xe^{3+} according to King and Gallimore's latest studies with their Molecular Beam Mass Spectrometer (MBMS), however the instrument was inconclusive as to the presence of Xe^{4+}.[20] Most of this plasma is within 45° of the thruster centerline, with the plume current sharply peaked at the centerline. Peak ion densities are around 10^{17} m^{-3}. A few meters downstream of the thruster this density has dropped several orders of magnitude.

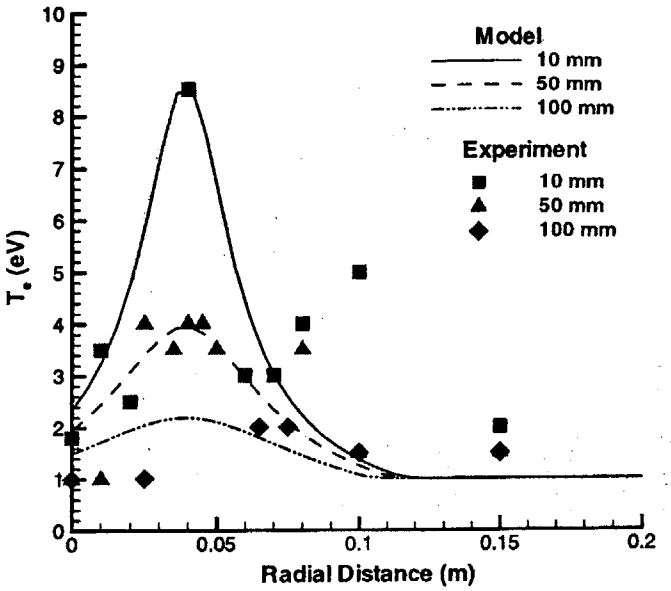

Figure 2.3. Electron Temperature[3]

The electron temperature may reach 10 eV very close to the thruster discharge chamber, but the temperature in the plume is around 2 to 4 eV and is often assumed to be constant in models. Some measurements of T_e are shown at left.

There are several analytical fits to Hall plume density in the literature. Those of Pencil et. al (1994, 1996) are very simple and useful. From these fits one can visualize the size and shape of the plume and plot a sample current density trace as would be sampled by a probe. They are derived from current density measurements on a 1500 watt SPT-100 thruster.

The first fit, a Lorentzian, is given and plotted below. It is based on measurements taken early in the life of the thruster. Note the inverse squared dependence on distance. The authors estimate an overall 30% uncertainty in this profile.[30]

$$j = \frac{1}{r^2}\left(a_0 + \frac{a_1}{\theta^2 + a_2}\right) \qquad \begin{cases} a_0 = 0.0014895 \\ a_1 = 103.1 \\ a_2 = 60.169 \end{cases} \tag{2.2}$$

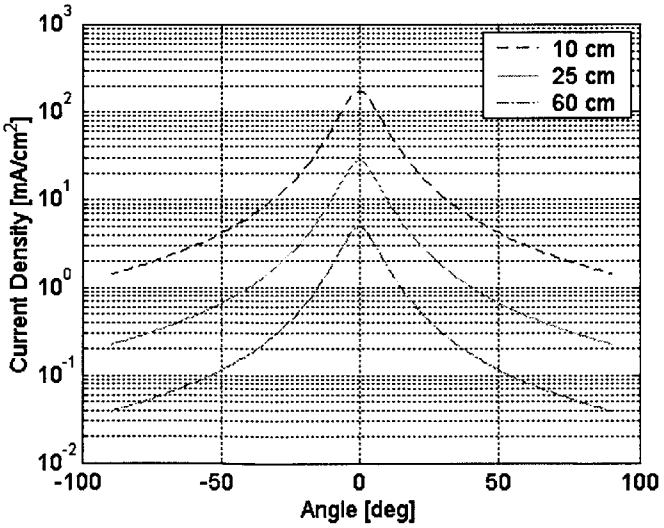

Figure 2.4. Plume Current (Pencil, 1994)

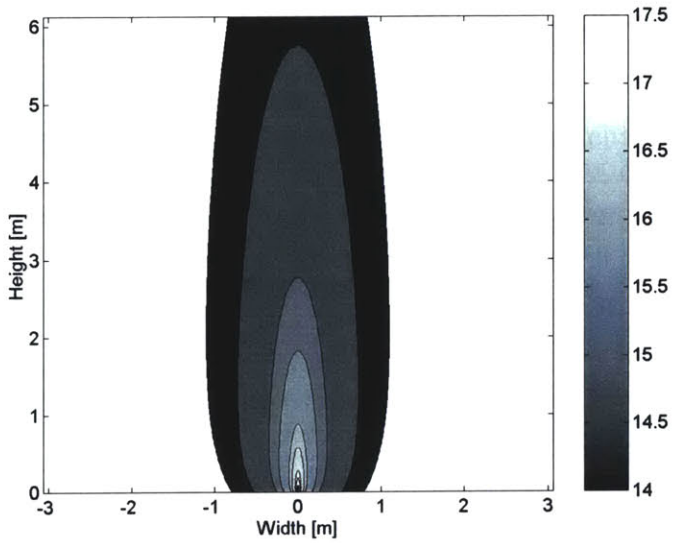

Figure 2.5. Plume Density Contours , $\log_{10}(n)$, $[n] = m^{-3}$

The second fit, derived two years later after tests at the end-of-life of the same thruster, uses a two-term Gaussian with collisionless expansion.[29] It underestimates the measured current density for $\theta > 60°$, as shown in Figure 2.7. This is believed to be due to the effect of facility-induced charge exchange ions, the creation of which is described in "Ion energy distribution" on page 23 below. This implies that the fit is a more correct extrapolation to true vacuum than the measurements themselves, which is supported by the reduction in measured current obtained by using a collimator, as described in "Facility Effects and Mitigation Techniques" on page 43.

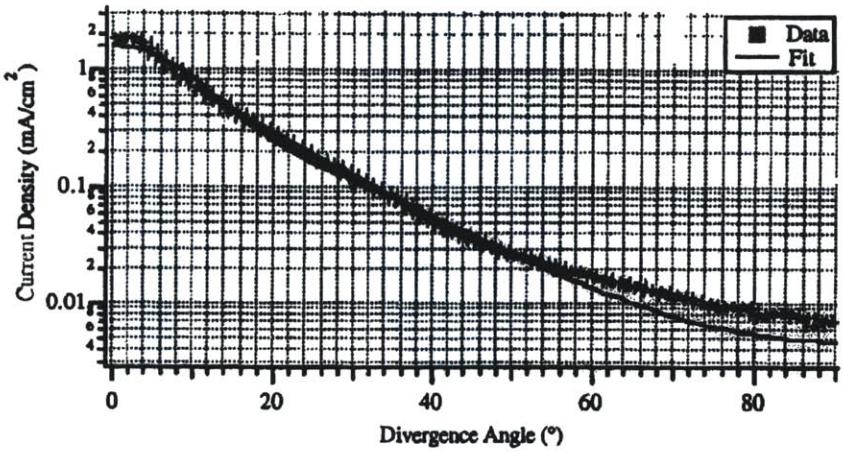

Figure 2.7. Plot of Measured Current Density at Facility Pressure of $<3x10^{-6}$ Torr and the Derived Analytical Fit from Pencil et. al. (1996)

Please note that there were typos in the paper presenting this function; by plotting and logical deduction the form given and plotted below was determined to be correct.

$$j = \frac{1}{r^2}\left(k_0 \exp\left[-\left(\frac{\sin\theta}{k_1}\right)^2\right] - k_2 \exp\left[-\left(\frac{\theta}{k_3}\right)^2\right]\right) \qquad \begin{cases} k_0 = 0.31732 \\ k_1 = 0.48743 \\ k_2 = -1.2279 \\ k_3 = 11.073 \end{cases} \tag{2.3}$$

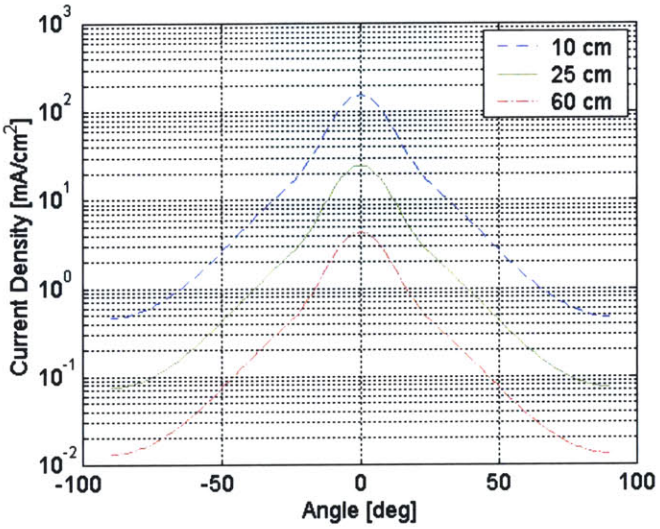

Figure 2.8. Plume Current (Pencil, 1996)

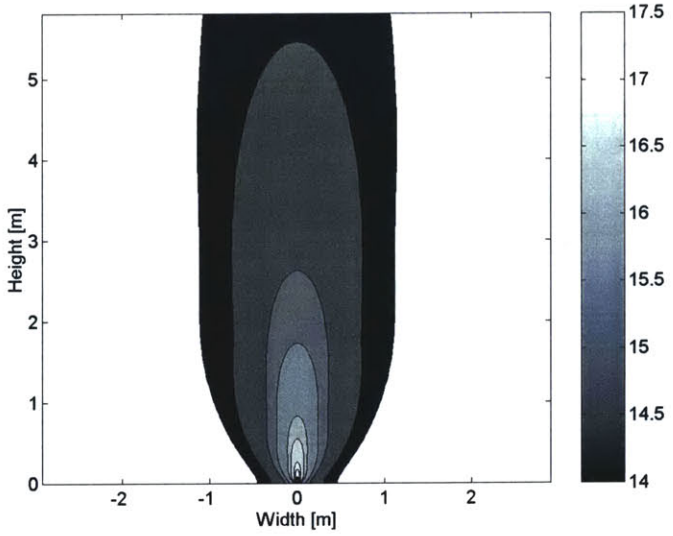

Figure 2.9. Plume Density Contours , $\log_{10}(n)$, [n] = m^{-3}

More rigorous analytic expressions for plume current density can be found in Reference [23], *Comparison between Plasma Plume Theoretical Models and Experimental Data* (1999).

2.3.2 Ion energy distribution

The ion energy distribution in a SPT-100 plume has been studied extensively, especially by Gallimore and his students at the University of Michigan. Pencil (1994) has a simple Lorentzian fit for mean ion energy versus angle from centerline, given and plotted below.[30]

$$E = b_0 + \frac{b_1}{\theta^2 + b_2} \qquad \begin{cases} b_0 = -185.59 \\ b_1 = 2.8984e6 \\ b_2 = 6839 \end{cases} \tag{2.4}$$

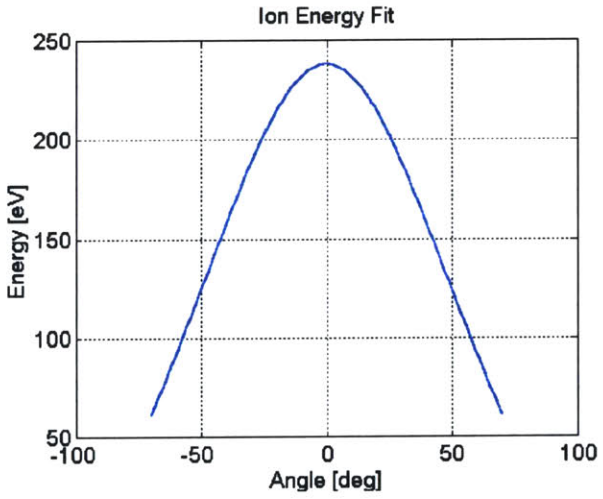

Figure 2.11. Ion Energy Analytical Fit

Usually, energy is given as a distribution over voltage, as is obtained from an Retarding Potential Analyzer (RPA) or the MBMS. In general, near the thruster centerline the ion-energy distribution is Gaussian-like with a peak near the discharge voltage, for example a peak of 270 V for a discharge of 300 V. At larger angles the distribution becomes broader, due to the appearance of low-energy ions.

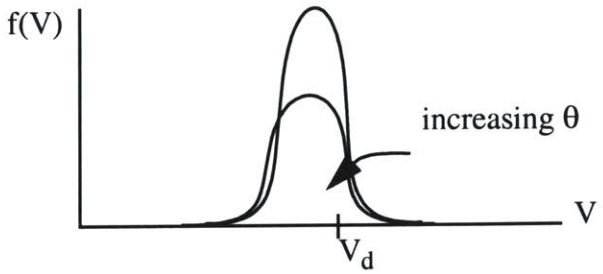

Figure 2.12. Effect of divergence angle on ion energy distribution

In the thruster, lower energy ions are believed to be created near the exit of the discharge chamber, while higher energy ions are created farther upstream. Ions have higher energy the closer to the anode they are when formed, as they are accelerated through a higher voltage. The lower energy ions have a greater range of exit angles as shown in Figure 2.13. below, which should cause them to be present in areas the higher energy ions can't reach. From calculating moments of the velocity distributions derived from energy distributions, researchers have found a very narrow low-energy core surrounded by a slightly higher energy annulus, which supports this theory of ion production. The core has a half-angle of about 5° at 50 cm for an SPT-100. Downstream of the engine this annulus is smeared out by beam divergence.[19]

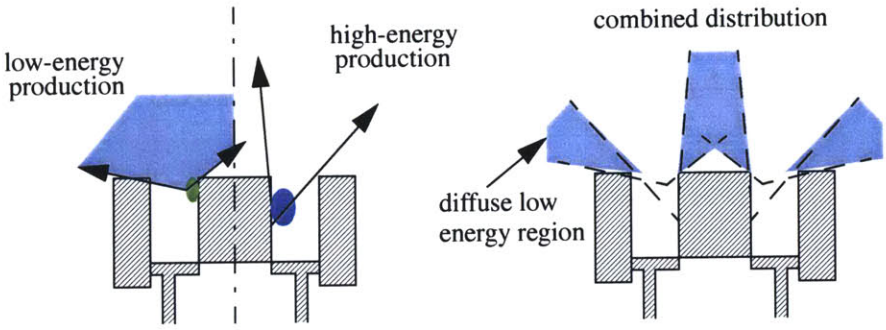

Figure 2.13. Ion production and energy distribution schematic according to Bishaev and Kim (1978)

In addition to low-energy ions, high-energy ions with voltages greater than the discharge voltage are also found in these distributions. Besides being created at different points in the thruster discharge chamber, ions with energies other than the discharge voltage are also created by collisions. Inelastic collisions allow charge exchange with negligible momentum exchange. Elastic collisions transfer momentum between particles. These effects are both believed to occur in the plume and are discussed in detail below.

Charge Exchange Collisions

This type of collision produces what are known as charge exchange (CEX) ions and neutrals. The particles involved in the collision may both be fast ions, or the collision may be between a fast ion and a stagnant neutral. During the interaction, one or more e^- are transferred between particles without any appreciable change in the particle momenta. This changes the voltage of the particles, for example if a Xe^{2+} loses one charge after accelerat-

ing through 300 V it will then be detected at 600 V. A given collision is capable of producing a certain set of voltages since $V = E/q$, as follows:

Table 2.1. Examples of Charge Exchange Collisions

Particle	Pre-Collision			Post-Collision		
	Charge	Energy	Voltage	Charge	Energy	Voltage
A	+1	E_0	V_0	2	E_0	$V_0/2$
B	+2	$2E_0$	V_0	1	$2E_0$	$2V_0$
C	0	E_{th}	0	+1	E_{th}	0
D	+2	$2E_0$	V_0	+1	$2E_0$	$2V_0$

In a collision with particles of charge 1 and 3, possible post-collision voltages are 3V, 3V/2, 3V/4, V/2, V/3, and V/4. In King's studies however, only the higher multiples of V were found in energy distributions, indicating that only interactions between fast charged particles and slow neutrals (for example **C** and **D** in Table 2.1. above) are likely. The shape of the energy distribution is in this case conserved, although it is broadened or narrowed depending on whether the resulting V is higher or lower than V_0, respectively.

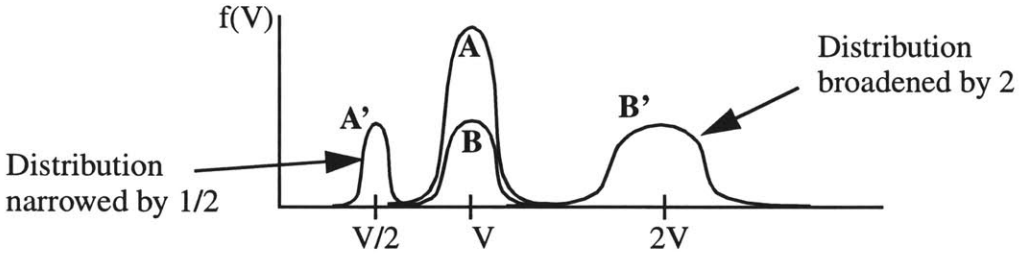

Figure 2.14. Energy distributions from charge exchange collision[18]

By integrating the ion current obtained in the energy distributions, King and Gallimore estimate that at 0.5 m from an SPT-100, approximately 20% of the ions at 50° from the thruster centerline are products of a CEX collision. At 1 m from an SPT-100, that percentage rises to 40% of the ions at 50° and 50% of the ions at 10°. These high percentages are due to facility background neutrals as the beam neutral density would fall with distance. At 1 m the ions have traveled twice the path length from the exit plane through the facility background. Since the cross sections for CEX collisions with neutral Xe scale with ion charge, there is a higher probability for Xe^{2+} ions than Xe^{+} ions to undergo these collisions.

The neutral products of CEX collisions cannot be seen in these energy distributions as they do not produce any current, however measurements of the neutral flux may be made with an adapted ionization gauge as described in "Neutral particle flux probe" on page 38. Data from such an instrument has showed a strong peak in the neutral flux within 25° of

the thruster centerline, and based on a convective heat-flux analysis, it can be showed that these neutrals are most likely the fast products of CEX collisions.[22] This makes sense since unionized propellant is expected to be uniformly distributed over the solid angle seen from the thruster discharge chamber and not peaked in the center of the plume. This taken together with the CEX ion percentages discussed above implies that the effect of the facility background neutrals on the measured ion energy distributions is substantial.

Momentum-transfer collisions

Momentum-transfer collisions between plume ions are believed to cause the high energy tail, extending beyond the discharge voltage, apparent in many plume studies with probe diagnostics as early as 1992.[20] Simply stated, an ion with a charge of 2 at the same potential as an ion with a charge of 1 will have twice the kinetic energy; if these two ions have an elastic collision, the ion of charge 1 could end up with a higher energy such that its post-collision potential is greater than its original potential. This can be seen by approximating the atoms as hard-spheres and considering the post- elastic collision energies,

$$E_1' = E_1 + (E_2 - E_1)\sin^2\frac{\theta}{2} \tag{2.5}$$

where all scattering angles θ are equally likely. In the thruster plume, the previously mentioned collision, high energy Xe^{2+} ions can transfer momentum to Xe^{+} ions producing high energy tails on the Xe^{+} distribution and low-energy tails on the Xe^{2+} distribution. Figure 2.15. shows the resulting energy distributions for collisions between two monoenergetic species of Xe^{+} and Xe^{2+} accelerated through the same voltage.

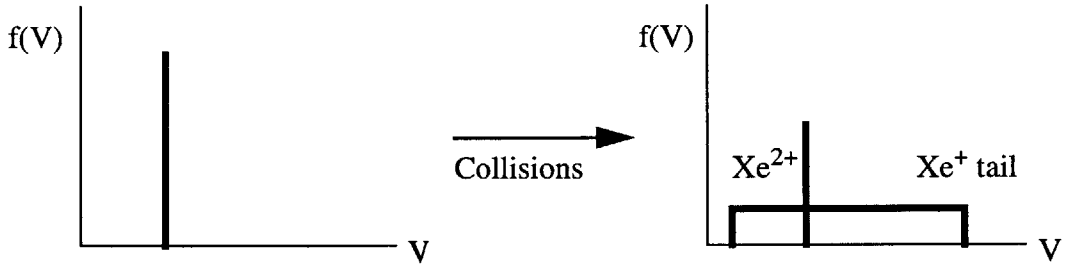

Figure 2.15. Xe^{+} and Xe^{2+} of same voltage with momentum transfer collisions [20]

With these collisions taking place over the true energy distributions of Xe^{+} and Xe^{2+} created in the thruster, monotonically decreasing low- and high-energy tails as seen in experi-

ments with probe energy diagnostics could be created. Physically, the tail height should be a function of the collision cross-sections involved.[20]

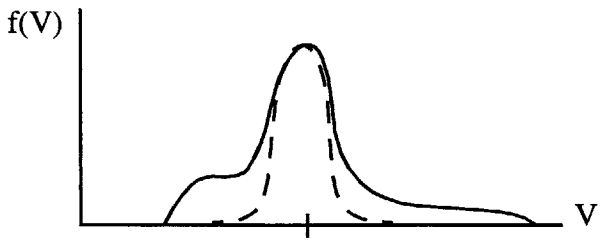

Figure 2.16. Energy distribution with tails from momentum-exchange collisions

Overall Effect of Collisions

The combined effects of these two types of collisions can be seen as smooth tails on the energy distributions with satellite peaks at multiples of the main peak. An example of an energy distribution obtained by the MBMS with these features is shown in Figure 2.17. below. Note the very high peak to the right of the fourth plot, showing the large effect of the facility-induced CEX ions

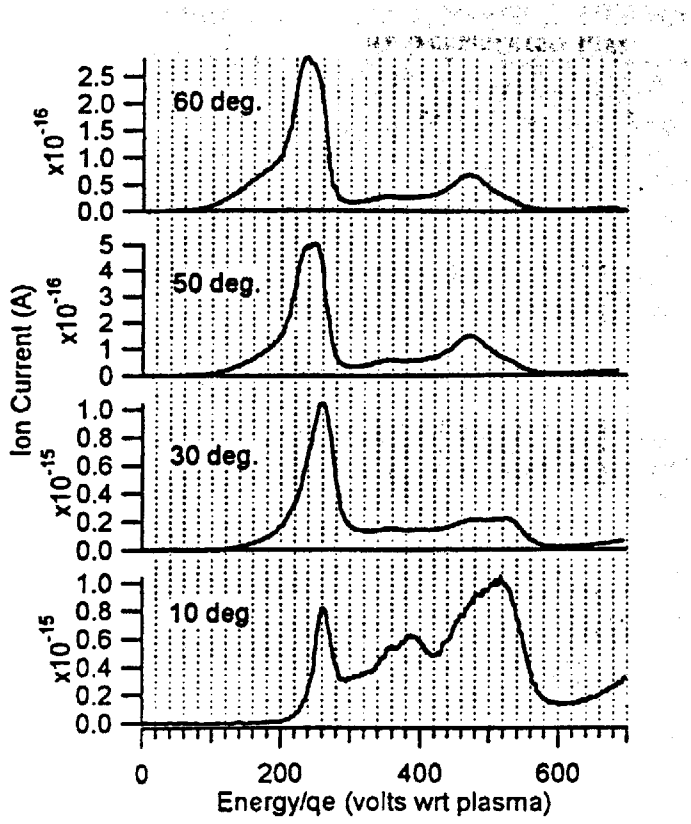

Figure 2.17. Scanned image of energy density with features discussed. Measurements taken 1 m from an SPT-100.[18]

2.3.3 Deposition of Eroded Materials

An SPT-100 may erode about 20-25 cm^3 of thruster material over its lifetime due to sputtering from high-energy ions. This erosion varies over the thruster lifetime, both in constitution, distribution, and overall volumetric rate. Eroded products contribute less than 1% to the total plume flow at BOL and less than 0.1% by EOL.[33] The makeup of the eroded products changes as insulation is completely eroded away and the metal parts underneath may be exposed. The angular distribution changes as the geometry of the thruster housing is altered.

The amount and effect of deposited products on collimated material samples can be tested in the lab many ways, such as

- Profilometer measurements to determine height of deposited film
- Mass measurements of the samples
- Surface resistance measurements
- Optical transmittance with a spectrophotometer
- Infrared emittance with an infrared reflectometer
- Chemical analysis with X-ray photoeletron spectroscopy

Pencil, Randolph, and Manzella have studied solar cell cover glass samples in these ways for a BOL and EOL SPT-100.[29], [30] They found that visible deposition at 1 m from the thruster exit occurred only for the EOL thruster, and only in a region between 70° and 80° from the centerline. This deposition was within the measurement uncertainty of the profilometer, 500 Å, which corresponds to $1x10^{-3}$ Å/s for the 200 hour tests. Although there was no measurable deposition in the BOL experiments, chemical analysis of a sample at 80° did reveal evidence of Boron indicating that thruster insulator material did reach that area. A model developed by the researchers to predict the incident deposition 1 m from the thruster as a function of angle has the following results.

Table 2.2. EOL Incident Deposition Rates, Å/s

	0°	40°	70°
Exterior Pole	$3.8x10^{-3}$	$2.9x10^{-3}$	$1.2x10^{-3}$
Exterior Insulation	$2.1x10^{-3}$	$1.6x10^{-3}$	$0.9x10^{-3}$
Interior Insulation	$0.9x10^{-3}$	$0.7x10^{-3}$	$0.4x10^{-3}$
Total	$6.8x10^{-3}$	$5.2x10^{-3}$	$2.5x10^{-3}$

Due to sputtering from incident plume ions, net deposition only occurs for $\theta > 70°$. At BOL there is no exterior pole component, because it is still insulated, and higher insulator components. Overall, it seems clear that there is at least $1x10^{-3}$ Å/s of deposition incident

on surfaces 1 m from this 1.5 kW thruster. For net deposition rates for a Hall thruster we can only assume $5x10^{-4}$ Å/s between 70° and 80°.

Although the deposited film height from the 200 hour test was within the measurement uncertainty, its effect on the optical properties of the sample was not. There was a large (7-16%) degradation in optical transmission, an increase in reflectance on 1 to 1.5%, and up to a 5% increase in absorptance for samples in the net deposition region.

2.3.4 Erosion of surfaces

Pencil et. al.[29], [30] measured the effects of net erosion on samples the same way they measured deposition, as listed above. 200-hour exposure tests were conducted on samples 1 m from the plume for divergence angles from -90° to +90°. At BOL, net erosion rates were measurable for $\theta < 80°$, while at EOL they were measurable for $\theta < 65°$. A comparison of the data from the two groups of tests is shown in below.

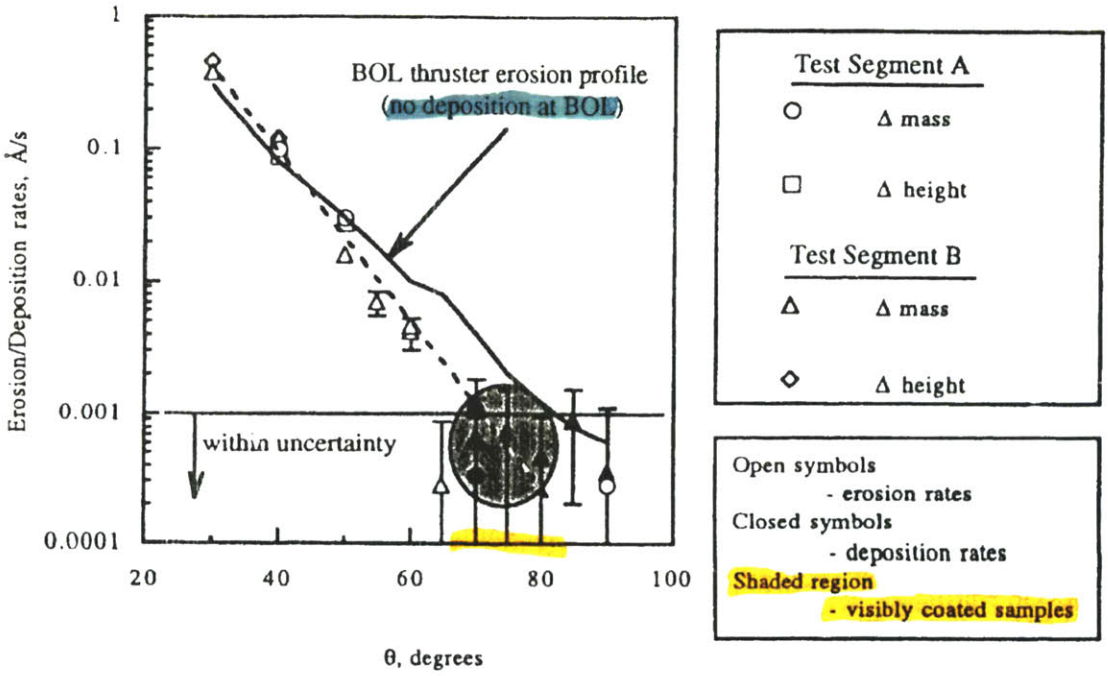

Figure 2.18. Erosion and Deposition Rate 1m from an SPT-100[29]

Anti-reflective coatings on the samples were completely removed in the high-erosion region. The EOL tests also included the effects of incidence angle, and at higher incidence angles erosion is found to be accelerated. Samples which were in the net deposition region in the EOL tests were eroded clean if placed at an incidence angle of 45°.

Different materials representative of solar cells were tested, including coated cover glass, silver coated connectors, and silver foil strips. The silver samples lost much more material than the cover glass due to the large volumetric sputtering rates of silver. Sample mass loss peaked at >20 mg while sample step height peaked at > 20 μm. The samples overall did

not show any changes in surface resistance or infrared emittance, indicating that there was no effect on surface conductivity or thermal properties. Changes in reflectivity due to removal of the AR coating in the high-erosion region were about 2%, while there was no measurable change in absorptance or transmittance.

Detailed models of thruster erosion were developed with these experimental data. Please see the references for more details.

2.3.5 Plume effects on communications

Past flight experience with Hall thrusters has not indicated any detrimental field effluxes or effects on communications. However electromagnetic signals are known to interact with plasma by changing phase, amplitude, direction, and power spectral density. Lab tests have provided more specific data on signals passing directly through plumes. A lab setup for this type of experiment is shown at right.

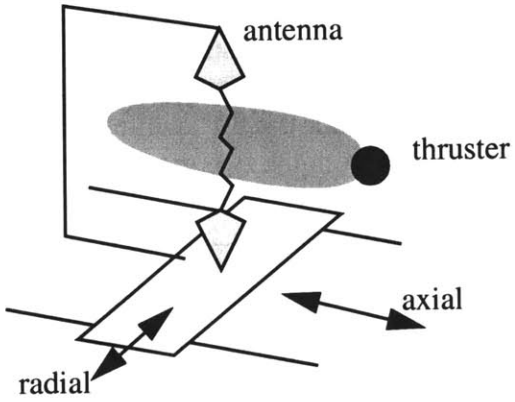

Figure 2.19. Communications Experiment[11]

In general, for kilowatt-class Hall thrusters, significant attenuation is observed in the lower microwave frequency bands, below about 8 GHz. Phase modification is significant throughout the microwave frequency range to above 20 GHz and well out into the plume. Both amplitude and phase temporal variations can generate frequency sidebands on microwave signals propagating through a plume. These effects are most signficant for higher power thrusters.[11]

In one experiment by Gilchrist et. al.[11], a 17 GHz signal was passed through the plumes of a 1.35 kW D-55 anode layer thruster and a 5 kW Hall thruster at different radial and axial distances from the thruster exit plane. Evaluation of the spectral modifications of the signal due to the plumes showed noticeable sidebands. For the D-55 thruster, first sidebands were present at +/- 100 kHz near the exit plane; second sidebands were present further downstream; and the changes approached the background noise by 40" (1.04 m) downstream. For the 5 kW Hall thruster, first sidebands were present at +/- 12 kHz; the changes approached background noise by 31" (0.79 m) downstream. The sidebands for both thrusters show variations with axial distance.

Models of the plume electron density which included azimuthal drift wave oscillations were found to better match the measured sideband levels and variations along the plume axis than symmetric models. The parameters of the instability were different for the D-55 and the 5 kW Hall, indicating that the resulting variations in spectral effects depend on the detailed operational characteristics of a given thruster.

2.3.6 Plume optical emissions

Manzella (1993) measured plume optical emissions of an SPT-100 in the range of 3000-9000 Å.[24] Most of the emission occurs in the blue spectrum, between 4200 and 5000 Å, due to Xe^+ transitions. A total of about 270 individual atomic and ionic transitions were identified in the emission spectrum from Xe, Xe^+, and Xe^{2+}. There was no evidence of emission from thruster erosion products such as B, N, Si, and O. A total of 250 mW of radiated optical emissions was measured from the exit plane of the thruster. The black-body radiation from the hot thruster has an expected peak between 1000 and 5000 nm.[33]

2.4. Instrumentation/ Diagnostics

2.4.1 Langmuir probes

There are many types of Langmuir probes, including spherical, planar, cylindrical, and multiple (double, triple, quadruple). All involve a metal probe which is placed in a plasma and either allowed to float or biased to some electric potential.

Classic Langmuir probe theory involves a small metal probe placed in a stationary plasma.[16] The current to the probe is a function of the potential to which it is held according to thin sheath plasmadynamics. One species will be attracted and one repelled: ions are attracted if V is below the local plasma potential V_p and electrons are attracted if V is above V_p:

$$I_{repelled} = qn_j A_{probe} \bar{c} \cdot \exp\left(\frac{V - V_p}{kT_j}\right) \tag{2.6}$$

$$I_{attracted} = qn_j A_{probe} \exp\left(-\frac{1}{2}\right) \sqrt{\frac{k(T_i + T_e)}{m_j}}$$

The characteristic produced by sweeping the probe over a range of potentials can be interpreted to estimate certain plasma parameters, as shown in Figure 2.20. If a probe is allowed to float unbiased in the plasma, it reaches the potential at which the net current to it is zero. This is known as the floating potential, V_f. At high negative potentials the ion current becomes saturated at a constant value, and at high positive potentials a corresponding electron saturation current is reached. The electron retarding region in between these two regions is exponential.

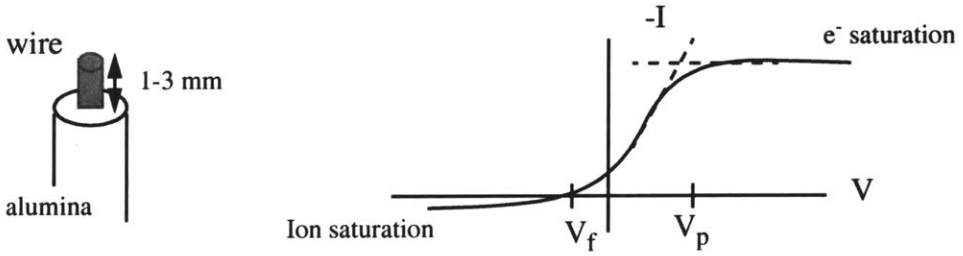

Figure 2.20. I-V curve for an electrostatic probe in stationary plasma

The slope of the logarithmic plot of the electron retarding region gives the electron temperature, or more precisely the equivalent temperature of the assumed Maxwellian population.

$$\log I = \frac{qV}{kT_e} + C \tag{2.7}$$

The intersection between the tangents to the electron retarding and the electron saturation regions gives the plasma potential V_p. The electron density is determined from the electron current at the plasma potential, where the electron current is obtained by subtracting the ion saturation current from the entire I-V characteristic.

$$I_e(V_p) = Aqn_e\sqrt{\frac{kT_e}{2\pi m_e}} \tag{2.8}$$

Spherical Langmuir probes are often used in low-density plasma such as found in ionospheric studies. The spherical shape means that the probe is not sensitive to the plasma velocity vector. Probes for high-density plasmas such as found in the center of thruster plumes are usually cylindrical and made of a small amount of uninsulated Tungsten wire sheathed in alumina. Single probes must be swept in voltage to explore the entire voltage-current (I-V) profile, while triple or quadruple probes are each held at a constant potential to simultaneously sample multiple points of the I-V profile around V_f. Either type of probe can be used to determine electron temperature, ion density, and plasma temperature in a stationary plasma. A quadruple probe also gives ion velocity.

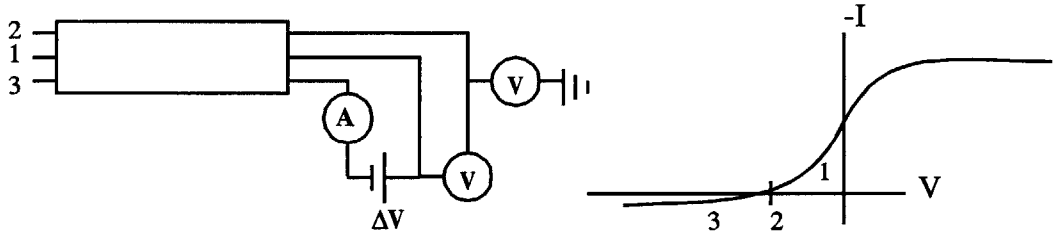

Figure 2.21. Schematic of a triple probe

Theory for Langmuir probes in a flowing plasma is very complicated and is examined in detail in Michael Fife's thesis[10]. Unfortunately there is no unique universal method of interpreting the characteristic in this case, and whenever a Langmuir probe is used in a plasma beam an error of 10-20% is incurred. In practice, the ion and electron saturation region of the I-V characteristic become linear. In the electron attracting case, this may reflect a transition to a 3-D orbital-motion limited regime, in other words, and infinite

sheath. A linear fit to this region can be used to estimate the plasma potential, but this method is not very accurate.

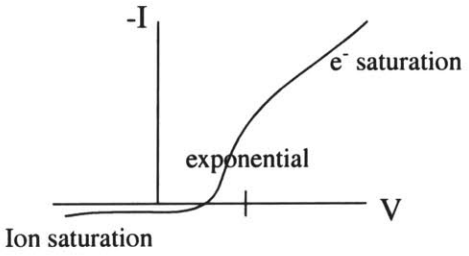

Figure 2.22. I-V Characteristic in Flowing Plasma[31]

2.4.2 Faraday probe

A Faraday probe is intended to measure the directed current flux at a point in the plasma. A planar Faraday probe generally is any metal surface which is allowed to collect ion current in a plasma. Often they may be simply a metal disk 2 cm or so in diameter, sprayed with or made of tungsten for reduced secondary electron emission, which is biased negative to repel electrons. A Faraday cup usually implies a deeper probe with an aperture leading to the collector. Faraday cups may have biased grids across the aperture similar to RPA's, which are described below; indeed in some cases the term RPA and Faraday cup are used interchangeably.

A guard ring may be used to protect the back or surface of a planar collector from stray current, to minimize edge effects of the probe, or to minimize the perturbation of the probe to the plasma. For these purposes the ring may be grounded, separately biased to the same negative potential as the current collector, or floating. Two typical designs are shown below.

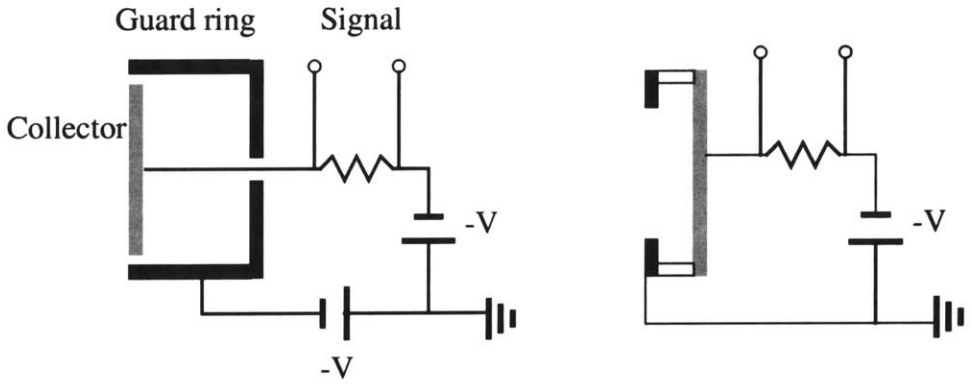

Figure 2.23. Schematics of planar Faraday probes with guard rings

The collected current can be used to estimate the ion density using the relation

$$j = I/A = nqv \tag{2.9}$$

Faraday probes are more robust than Langmuir probes, but they only provide current density and not electron temperature. Sweeping a Faraday probe through the entire plume provides the total beam current for thruster performance calculations. Data from Faraday probes is considered fairly easy to interpret, although in a vacuum chamber the effect of charge exchange ions at higher background pressures must be considered. The net result of charge exchange ions on the current density is that some current is removed from the beam center, replaced by fast ions, and spread around at larger beam angles on the previously randomly distributed slow neutrals. The net increase in current at angles above 50° between pressures at 10^{-6} Torr and 10^{-5} Torr can be an order of magnitude.[25] Collimators may mitigate this effect, see "Facility Effects and Mitigation Techniques" on page 43.

2.4.3 Retarding Potential Analyzer (RPA)

Retarding potential analyzers consist of a current collector shielded with biased grids or electrodes. A positively biased grid repels ions with energies below the cutoff voltage *V*, while some number of grids are biased negative and used to repel electrons and secondary electrons. The collector may also be biased negative to ensure good ion collection. Usually, the first grid is allowed to float in the plasma to reduce the perturbing effect of the device; the second grid is biased to repel electrons; the third grid is varied to selectively repel ions; and the fourth grid is biased to repel secondary electrons. The potential of the positive grid is varied (e.g. 0 to 500 V) and the current on the collector is measured. The spacing between the grid wires must be sized according to the Debye length of the species they repel, with a maximum wire spacing of 4 Debye lengths a typical rule of thumb[16]. The grids themselves must be spaced on a similar scale to mitigate space charging effects. RPA's can be effectively miniaturized as there are no time-of-flight requirements.

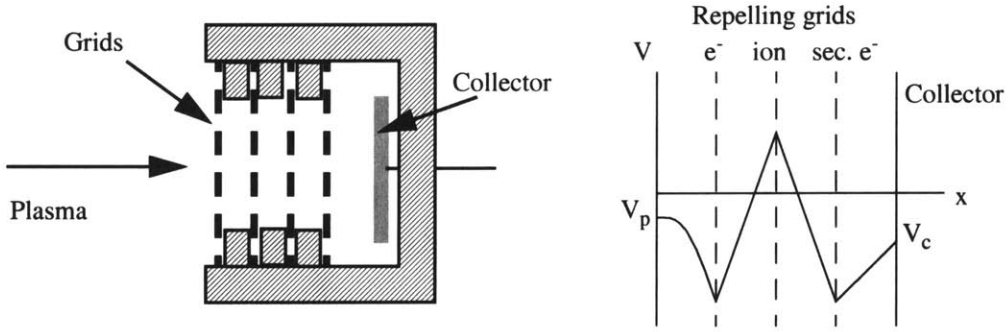

Figure 2.24. Schematic of an RPA

The derivative of the current-voltage characteristic obtained from the RPA data is proportional to the ion energy distribution. This can be seen by starting with a normalized distribution function for ion density expressed in velocities,

$$\int_0^\infty f(v)dv = 1 \tag{2.10}$$

Then, using the relation for current in Equation (2.9) and applying the cutoff potential V of the RPA, the current collected is

$$I = A_{coll} n_i q \int_v^\infty f(v')v'dv' \tag{2.11}$$

where the velocity is related to voltage by

$$v = \sqrt{\frac{2qV}{m_i}} \tag{2.12}$$

Changing variables from v to V and differentiating the new expression for current by voltage gives the desired relation,[22]

$$\frac{dI}{dV} = -A_c n_i q \cdot f(V)v(V)\left(\sqrt{\frac{2q}{m_i}}\frac{1}{2}V^{-\frac{1}{2}}\right) = -\frac{A_c n_i q^2}{m_i} f(V) \tag{2.13}$$

An example of raw data and the corresponding energy distribution are shown below.

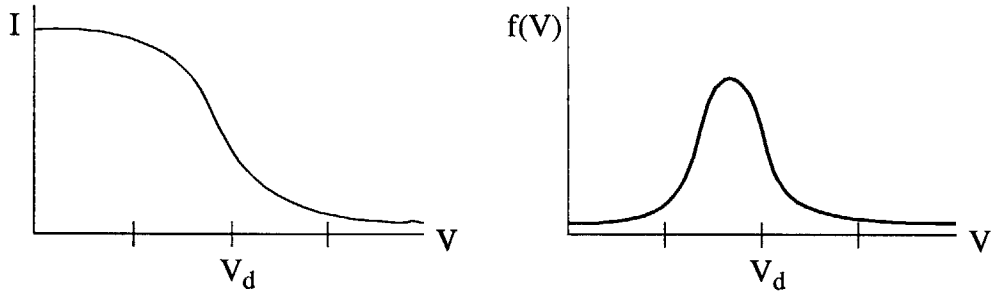

Figure 2.25. Sample RPA data and corresponding energy distribution

Although the RPA may be easy to implement, it does have some drawbacks. To analyze RPA data the assumption must be made that there is only one species, i.e. Xe^+, in the plume. The differentiation required to calculate f(V) introduces noise to the data, so that acceptable signal-to-noise ratios may not be attainable for the low currents at divergence angles past about 60°.[19] Also, the internal pressure in RPA due to the ram effect of flowing, high-density plasma entering the probe causes some entering ions to undergo collisions before they reach the detector. The net effect due to collisions of incoming plasma with this background is attenuation of the energy peak and broadening of the distribution in the direction of lower ion energy.

2.4.4 Molecular beam mass spectrometer (MBMS)

The Molecular Beam Mass Spectrometer is an instrument developed at the University of Michigan.[21] It combines an electrostatic energy analyzer with a time-of-flight mass spec-

trometer, allowing species-dependent measurements of energy distributions. This instrument improves upon the basic operation of an RPA by using differential pumping and a small diameter ion beam to eliminate collisional energy broadening, attenuation, and space charge shielding effects.

The current collectors, either a Ceramic Channel Electron Multiplier (CEM) or a high-gain picoammeter, allow measurements over a 360° envelope about the SPT-100. Ion currents as low as $1x10^{-18}$ A are measurable. A Langmuir probe is used to measure the local plasma potential for corrections for energy imparted to ions as they fall from ambient potential to ground potential.

The basic 45-degree parallel plate energy analyzer at the heart of the MBMS is shown in Figure 2.26. The plasma beam enters a region of constant electric field V_p/d with a trajectory of 45°. In order for an ion to leave the analyzer, it must have an energy per charge E/q such that its trajectory exactly intersects the exit aperture. The electrons are deflected in a direction opposite the ions and are removed from the beam.

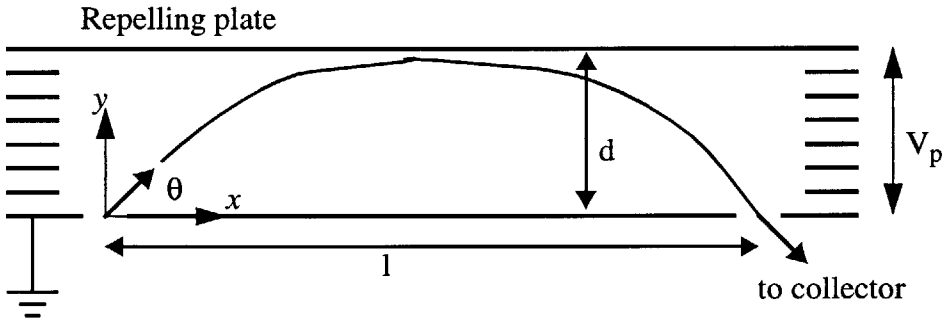

Figure 2.26. Schematic of 45° energy analyzer

The spatial trajectory of the ions depends on their velocity, mass and charge, so that

$$y = v_{y_0} \cdot t - \frac{q_i|\vec{E}|}{m_i} \cdot \frac{t^2}{2} = x - \frac{q_i(V_p/d)}{m_i} \cdot \frac{x^2}{2(u_i^2 \cos^2\theta)} = x - \frac{1}{2d}\frac{V_p}{(E_i/q_i)}x^2 \qquad (2.14)$$

$$E_i = \frac{1}{2}m_i u_i^2$$

$$\cos^2\theta = \frac{1}{2}$$

where d is the height of the analyzer, V_p is the applied deflection voltage, and x is the distance into the analyzer.

Only ions with the pass energy and resolution which allows them to reach the points $y = 0$, $x = l \pm w/2$ reach the current collector:

$$\frac{E_i}{q_i} = V_i = \frac{l}{2d}V_p \qquad (2.15)$$
$$\frac{\Delta V_i}{V_i} = \frac{w\sin\theta}{l}$$

where w is the width of the exit aperture. The length of the analyzer and exit aperture were chosen to achieve a resolution of $\Delta V/V = 0.004$, with the height of the analyzer then chosen to accommodate the resulting parabolic trajectories. As a result, the Michigan energy analyzer is 57 cm long and 16 cm tall with an exit aperture 3 mm wide.

The current collected is related to the pass energy by

$$I = Aqn_{V_i}\sqrt{\frac{2qV_i}{m}} \qquad (2.16)$$

where n_{Vi} is the number density of ions with the selected voltage V_i. According to reference [19], this n_{Vi} is exactly equal to the ion energy distribution function, so that

$$F(V_i) \propto \frac{I_i(V_i)}{\sqrt{qV_i}} \qquad (2.17)$$

However, the exact definition of this $F(V_i)$ is not clear. From this equation it is seen that this ion energy distribution function for a constant q/m is not directly proportional to the collected current, but no differentiation of the collected ion current is required to calculate $F(V_i)$.

A time-of-flight technique is used to provide species mass analysis. The travel length of the MBMS is 2.35 m, and the time for ions to arrive at the detector is on the order of tens of microseconds. A sample spectrum is shown below.

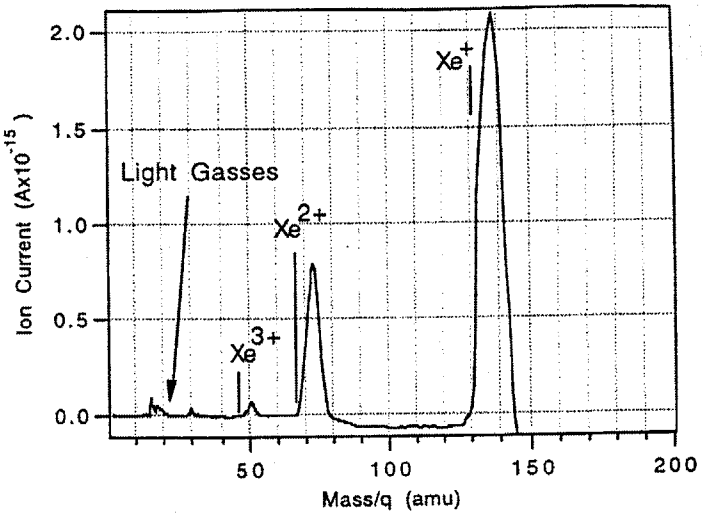

Figure 2.27. Mass spectra from MBMS[20]

Using this capability with the electrostatic analyzer, the MBMS can obtain energy distributions for each species (Xe^{+}, Xe^{2+}, Xe^{3+}) individually.

2.4.5 Neutral particle flux probe

The neutral flux probe developed by Gallimore et. al.[17] is a gridded retarding pressure sensor, a type of hybrid between an RPA and vacuum-pressure gauge. Electrostatic grids are mounted at the inlet of a hot cathode ionization gauge tube to repel all electrons and ions. Therefore the tube can measure only the neutral component of the plasma in the standard method of hot cathode ionization gauges. A schematic is shown in Figure 2.28. The gauge output is monitored on a controller calibrated for Xenon.

Free molecular theory is used to determine the escape flux from the tube. By conserving flux and using the ideal gas law it was shown that the pressure measured inside the tube is directly proportional to the plume neutral particle flux entering the probe if the gauge temperature is constant.

$$(\bar{u})_{out} = \sqrt{\frac{kT}{2\pi m}} \tag{2.18}$$

$$\Phi_{in} = (n\bar{u})_{in} = \frac{P_{tube}}{\sqrt{2\pi mkT}} \tag{2.19}$$

The gauge has an overpressure protect set point, as high pressures can damage the tube filament. This means that may not be possible to operate the gauge in some range around the

plume center. In Gallimore's study the pressure point was set to 0.8 Pa and measurements were limited to greater than 10° from centerline for an SPT-100.

An example of the output from this probe is shown below. Note the large peak near the centerline; since the probe measures flux, this peak is due to the high velocity of the CEX neutrals in this region. The neutral density is expected to have a wider angular distribution than this flux peak.

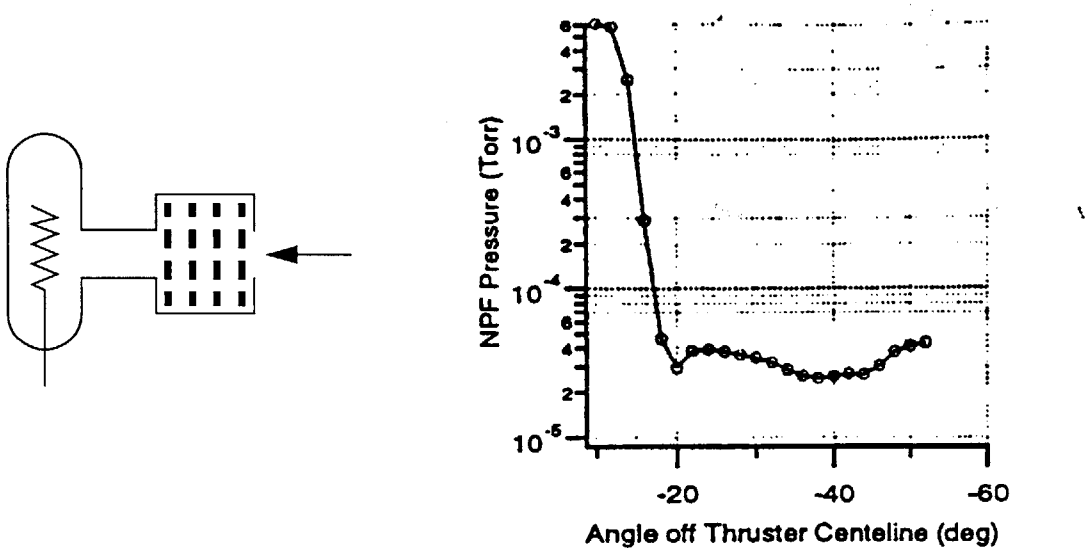

Figure 2.28. NPF probe schematic and output at 0.5 m from an SPT-100[17]

2.4.6 QCM's

A Quartz Crystal Microbalance consists of two carefully matched quartz crystals, one exposed to the environment in question and one shielded as a reference. The difference in frequency between the two crystals gives and indication of the mass accumulated on the sense crystal. QCM's are sensitive enough to measure less than a monolayer of atoms. The sensitivity of the crystal varies with the fundamental frequency and is experimentally determined. For uniform condensate density ρ, the beat frequency increase is linear with time, according to the basic operation equation of the QCM:

$$\Delta F = S_f\left(\frac{\Delta m}{A}\right) = S_f(\rho\tau) = S_f(\rho\dot{\delta}\Delta t) \tag{2.20}$$

where S_f is the crystal sensitivity, $\Delta m/A$ is the change in mass per unit area, τ is the film thickness, and Δt is time, and $\dot{\delta}$ is the rate of deposition.

The schematic for one model of QCM available from QCM Research is shown below.

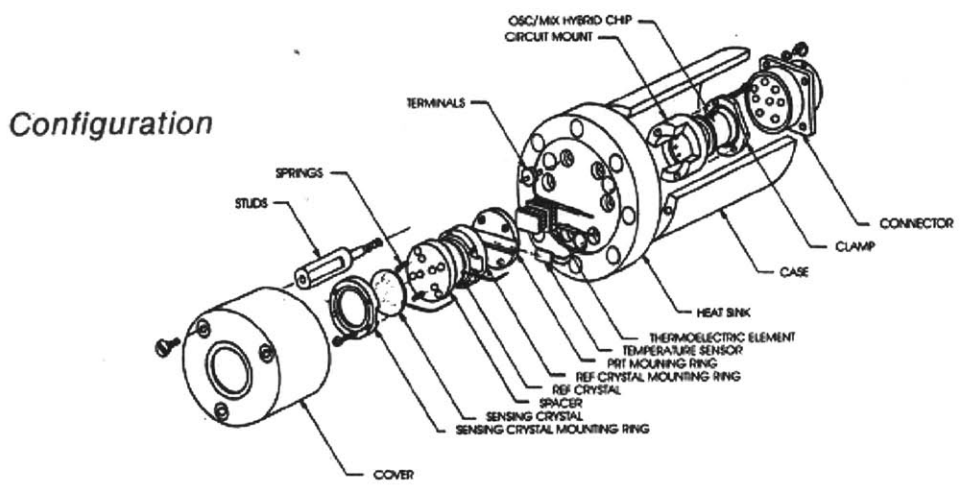

Figure 2.29. Configuration of a Thermoelectric QCM from QCM Research

QCM's are very light and small, require little power, and they have an extensive flight heritage. QCM Research has several models which are fully flight qualified. On most of the models, it is possible to perform thermogravimetric analysis on the deposited film. In this process, the crystal is slowly heated, causing constituents to boil off as their vapor pressure is reached.

2.4.7 Witness plates

Witness plates describe any material sample deliberately exposed to the plume to measure its effects. Different materials used include quartz and metal; usually the intent is to mimic solar array surfaces or other spacecraft surfaces commonly exposed to plumes. Masks are used to protect an edge of the sample as a control surface for height change measurements. These masks may be made out of tantalum foil. Plates may also be analyzed chemically, optically, and thermally.

Collimators may be used to restrict the view of the sample, such as to prevent contamination from material sputtered from nearby surfaces. Unfortunately they may also introduce sputtering from the collimators themselves. A collimator design is presented in "Facility Effects and Mitigation Techniques" on page 43.

2.4.8 Emissive probe

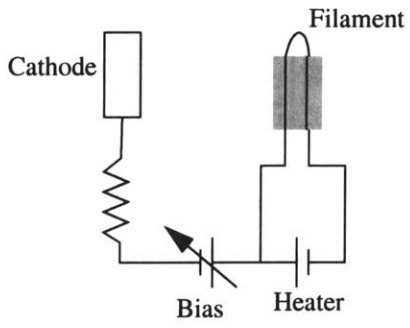

Figure 2.30. Emissive probe schematic

Although Langmuir probes may be used to estimate the plasma potential based on the "knee" between the electron retarding region and the electron saturation region, this is not a very accurate method. An emissive probe can provide a reliable measure of plasma potential with a very small perturbation to the plasma. The idea is that if the probe is positive with respect to the plasma, the electrons emitted with low energy are attracted back to the probe. In this case the probe current is unchanged by the electron emission. If the probe is negative with respect to the plasma, the emitted electrons can escape, and the probe current is decreased from the positive case. In other words, the emission current from such a probe drops to zero as the probe voltage approaches the plasma potential from the negative side, because emitted electrons begin to be reflected back to the probe by the plasma. The plasma potential is determined by the inflection point between the two regions of the probe's current-voltage characteristic.

An emissive probe consists of 5 to 10 mm of exposed filament, usually tungsten; a support structure with insulated copper leads which must be reliably attached to the tungsten, and power supplies to heat and bias the filament. The filament is heated to about 0.18 eV. There is a certain voltage drop along the emissive probe wires, of about 1 V, which introduces a systemic error. Compensating resistors in the circuit can be used to minimize this error. The tungsten filament may be spot welded to or braided with the copper leads.

Besides sweeping the emissive probe over a range of potentials, another method for determining the plasma potential allows the probe to float in the plasma while the heater current is varied. Increasing the heater current causes the probe to emit more electrons, until the probe reaches an equilibrium where it emits as many electrons as arrive. At this point the probe potential will be near the plasma potential, and the probe potential varies only slightly with increasing heater current. This method however is not necessarily accurate as a potential minimum may form between the probe and the plasma, which prevents it from floating at the true plasma potential. The electronics for a floating probe are simpler however as sweeping the probe bias is not required.

2.4.9 Heat flux probe

The heat flux probe used by Gallimore and King used transducers to measure the convective heat flux.[22] The probe consists of two commercially available transducers, one of which is covered by a sapphire window. The transducers are mounted in a copper housing which is water-cooled. This housing is instrumented with a thermocouple. The probe is shown schematically at left.

The main heat transfer mechanisms in the plume are convective heating, radiant heating, ion recombination heating, electron current heating, and ablative cooling. Convective and radiant heating dominate the transport of energy due to the high exhaust velocity of the thruster and the intense radiation from the plume and the hot thruster body; the ion recombination heating is estimated to be only 2% of the convective heating and is ignored, the probe is biased to ground potential to eliminate electron heating, and the ablative cooling is assumed to be insignificant. This leaves only the convective and radiant heating. The transducer behind the sapphire window is protected from the convective heat flux, so that it provides a measure of radiant heating only. The other transducer is exposed to obtain the total heat flux. With the assumptions outlined, this allows the convective heat flux to be derived.

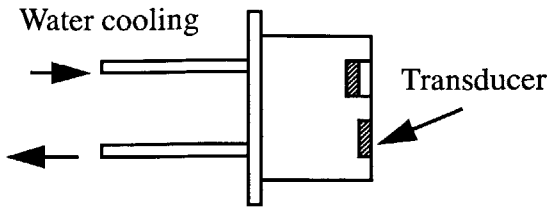

Figure 2.31. Schematic of heat-flux probe[22]

The sapphire window has a useful transmission-wavelength of 200-5500 nm, so it is transparent to the known radiated energy of an SPT-100 plume (see "Plume optical emissions" on page 31). The convected heat flux to the probe, assuming complete ion accommodation in one collision, is given as the difference between the incident plume heating and the reflected convective cooling.

$$q_{conv} = n_i\left[\frac{1}{2}m_i\int_0^\infty u_i^3 f(u_i)du_i - 2kT_p\int_0^\infty u_i f(u_i)du_i\right] \tag{2.21}$$

A direct measurement of q_{conv} can be combined with known values of the first and third moments of the ion-velocity distribution function and the probe body temperature to solve for the ion density. However this analysis does not account for the neutrals which might also carry heat convectively to the probe, so it is possible to derive information about the neutral component by comparing the heat-flux-derived ion density to Faraday-probe-derived ion density.

2.4.10 Radiometer

Radiometers are used to assess material degradation due to thermal radiation. Temperature measurements of the radiometer sensor and base are used to calculate the heat flux through the radiometer coating according to[35]

$$Q_{in} = Q_{rad} + kA\frac{dT}{dx} + mC_p\frac{dT}{dt} \tag{2.22}$$

and changes in this heat flux over time are used to infer changes in the thermal properties of the radiometer coating. For example, if the total heat flux to the base during thruster operation increases with time, then the coating has been degraded. One possible such coat-

ing is S13-GLO white paint with an emissivity of 0.25 in the visible range; this is a commonly used spacecraft thermal coating.

The radiometer used on ESEX is shown schematically below. The sensor consists of a titanium witness plate coated with S13-GLO and supported by a titanium strut and an insulating nylon bushing. A reflective aluminum housing surrounds the assembly.

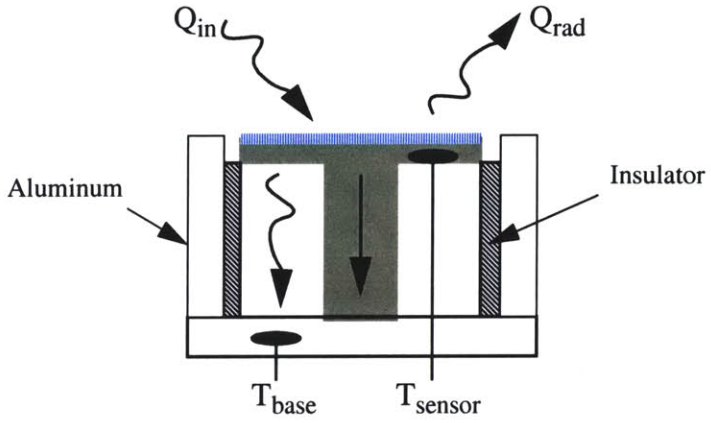

Figure 2.32. Radiometer schematic[35]

2.5. Facility Effects and Mitigation Techniques

A mentioned in Section 1.0., facility effects on plume experiments include results of the backpressure, sputtering of material from the chamber walls and support structures near the instruments, and recirculated plasma.

Manzella (1994) documented clear evidence of the ingestion and ionization of facility background gas by the SPT-100 thruster using emission spectroscopy. The background gas consists of nitrogen, oxygen, etc. with water vapor. Manzella estimated that the parasitic ions, which are accelerated back out of the thruster with propellant ions, contribute the equivalent of 2% of the main propellant flow. King et. al. found evidence of ingested gas products with their MBMS, identifying H^+, H_2^+, N_2^+, O_2^+, O^+, OH^+, and H_2O^+ and C^+ ions. The carbon came from surfaces in the facility that were protectively covered in graphite.

The CEX ions caused by collisions between thruster ions and facility background neutrals add to the current collected by Faraday cups, especially at larger divergence angles. Grys, Tilley, and Aadland[7] have designed a single-aperture collimator which protects the current collector from 99% of the random CEX ion current. The collimator was tested with a BPT-4000 thruster. The collimator also blocks some of the beam current, so a scale factor must be carefully determined from geometry. For the BPT thruster the collimator was tested with, the scale factor varied from 2 at the thruster centerline to 1 at 90°. Varying the back pressure and comparing against a regular Faraday cup showed that the collimated probe was much less affected by back pressure, which proves that it effectively blocks ions produced by collisions with the facility background.

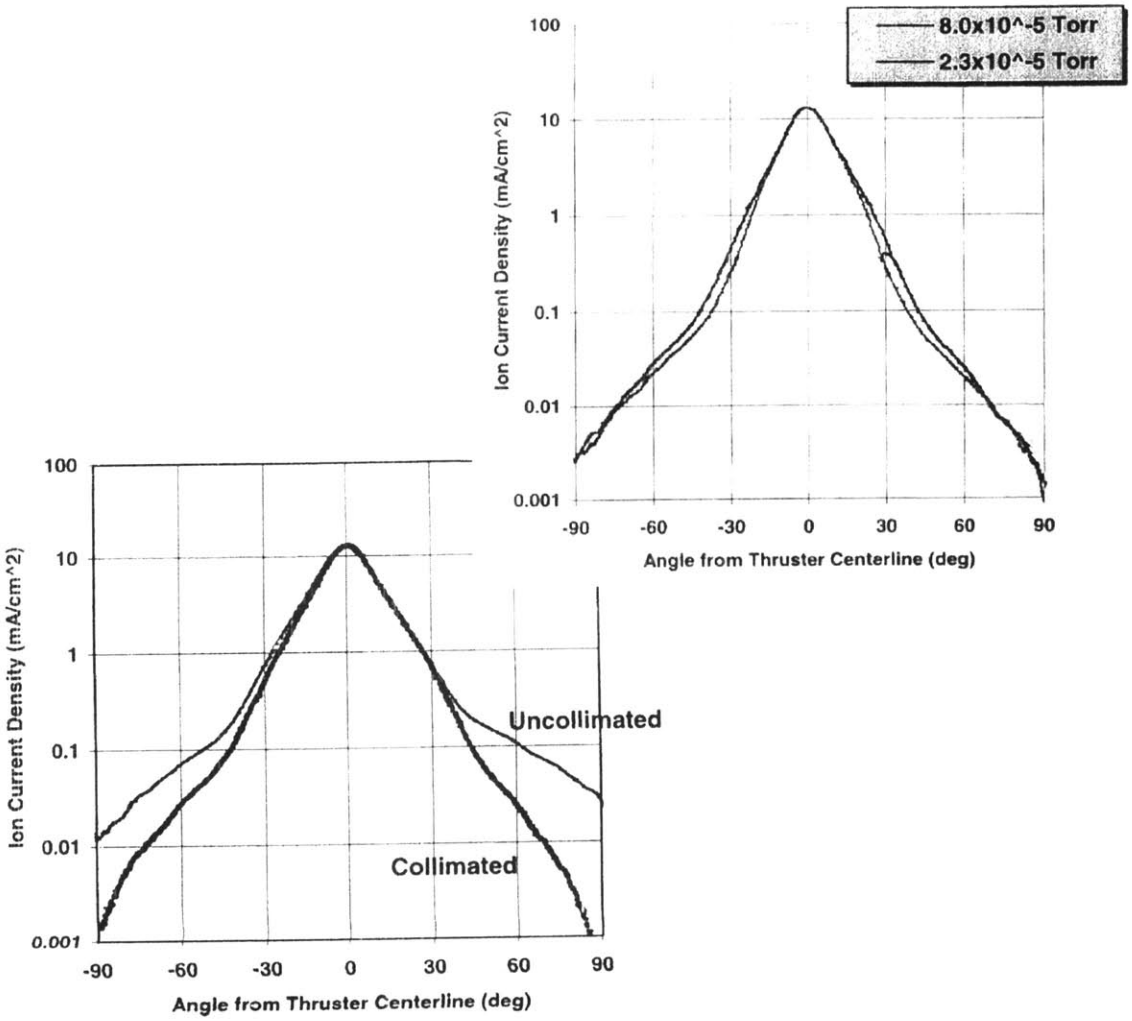

Figure 2.33. Effect of back pressure on collimated Faraday probe[7]

The collimator has 12 vents to reduce the buildup of neutral gas inside and an aperture of 2.3 cm, the same diameter as the current collector. The overall dimensions of the collimator are 5 cm diameter and 8 cm long. The collimator is biased to the same potential as the collector and the guard ring to prevent potential gradients which could overly disturb the plasma. Since the collimator collected as much as 2 A of current, a separate circuit is used for it so that the shunt voltage of the collector is not influenced. The measured and scaled beam current can be extrapolated to true vacuum with the equation

$$\ln J(\theta) = \ln J_0(\theta) + m(\theta) P_b \tag{2.23}$$

where J is the measured current density, J_0 is the true vacuum current density, P_b is the measured back pressure, and m is a slope determined experimentally by measuring the collimated beam current at a number of back pressures. This technique is independent of

the vacuum pressure gauge calibration and allows for accurate ion current density measurements even in modest facilities.

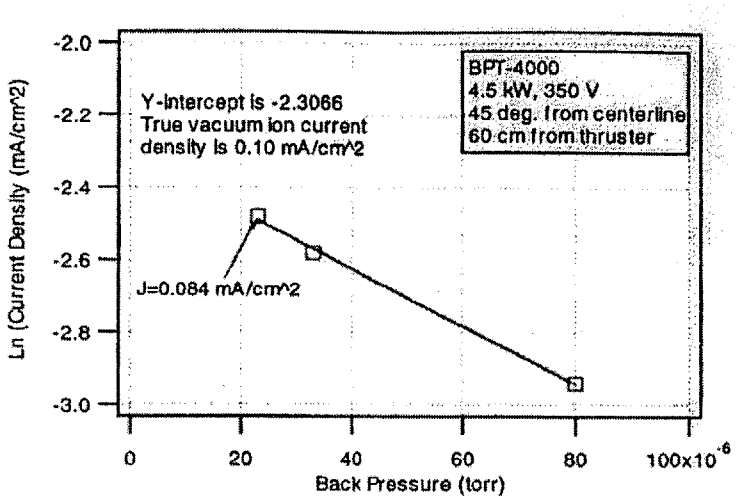

Figure 2.34. Back pressure correction for true ion beam current density[7]

Uncollimated witness plates at large angles from the thrust axis tend to be contaminated by material sputtered from the facility walls. A double aperture collimator to protect samples from this material was designed by Pencil et. al.[29] All direct line-of-sight trajectories for sputtered material are eliminated through axial placement of the apertures and the thruster exit is imaged on the entire sample. The collimators were constructed from tantalum foil line stainless steel tubes with molybdenum disks for the apertures. Chemical analysis of samples tested in the collimators after a 200 hour exposure to the SPT-100 indicated no evidence of aluminum or stainless steel, indicating that the collimator successfully blocked facility and support structure material.

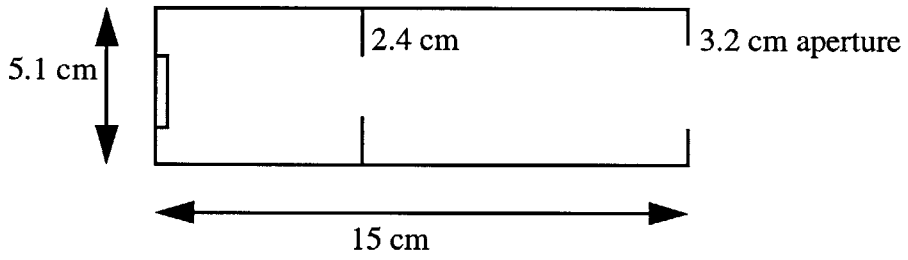

Figure 2.35. Double aperture collimator[30]

2.6. Electric thruster plumes in space

Recent and planned studies of electric thrusters in space are described below. All of the missions are by government civilian agencies, such as NASA, or military groups such as the US Air Force. The first missions presented are those which have already launched. These all represent entire spacecraft where testing electric propulsion was a primary

objective of the mission. The missions presented next are those which are planned for the near future, and include some packages which will not be launched as key elements of spacecraft but as pallets mounted on either the ISS or the shuttle.

2.6.1 Deep Space One [39]

NASA's Deep Space One (DS1), launched in October 1998, represents the first ever comprehensive in-flight investigation of ion propulsion-induced interactions and their effects. It was also the first in-situ measurement of the propulsion-induced environment near an interplanetary spacecraft.

A 30 cm Xenon ion engine provided the main propulsion for DS1. An Ion Propulsion Diagnostic System (IDS) was mounted 1 m from the thruster exit and well outside of the primary plume. The IDS contains the following instruments: 2 quartz crystal microbalances, 2 calorimeters, 1 RPA, a planar and a spherical Langmuir probe, 2 fluxgate magnetometers, a search coil magnetometer, and a plasma wave antenna. The measurements which can be obtained from the IDS are the velocity distribution of the Xe ions, the CEX ion energy and flux, the electron temperature, the plume potential, the magnetic field, and low and high frequency plasma waves.

Preliminary results have been reported for the RPA and the planar LP. The RPA successfully measured the saturated ion current and the ion energy relative to the spacecraft potential for the CEX ions. The planar LP, which is swept over about 15 V, measured the local plasma potential and the electron temperature.

A set of particle-in-cell numerical models were developed to assist in the data analysis and interpretation over the 3-D volume around the spacecraft as the IDS is located at a single point.

2.6.2 ESEX [35]

ESEX is a US Air Force Electric Propulsion Experiment which was launched in early 1999. The purpose of the mission was to demonstrate the readiness of a 30 kW ammonia arcjet for integration and use on new spacecraft. ESEX flew a sensor suite of 4 cryogenic QCM's, 4 radiometers, and 2 sections of GaAs solar array cells to assess the effect of the arcjet on the spacecraft.

The sensors were arranged in the backplane at distances of 40 to 93 cm from exhaust plane and angles from 120 to 160 degrees. A temperature of 218 degrees K was found to be

maintainable over the solar cycle. During thruster firings, a frequency change of 20 Hz was easily distinguishable from the overall QCM readout.

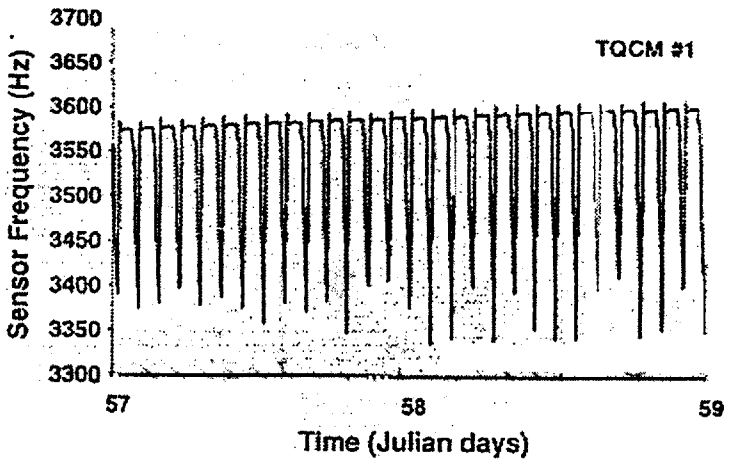

Figure 2.36. Representative QCM data showing a slow frequency increase due to mass deposition is distinguishable from the larger solar cycle.[35]

The cryogenic QCM's had the capability for thermogravimetric analysis to bake off constituents, and at least 5 bakeoffs have taken place during the mission. Results of the analysis were not available at the time of this writing.

The use of QCM's on ESEX highlighted the difficulties of interpreting the QCM signal. Net mass change of the QCM can be caused not just by mass deposition, but also by a local temperature rise, radiative impingement from the plume, atomic oxygen erosion, and expulsion of reactive species from the thruster which then remove deposited mass. All of these effects must be considered in making final judgements about the net effect of the thruster on surfaces located near the QCM.

In terms of the other instruments, one radiometer with a full view of the plume and thruster body showed a small degradation of characteristics of its thermal coating; the other radiometers showed no effects from the thruster firings. The solar array samples impinged by the plume did show some degradation in solar cell voltage, which is most likely a result of the plume plasma forming an alternate, shorting current path. Successive firings seemed to erode the array insulation at the short causing the effects to increase with successive firings. The authors note that simply placing the array farther from the plume would prevent these effects.

In summary, there were no contamination effects in the thruster backplane due to the arcjet firings. Only sensors placed unrealistically close to the thruster showed significant effects.

2.6.3 Stentor Satellite [5], [39]

The STENTOR is a French satellite which is dedicated to electric propulsion, specifically Hall thrusters. Four Hall thrusters will be onboard for North-South stationkeeping, 2 of

Russian technology and 2 French PPS 1350s. A Plasma Diagnostic Package (PDP) which weighs less than 2 kg, including the electronics, has been developed for in-flight plasma characterization. A unique feature of this package is that all the instruments are mounted on the satellite's solar panels, which provides sweeping movement as the panels track the sun. The plasma probes included are a retarding potential analyzer and a spherical Langmiur probe; these two instruments are collocated in one box. The contamination sensors are two QCM's and a portion of the satellite's solar panels dedicated to measuring thruster-induced effects on performance. The requirements used for this package are shown below.

Table 2.3. Summary of the PDP operating requirements

Parameter	Value
Ion Energy Range	0 to 400 eV
Expected Energy Peak for the largest ion population	150 eV
Electron Energy Range	1.7 to 3.5 eV
Plasma Potential Range	-150 to 100 V
Plasma Density	10^7 to $3x10^8$ cm^{-3} (10^{15} to $3x10^{16}$ m^{-3})
Ion Current Density Range	0.002 to 0.05 mA/cm^2

The plasma probes achieve a high dynamic range by automatic switching between two amplifier gains. The gain steps up if the collected current is less then 3.9 μA for the RPA and 60 μA for the LP. The power for the probes is stepped up from the 50 V bus voltage. The AIAA paper on this package includes block diagrams of the electronics.

The solar cells will be monitored for temperature and leakage current and a three-point measurement of open, circuit-short, and circuit-load. They will be mounted near the QCM's to relate solar cell degradation to the mass deposition rate. The premeasured control deposition rate must be separated out from the QCM results.

Table 2.4. PDP Mass and Power

Subsystem	Mass (g)	Maximum Power (W)
Probe Assembly	400	4.7
QCM Assembly	50	0.3
Solar Call Assembly	100	0.3
Electronics	1150	14

The STENTOR is expected to launch in 2001. Prior to launch, the package will be tested with a Hall Effect plasma source and a low energy, low current gridded ion source. Laboratory plasma diagnostic instrumentation, such as probes of different shapes and dimensions, will be used to verify the PDP's output. The PDP is expected to fly again on ESA's SMART 1.

2.6.4 SPIRET [37]

This project consists of three sequential tasks: first to develop facility and perform initial STS space tests, second to correlate space results with ground tests, and third to prepare for operations on ISS. SPIRET is collaborative with AEDC, Teledesic, Lochkeed Martin Space Systems Co., AFRL, NASA, UTSI. The end goal is a space-based facility for plume integration testing of electric thrusters.

Table 2.5. SPIRET Target Issues

Hall Integration Issues	Required Measurement	SPIRET Component
Spacecraft Contamination	Plume Density Plume ion energy Plume backflow	In-situ space measurements of a thruster using a traversing Xe and Xe^+ diagnostic suite
Communications	RF Transmission through plume Optical transmission through plume	In-situ space measurements using RF transmitter & receiver sets during thruster operation
Spacecraft Drag Estimation Uncertainty	Surface effects	In-situ surface contamination diagnostic suite in proximity to thruster

This program is relevant to the engineering design of spacecraft in industry and to the operational experience of EP propulsion units for the DoD. The program also sees some relevance to academia in terms of the development of measurement diagnostics and validation data for numeric plume models.

SPIRET will weigh 88 kg and use a 4.5 kW BPT Hall thruster. It will fly on a Spacehab QuEST tray, which is 1m x 1m, on the roof of the research module. The package is manifested on STS R3. The operational plan is to operate in 6 one-hour intervals. Power for the thruster will be limited to 3 kW due to Shuttle power limitations. The same arrangement will be used on ISS.

The primary science objectives for the experiment, listed with the instruments intended to measure them, are:

- Xe+ density and energy off-axis w/RPA and Faraday cup
- Plume e- density off-axis w/Langmuir probe

- Plume potential w/Langmuir probe
- RF signal propagation phase shift w/RF transmitter
- Environment density and potential

The secondary objectives are:

- Optical emissions from thruster w/spectrometer
- Material sputtering w/ witness plates
- Potential contamination w/ QCM

The table below shows the preliminary instruments selected for the diagnostic package.

Table 2.6. Preliminary SPIRET Instruments

Sensor	#	Location
RPA	2	Arm
LP	2	Arm
QCM	2	Pallet
UV/Vis spectrometer	1	Pallet
RF antenna	1	Pallet
CCD Monitor	1	Pallet

The mechanical arm holding the RPA's and LP's will rotate from 0 to 100° to interrogate the plume.

2.6.5 SMART 1

SMART 1 will be the first European spacecraft to travel to the moon and the first interplanetary spacecraft to use a Hall thruster. SMART 1, due to launch at the end of 2002, will have a 17 month cruise phase to the moon using its French PPS-1350 Hall thruster followed by a 6 month polar lunar orbit phase.

The spacecraft will carry two diagnostics packages. One will be the same as the Electric Propulsion Diagnostic Package that will fly on Stentor. The second package, called Spacecraft Potential, Electron, and Dust Experiment (SPEDE), contains two Langmuir probes on 60 cm booms. These probes can be operated either in a current-driven mode to measure the potential difference between the sensor and the spacecraft or a voltage-driven mode in which it measures electron flux. Using data from both packages, estimates will be made of the CEX ion density.

The SMART 1 diagnostics will be complemented with an extensive numerical simulation. Ground test data will be used to validate this simulation for predictions of the spacecraft/ thruster interactions.

2.6.6 TechSat 21

The TechSat 21 mission will include the 200 W Hall thruster by Busek and a set of micro-PPTs. Through measurements of the propulsion systems chosen the Air Force hopes to develop an "Integration Handbook" for using these thrusters on other USAF spacecraft. The satellites will have some form of onboard sensors designed to minimize mass while complementing ground testing and modeling resources. Sensors under consideration for the spacecraft include an energy analyzer with a magnetic mass separator, a CCD camera, a radiometer, and some kind of solar array instrumentation to measure changes in performance. TechSat 21 is scheduled for a demonstration flight in 2003 with full operation expected in 2007.

2.7. PPT Overview

Pulsed Plasma Thrusters (PPTs) are low power, high Isp devices which produce thrust by inducing a spark over the face of a fluorocarbon propellant bar, ablating it an accelerating the ionized discharge away from the bar surface. PPTs have a specific impulse of greater than 1200 seconds and a power requirement generally less than 120 Watts. The chief components of the thruster are the propellant bar, often teflon, and the high voltage capacitor and spark plug. The PPT operation is characterized by the energy for each spark, usually between 5 and 45 Joules. The sparks occur in finite time, usually at a rate of 1-2 Hz, with hundreds of msec required for charge-up time and tens of μsec for a spark. This method of operation produces a highly variable plume which never reaches steady-state.

Ground-based studies of PPT plumes have characterized the electron temperature and density, ion energy, backflow contamination, erosion and deposition, and particulate emissions. PPT's do have a flight heritage including the LES-6 spacecraft in 1968, where the PPTs were used for east-west stationkeeping, and Navy TIP/NOVA navigation satellites in 1975, where the PPTs were used for drag compensation. These missions did not indicate any major contamination, EMI effects, or solar array degradation from the PPTs. However there is a need for PPTs to be flown in space with more extensive diagnostics, especially in light of the very sensitive formation flying missions for which they are now being considered.

The plume of a PPT consists of both accelerated particles and slow neutrals. The constituents of the plume are carbon, fluorine, and a variety of fluorocarbons including CF, CF_2, CF_3 from the propellant and Cl, Fe, Ni, N, and O from other PPT components.[2] Centerline ion velocities range from 30 to 60 km/s. Slow neutral particles have been detected up to 1 ms after a discharge.[9]

Electron densities in the PPT plume range from 10^{17} to 10^{21} m^{-3}, depending on the energy of the discharge from 5 J up to 40 J, while the electron temperature is around 1-3 eV at all energy levels.[8]

Of particular concern are films which may collect on interferometer surfaces and negatively impact the optics. In general, net deposition is seen for angles greater than 30° from the PPT thruster centerline while net erosion is seen inside this half-angle, although in the plane containing the cathode and anode there are asymmetries which may need to be accounted for in positioning the PPT. In one test of more than 1 million pulses of a PPT, the maximum mass deposition on a 2 cm x 2 cm witness plate 61 cm from the exit plane was 1 mg at 30° while the maximum erosion was more than 19 mg at 10°, corresponding to height changes of 8000 Å and 167,000 Å respectively.[2]

Section 3.0. Shuttle Experiment Design

3.1. Introduction

This chapter will present work done to refine the concept of the Hall and PPT Hitchhiker Shuttle experiment, now known by the acronym ETEEV. Initially, the project included a Pulsed Plasma Thruster and a small Hall thruster, but whether these should be one or two payloads had not yet been decided. Instrument selection was still open, with Langmuir probes, Faraday cups, witness plates, quartz crystal microbalances, retarding potential analyzers, and a thrust balance under consideration. A grant from the Massachusetts Space Grant Consortium allowed more serious design studies to begin in January 2000.

These initial studies included a review of the thruster plume literature, presented in Section 2. This review was used to help determine what plasma conditions to expect from the thrusters under consideration. Also, the review identified the types of instruments used by researchers for plume studies in vacuum chambers as well as the instruments used in space-based plasma diagnostics packages such as on NASA's Deep Space 1. The application of this information to developing the Hitchhiker package is described in this section.

Starting in spring 2000, the experiment design process also included interaction with Goddard's Shuttle Small Payload Projects office. A teleconference in June, 2000, presented Goddard with a conceptual overview of the experiment's science objectives and expected subsystem parameters. Their feedback was very useful and helped solve some outstanding design questions.

Lastly, the experiment design process has included extensive analysis of a few instruments for their use in the space and ground experiments. These analyses are presented in this section.

3.2. ETEEV Team

ETEEV is a collaborative effort, with many different groups expressing interest in helping out with instruments and testing facilities. The universities involved are MIT and Worcester Polytechnic Institute (WPI). Busek is providing, and supporting the use of, the Hall

thruster. The AFRL at Edwards has loaned their set of 4 QCM's and a laboratory controller for ETEEV use. Other potential contributors are listed in Table 3.1. below.

Table 3.1. ETEEV Team Members and Responsibilities, January 2001

Institution	Participants	Roles
MIT	Manuel Martinez-Sanchez[a] Paul Bauer Stephanie Thomas* Anne Pacros*	Overall coordination Experiment design Instrumentation
WPI	Nikos Gatsonis Jurg Zwahlen* Andrew Suryali*	
Busek	Vlad Ruby Bruce Pote	200 W Hall thruster
AFRL Edwards	Greg Spanjers	QCM's
Potential:		
Michigan Space Grant	Alec Gallimore	NPF probe Large vacuum facility
Draper Lab	Michael Socha	Systems integration Thrust balance
NASA GRC	TBD	100 W PPT
AFRL Hanscom	David Cooke	DIDM instrument

a. Principal Investigator
* Student researchers

3.3. Science Objectives

ETEEV is designed to complement detailed lab measurements of electric propulsion environmental interactions with carefully selected checks against in-space data. Since space data are much more difficult and expensive to obtain than ground data, little has been obtained on these thrusters to date. Therefore, the experiments will focus on those areas where the difference between space data and vacuum chamber data could be critical, as outlined in Section 1.

The primary objectives of ETEEV are:

1. Surface film deposition measurements in the plume backplane, > 70° from centerline for the Hall thruster and >50° for the PPT at mid-range distances of 10 to 30 cm.
2. Diagnostic measurements of plume plasma parameters in the near and mid plume, including surface erosion, out to 60° and also at mid-range distances.

Secondary objectives are:

3. Thrust measurements for a complete performance characterization of the Hall thruster.
4. Optical observations of the farfield plume, >1-2 m, for various orientations of the shuttle ram and geomagnetic field.
5. Optical emission from the plume at a few chosen spectrum lines

The secondary objectives will be met if they prove fairly simple to implement and feasible financially. These objectives involve instruments such as cameras and a thrust balance which are not candidates for student construction and may need to be procured at extra cost. Expanding on these objectives, target issues for the Hall thruster experiments are:

- Debris deposition at 70°-90°
- Ion fluxes/energies at angles of 30°-60° from centerline
- Surface erosion at 30°-60°
- Ion current density profile throughout the main plume
- Thruster performance and operating regime at selected settings
- Distant plume distortions due to the geomagnetic field

Likewise, target issues for the PPT are:

- Electron density and temperature throughout the main plume
- Ion energy throughout the main plume
- Contamination deposition at angles from 30° to the backplane
- Erosion near the plume center

3.4. ETEEV Thrusters

The Hall thruster and PPT were chosen for ETEEV because they are mature thrusters currently being considered for a variety of missions. Hall thrusters can be used for orbit raising, north-south stationkeeping, and attitude control, depending on the size of the thruster and spacecraft. They are now baselined on some commercial satellite models, and the Busek 200 W Hall thruster has been selected for use on the Air Force's TechSat 21 mission. PPT's are popular due to their simple propellant design, high specific impulse and precise impulse bit. They are considered for applications like spacecraft attitude control and high-precision positioning. They hold particular promise for high-performance formation flying systems and thus they are being considered for spaceborne interferometers such as Terrestrial Planet Finder.

The Hall thruster for ETEEV is a 200 W model provided by Busek. The design of this thruster and the miniature hollow cathode used with it was funded by the U.S. Air Force. This model is called a "tandem" thruster because the magnet coil is located upstream of the discharge chamber, which allows the large magnetic field required for such a small Hall thruster to be generated in a thermally manageable way. The specifications for this

thruster are 1380 seconds Isp and 38% efficiency when operated at 300 V with 0.7 mg/s Xe flow. The nominal thrust at these conditions is 10.5 mN. The cathode self-sustains its discharge at a flow of about 0.08 mg/s.[15]

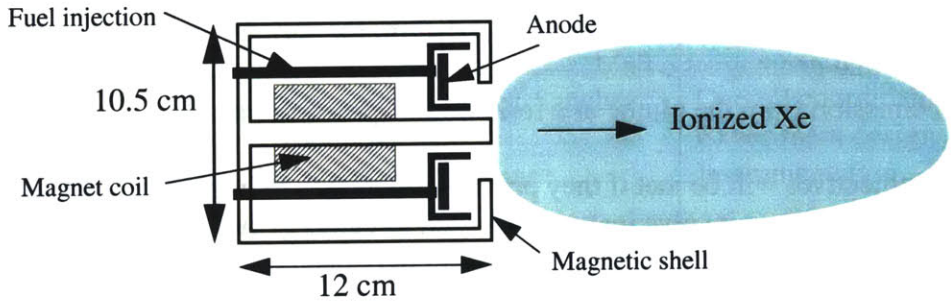

Figure 3.1. Schematic of Busek BHT-200-X2B

A picture of the BHT-200 with its hollow cathode is in "Basic Hall Thruster Characteristics" on page 18. For more details on the design of this thruster, please see *Low Power Hall Thruster Propulsion System*, reference [15].

The PPT for ETEEV has not yet been specified but it will also be a low-power (about 100 W) thruster. Example performance numbers from a breadboard PPT recently tested at NASA Glenn[2] at a spark energy of 43 J are an impulse bit of 710 μN-sec with an average mass loss of 60.3 μg/pulse. A schematic of a simple PPT and a picture of PPT operation from experiments by WPI students are shown below.

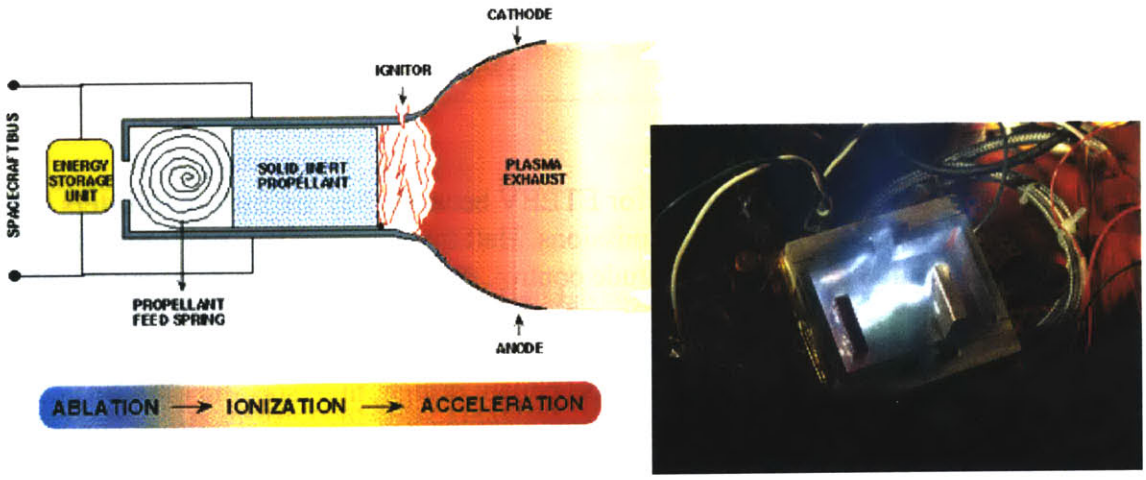

Figure 3.2. PPT schematic, right and PPT firing, courtesy WPI

Although other electric thruster experiments have been conceived since work began on ETEEV, ETEEV remains unique since it will test only low-power thrusters. Therefore it will complement other space-based propulsion experiments and not compete with them.

3.5. Hitchhiker Carrier Capabilities

The Hitchhiker Shuttle carrier is designed for small payloads which require power, data, or command services. As of January, 1999, the Hitchhiker Project has flown 58 Hitchhiker experiments. The system provides real-time communications between customers at the control center at Goddard Space Flight Center and their payloads on the Shuttle. It can also provide crew control and display capability if necessary. Hitchhiker payloads may request payload-unique Shuttle attitudes. NASA has extensive documentation on the small payload carriers on their web site (http://sspp.gsfc.nasa.gov/).

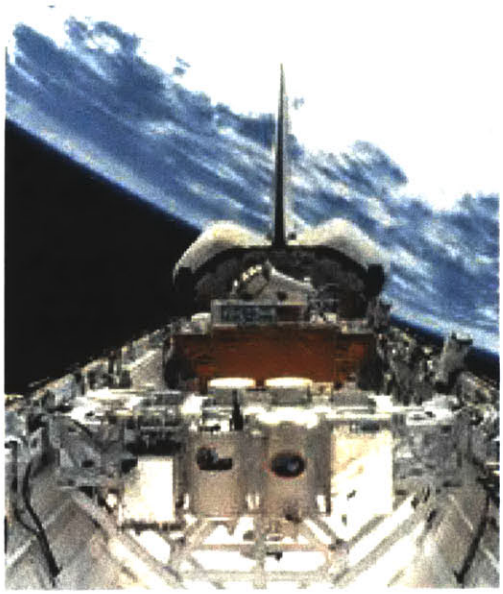

Figure 3.3. Hitchhiker Cross-bay bridge

Hitchhiker carriers are available in several configurations, including sealed canisters, canisters with motorized doors, and three different sizes of flat plates. These carriers can be mounted on a cross-bay bridge which can be located anywhere in the Shuttle payload bay, with a maximum combined customer weight of 3000 lbs. There are seven canister or side-plate slots along the side of the bridge and four pallet slots along the top. Canisters and side-mounting plates may also be mounted on the side of the payload bay using the GAS (Get-Away Special) adapter beam. Side plates can hold up to 200 lbs. while pallets can hold up to 500 lbs. each.

A standard Hitchhiker avionics unit provides eight standard electrical interfaces or "ports". This avionics unit is in the process of an upgrade which will significantly improve its data rates. The current units provides the following capability per port:

- Two 28V/10A power lines which are turned on by ground command
- One asynchronous 1200 baud uplink command channel
- One asynchronous 1200 baud low-rate downlink channel, available real-time about 85% of the time; data can be recorded onboard for later recovery
- One 1-14 kb/s medium rate downlink channel, available about 50% of the time
- Three channels for temperature sensors
- Several other analog interfaces and signals

Hitchhiker payloads rarely use onboard data-storage devices due to the excellent avionics capability provided. There is a limit of 1500 W and 1.4Mb/s on all combined Hitchhiker payloads, and individual payloads are not necessarily limited to only one port. It is also common for data to be ftp'ed to the ground through the onboard network of crew laptops, which does not require crew involvement. All downlinked data are available on CD-ROM 1 month after the flight.

At Goddard, Customer-provided Ground Support Equipment (CGSE) can be used to command the payload and display data during payload-to-carrier integration, verification testing, and flight operations. The avionics interfaces are designed to be transparent, so that the same CGSE can talk directly to the payload during development or through the avionics without any conversion of the data streams. Real-time orbiter attitude and position are also available to the CGSE.

Thermal control is the responsibility of the customer. Thermal blankets, heat pipes, radiators, and heaters are generally used. Experiments must be able to withstand 30 minutes of full sun and the orientation of the payload bay to the earth indefinitely. Mechanically, the experiment must be able to withstand launch and landing loads in any orientation. Goddard is responsible for aiding the customer with their thermal and mechanical models.

Although not technically a part of the Hitchhiker carrier system, there are numerous cameras in the payload bay. Most of these are black and white but several are color. In addition, the astronauts frequently take pictures of the payload bay from the middeck. All of these systems may be used for free if the Shuttle mission allows it.

ETEEV poses several safety issues with regard to the Shuttle. ETEEV has pressurized containers, exposed high-voltage surfaces, expelling gases, and moving parts, all of which require special consideration.

In terms of programmatics, the first milestone is the Request for Flight Assignment, Form 1628, which must be filed with the appropriate NASA Headquarters discipline office. The Customer Payload Requirements document is due as soon as possible after the Form 1628 has been accepted; this document begins the contractual process of defining the information needed for the preparation, flight, and disposition of the payload. Further documentation, including an extensive safety data package, is due 24 months before the scheduled flight. The hardware is due at Goddard 6 months before the flight, where the hardware is integrated to the carrier and functional and EMI tests are performed. Any tests required to verify proper operation or for safety certification must be performed before this date. After the tests at Goddard the payload is shipped to Kennedy Space Center and integrated into the Orbiter. Launch is typically 4-10 weeks after this integration.

3.6. Expected plasma parameters

To perform instrument selection, and to determine if the instruments for the two different thrusters were at all compatible, the expected plasma parameters for each had to be determined.

The expected current density from the Hall thruster was estimated by scaling Pencil's analytic fits given in "Density and composition of the plume" on page 19. The current was assumed to scale with thruster power, which corresponds to a 2/15 scaling factor from an SPT-100 to the 200 W thruster. The current density scales with inverse distance squared, which is already incorporated into the model. The resulting density profiles from the 1996 fit are shown in Figure 3.4. and Figure 3.5.

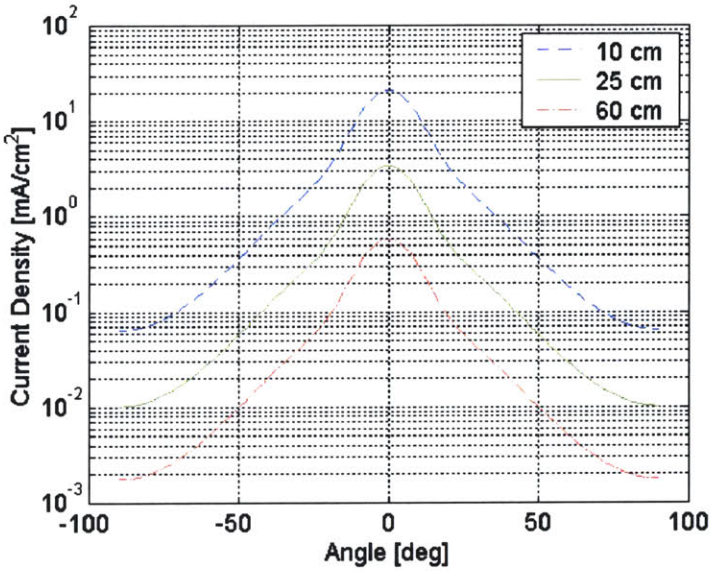

Figure 3.4. 200 W thruster predicted current

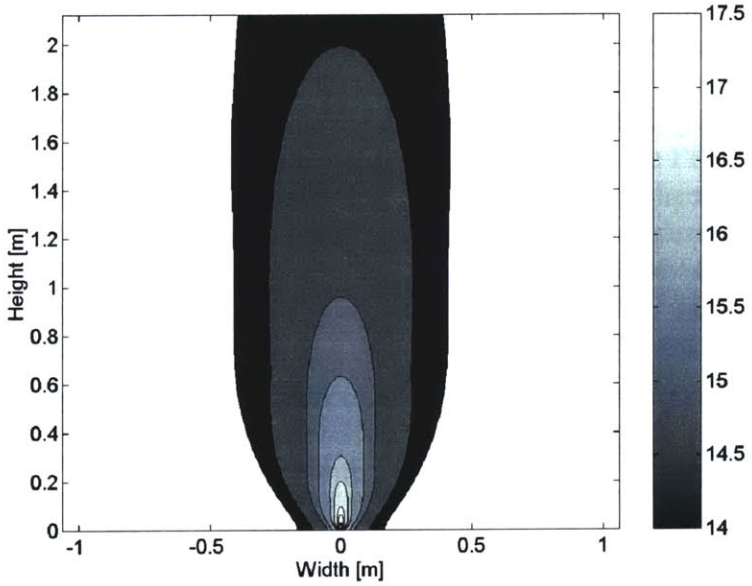

Figure 3.5. 200 W thruster predicted density contours, $\log_{10}(n)$, $[n] = m^{-3}$

The ion energy distributions are not expected to differ much from a standard SPT-100. This suggests that the most probable voltage will be somewhat less than the discharge voltage and that voltages up to 600 V are expected due to particle collisions. Please see "Ion energy distribution" on page 23 for more details.

Hall thruster deposition rates were also assumed to scale roughly with thruster power and inverse distance squared. By bringing the QCM's and witness plates to 25 cm from the exit plane the flux of contaminants will be 16 times that at 1 m, so that taking the power scal-

ing into account the flux for the 200 W thruster at 25 cm is about twice that of an SPT-100 at 1 m. Therefore the estimated deposition at 25 cm and 75° is $1x10^{-3}$ Å/s or 3.6 Å/hr. Erosion rates may be scaled similarly, giving an erosion rate of about 0.1 Å/s or 360 Å/hr at 25 cm and 45°.

The expected PPT parameters cannot be defined until the PPT for ETEEV has been selected. Please see "PPT Overview" on page 51 for some typical PPT plume characteristics.

3.7. Instrument Analysis

Any of the instruments listed in the plume literature review could be considered for ETEEV. However, instruments required for optical or electromagnetic study of the plume can be excluded since this is not an objective of ETEEV, excepting simple photography. A time-of-flight mass spectrometer is too cumbersome for a compact space experiment due to path length requirements, and the same is true for a 45° electrostatic analyzer. A magnetic deflection spectrometer may be smaller but they have not been used extensively for plume studies and would require significant development effort. Therefore consideration of instruments is limited to those that are frequently used in plume research and easily miniaturized, which leaves RPA's, Faraday and Langmuir probes, QCM's, and witness plates as primary candidates. A few slightly larger instruments are under consideration including DIDM, described below, and Gallimore's neutral flux probe. In addition to plume diagnostics a thrust balance is required for the performance measurements; this will probably be physically the largest instrument.

After considering the plasma parameters for both the PPT and the Hall thruster, it was determined that different instruments suites were required for each. Analyses of instruments for use with the Hall thruster are given below.

3.7.1 QCM and Witness Plate Analysis

QCM's are available in different operating frequencies, with increasing sensitivity for increasing frequency. The following analysis shows the performance of each frequency under conditions expected for the 200 W Hall thruster.

The available frequencies of QCM's are 5, 10, 15, and 25 Mhz with sensitivities of $5.7x10^{7}$, $2.3\ x10^{8}$, $5.1x10^{8}$, and $1.4x10^{9}$ Hz-cm^2/g respectively. As mentioned in "Expected plasma parameters" on page 58, a film growth rate of $1x10^{-3}$ Å/s is assumed at 25 cm and 75° from the exit plane of the thruster. Also, a film density of 2.2 g/cm^3 is assumed to calculate the mass deposition rates. This gives a mass per unit area rate, $\dot{\rho\tau}$ of $1.9x10^{-6}$ g/cm^2/day. The sensitivities of the different crystals and the resulting frequency change per hour of thruster operation is obtained by applying $\Delta F = \rho\tau S_f$ is shown below.

$$\dot{\Delta F} = \dot{\rho\tau}\begin{bmatrix} 5.7x10^{7} \\ 2.3x10^{8} \\ 5.1x10^{8} \\ 1.4x10^{9} \end{bmatrix} = \begin{bmatrix} 4.5 \\ 18 \\ 40 \\ 110 \end{bmatrix} \text{Hz/hr} \tag{3.1}$$

The optimum crystal frequency for this application nominally depends on the number of hours available for the test. For a test with very limited time available, as for ETEEV, a 25 MHz crystal would be optimal. However, QCM's at this frequency are the most expensive, and the QCM's available from the Air Force are 15 MHz. Given a 15 MHz crystal, ETEEV should ideally operate for at least one day, which would give about 960 Hz change.

Comparing the results from this QCM with those likely to obtained by witness plates, the actual height and mass of the film after 24 hours would be about 86.4 Å and 7.6 μg for a 2 cm x 2 cm sample. This is well below the measurement uncertainty of 500 Å for profilometry and 0.02 mg for an electronic balance. Conversely, 500 Å on a 15 MHz QCM corresponds to about a 5.6 kHz change in crystal frequency, which highlights precisely how sensitive QCM's are compared to other methods. Only a QCM has a chance of measuring the actual deposited mass from the Hall thruster on ETEEV.

The PPT presents a completely different picture to the QCM. Unlike a Hall thruster, the maximum deposition from a PPT is close to centerline (<50°). Mass measurements from a LES 8/9 give about 0.0025 μg/cm^2-pulse at 30° and 24 cm from the PPT exit.[30] This corresponds to a $\dot{\rho\tau}$ of about 4.75x10^{-4} g/cm^2/day, 250 times greater than from a Hall thruster! For the 15 MHz crystal this would give 2.45x10^5 Hz/day during operation, or equivalently almost 1 mg of mass on a sample 2 cm x 2 cm. This level of deposition would flood the QCM, so if the 15 MHz QCM's are used for the PPT they will have to be placed in a lower deposition area.

To see if this intended usage of QCM's is reasonable, compare it to the usage of QCM's on other flight experiments. On the Midcourse Space Experiment, between 8 and 160 Å was measured after 10 months in the wake and at the primary mirror of the spacecraft's telescope, respectively.[41] On ESEX changes as small as 21 Hz were easily distinguishable.[35] So even if ETEEV only operates for few hours the deposition should still be well within typical QCM usage.

Although the data from a QCM can be obtained real-time through telemetry, the interpretation of the does require a lot of post processing. The solar cycle causes a regular change in the QCM frequency, while water dumps or Shuttle thruster firings could cause extra contamination which must be separately accounted for. A detailed history of the Shuttle's movements and any possible effects from nearby experiments will be required for interpreting QCM's on ETEEV. A control QCM which is shielded from ETEEV's thrusters but not from the general Shuttle background could help with this interpretation.

The MK16 QCM is capable of thermogravimetric analysis, or selectively boiling off constituents at different temperatures. Unfortunately boron, a main constituent of the Hall thruster insulation, is not a common material and is not listed in the vapor pressure tables which come with the QCM. However with further research it may be possible to identify the vapor pressures of all possible constituents from ETEEV and the Shuttle bay.

Although the operational time ETEEV will have on the Shuttle will not be enough to get measurable deposition on a witness plate, it may be possible to get useful compositional measurements using post-flight spectroscopy. This idea is reinforced by the fact that researchers at Lockheed claim to get useful results from witness plates exposed to their Hall thruster in a few hours. Careful contamination avoidance procedures will be required to protect the plates at all stages of integration with the Shuttle.

Despite the limitations on deposition measurements, witness plates are very useful for measuring Hall thruster erosion in the mid- and main plume regions. An erosion rate of about 360 Å/hr is expected for quartz samples at 25 cm and 45°, which will be easily measurable with a profilometer. Silver is an especially good material candidate for reliable erosion measurements in the limited time available for ETEEV operations as it erodes even more quickly than quartz. Since there is a good chance for useful data and witness plates are cheap and easy to add to the experiment in quantity, ETEEV will have plates of several different materials collocated with the RPA's and the QCM's.

3.7.2 Langmuir Probe Analysis

When multiple Langmuir probes are used together, they must be placed far enough apart so that they don't interact electrically. Usually, a spacing of the order on some number of Debye lengths, such as 5 to 10, is considered sufficient. Figure 3.6. shows the plume Debye length at 10 cm and 25 cm from the 200 W Hall thruster exit plane and for two estimated electron temperatures, using Pencil's plume model (1996) and the formula for Debye length

$$\lambda_d = \sqrt{\frac{\varepsilon_0 kT}{ne^2}} \tag{3.2}$$

From this plot, one can see that while probes could be spaced just a millimeter or two apart in the center of the beam, to measure near the backplane the probes would have to be almost a centimeter apart to guarantee electrical isolation. Unfortunately, this doesn't allow for very good spatial resolution on a linearly spaced triple probe. A compromise

probe which could measure from the center out to about 50° could have a probe spacing of 3-5 mm.

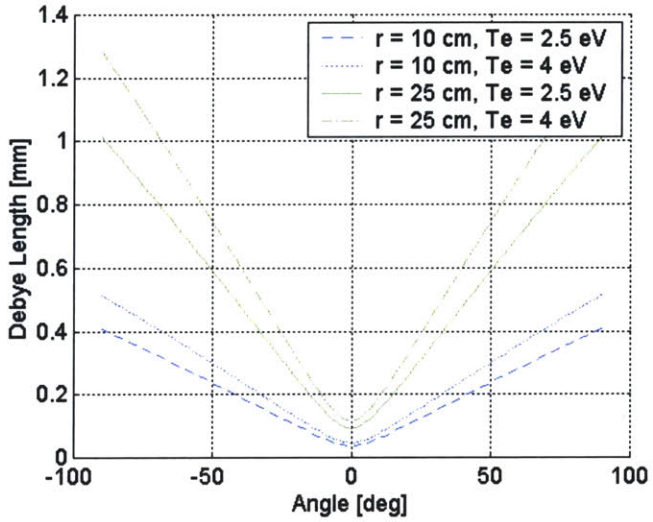

Figure 3.6. Plume Deybe Length

There are two possible configurations for a triple probe, linear and bundled, shown in the sketch below. It is clear that for a given probe separation d, the bundle has the smallest overall dimension *l*, which means the smallest impact on the plasma.

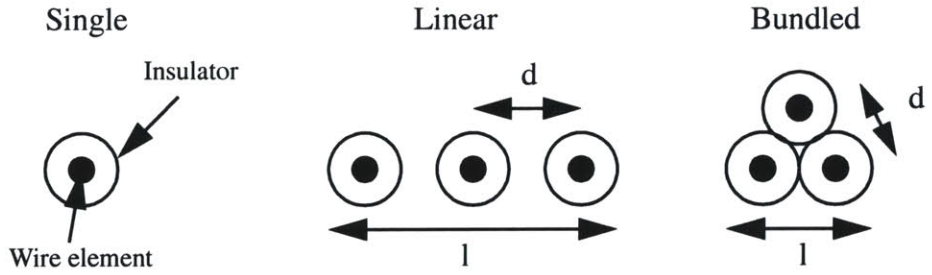

Figure 3.7. Triple Probe Configurations

Obviously, a single probe by itself has the least impact on the plasma and the best spatial resolution.

Using the analysis presented in Mike Fife's thesis (1998) for the current to a probe in a flowing plasma, estimates for the current to be received by probes in the plume of Busek's 200 W Hall thruster were made to allow sizing of the probe current-collecting elements and ammeter. The plot below shows an I-V profile for a probe 3mm long and 0.4 mm in diameter, for a number density of 10^{15} m^{-3} which occurs in the plume near 25 cm and 45°.

The results indicate that for a probe of this size currents of 1 to 500 μA can be expected. The spreadsheet with these calculations is in Appendix B.

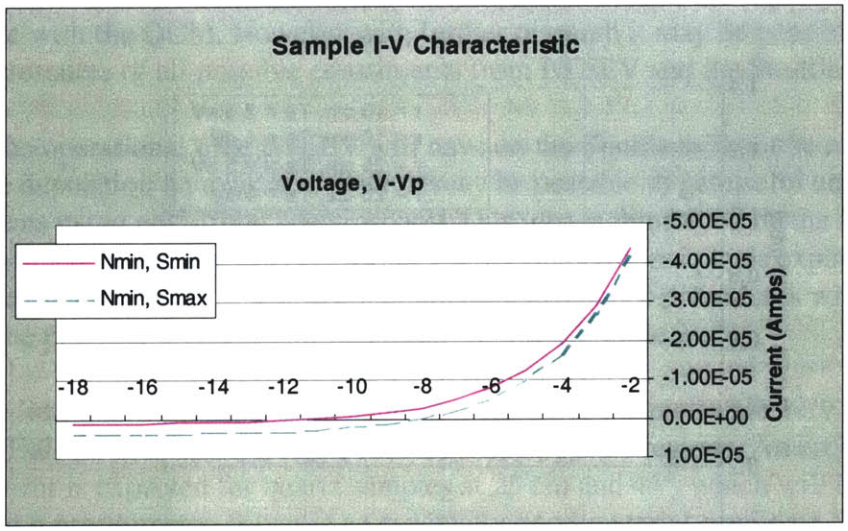

Figure 3.8. Sample Langmuir Characteristic for 200 W Thruster

Considering the physical layouts and required electronics of these probes, there are trades to be made between different types of Langmuir probes.

A single probe must be swept in voltage to produce a current vs. voltage (I-V) profile, which is then analyzed to determine the electron temperature and plasma potential. The profile must be corrected based on the spacecraft's potential, but if this is known the data analysis is considered simple but time-consuming. Although it is possible to mostly automate this data reduction, inspection of each characteristic is required to ensure that the correct regions of the I-V characteristic are used for calculating the plasma parameters. This essentially prevents real-time knowledge of the plasma parameters during probe operation. Other advantages however are that a swept single probe provides the most information about the shape of the electron distribution function of any Langmuir probe configuration, and since a single probe is easy to duplicate, redundancy is easy too.

A triple probe configuration allows each probe to be maintained at a fixed voltage, which allows for simpler electronics and operation and allows the triple probe to avoid being dependent on the Shuttle's potential. Also Newton's method, used to solve the three equations for the selected points of the characteristic, is very fast and may be done on the flight computer for real-time knowledge of the plasma properties. However the triple probe is physically larger, which has two consequences: disturbing the plasma more and having a lower spatial resolution. All three probes must operate reliably for useful data to be obtained, which introduces risk to the instrument since only one of the probes needs to be irreparably contaminated for measurements to be ruined. Also, triple probe theory was developed for stationary plasmas, and applying it to a rapidly flowing plasma such as a thruster plume introduces issues of theoretical correctness. Attempts have been made to

extend the theory to flowing plasmas, but as mentioned in Section 2 there is no universal method of interpreting the characteristic in this case.

The final determination between swept single probes and triple probes for ETEEV is expected to be made only after extensive testing of both types of probes on the ground. However a Langmuir probe of the chosen type will be swept through the plume out to about 50°.

3.7.3 Faraday Cup Analysis

Traditional planar Faraday probes with a negatively biased guard place a large electrically disturbing surface directly in the plasma. A more Faraday cup-like configuration is similar to a retarding potential analyzer, but without the retarding grid. The entire assembly is inside a metal cage which is allowed to float to minimize impact on the plasma. Inside this cage, a grid with a negative potential collects secondary electrons while a plate below it, biased a few volts more negative than the grid, repels electrons and collects ions. The two configurations are compared below.

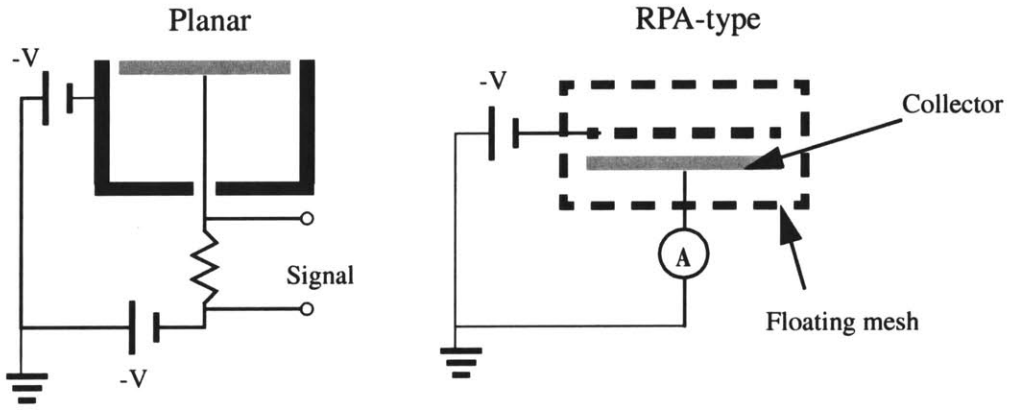

Figure 3.9. Possible Faraday probe schematics

The RPA-type has more complicated construction, but can have the least impact on the plasma. Considering the small plume dimensions of the 200-W Hall thruster, small size and low impact are both key requirements for the instrumentation. A third possible configuration would be a planar probe with a guard ring in front to minimize edge effects and a coating of ceramic on the back to protect the probe from stray current.

To determine the appropriate size for the current collector, values of the current density as estimated using Pencil's model in "Expected plasma parameters" on page 58 were used. The angle at which 95% of the beam current is contained is about 35°, and the current density at this angle at a distance of 25 cm is about 0.16 mA/cm^2. The current density in the center of the beam at the same distance is 3.3 mA/cm^2. Being conservative, this gives a range of 0.1 to 5 mA/cm^2 that the Faraday cup should comfortably measure.

So, depending on the capabilities of the ammeter to be used for the measurement and the region of the plume to be tested, a minimum size collector area can be determined. Ten microamperes is a reasonable minimum current, which gives a minimum area of just 6.25 mm^2, or a disk of diameter 3 mm. Since the Debye length at 35° and 25 cm is about 0.5 mm, a disk this small is not quite large enough to appear planar to the plasma, although it is large enough to collect a reasonable current. A disk of about 1 cm in diameter makes more sense, and is more comparable to the sizes used in other experiments, but scaled down to our thruster (see "Hall and PPT Research Overview Spreadsheets" on page 113 for descriptions of some other Faraday probes).

For ETEEV, it may be desirable to sweep past 35° and obtain the full current density profile, as it can then be compared against the results from collimated and uncollimated Faraday probes on the ground. A probe 1 cm in diameter would collect about 25 μA of current at 90°, and is about ten times the size of the local Debye length, so this size is still a good choice.

The configuration of the Faraday probe for ETEEV will be determined by the results of ground testing. The simplest planar designs will be compared against those with a protective floating shell. The mechanical robustness of the design will be important for the flight instrument, which may eliminate designs with guard rings as the necessary structural support may make the probe too large for the desired spatial resolution. The required dimension of 1 cm for the collector is already somewhat limiting without yet being complicated by additional structures.

3.7.4 RPA Analysis

RPA development for ETEEV is taking place at WPI. These instruments can be made very light and small, as in the RPA for Stentor, where the Langmuir probe and RPA together weight only 400 g. There is a flight heritage for them including Deep Space 1 and they are planned on future missions including SMART 1.

Although the RPA from WPI will be designed for PPT plumes, changing the repelling grids should be sufficient to make them appropriate for the Hall thruster as well. The rough specifications of the grids required for the Hall thruster at divergence angles around 45°, where the Debye length is about 0.6 mm, are an open fraction of 0.8, a wire diameter of 0.13 mm, and a wire spacing of 1.5 mm. The total RPA grid transmittance is determined by the number and orientation of the grids and should be calibrated experimentally.

3.7.5 DIDM

The Digital Ion Drift Meter[6], or DIDM, primarily measures ion drift velocity. In so doing it also measures the ion density and temperature. The component of the velocity perpendicular to the meter is determined by imaging the particle distribution; this is the drift meter function. The component normal to the meter is measured with a spherical RPA function. DIDM has drift meter rates of up to 16 Hz and RPA sweep rates of up to 8 Hz. The resolution of the drift meter is less than 1 degree. The instrument weighs less than 5

pounds and uses 5 W when powered. DIDM's specifications are for ion densities up to 10^{12} m^{-3} and energies up to 5 eV.

The DIDM also has a Langmuir probe integrated with the meter as errors in the knowledge of the local potential produce large errors in the measured drift velocity. DIDM already has a flight heritage, it flew on the German spacecraft Challenging Minisatellite Payload (CHAMP), which launched on July 15, 2000. The next generation of DIDM is scheduled to fly in 2003. Sample images from the CHAMP flight are shown below.

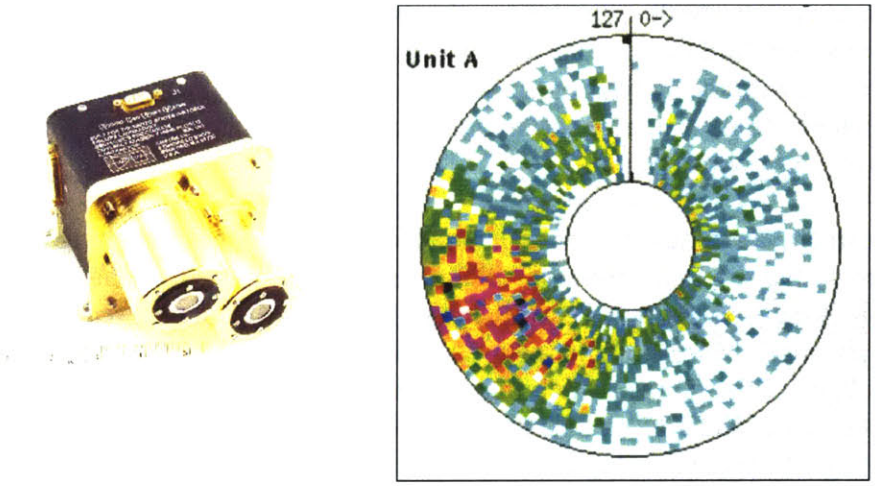

Figure 3.10. DIDM together with a sample ion velocity distribution image

On ETEEV, DIDM has to be placed in the backplane and pointed away from the thruster plumes so that it is not bombarded with high energy ions. It will be used to characterize the Shuttle background plasma environment and possibly the Shuttle floating potential.

3.7.6 Thrust balance

The thrust balance for ETEEV would be developed at Draper lab. This instrument provides quite a design challenge, as traditional balance designs depend on gravity, an obvious drawback, and thin flexures which could prove a safety hazard on the Shuttle. The ETEEV balance must have the capability to lock down safely to withstand launch and landing loads, to be robust mechanically while unlocked to expected disturbances in the Shuttle environment, to be recalibrated in-situ, and to detect 10 mN of thrust with an accuracy of about 0.1 mN. The Shuttle microgravity environment, such as the timing of attitude control thruster firings, must be monitored closely during operation so that measurements can be taken from the quietest periods.

These design issues and the financial resources required to develop a balance which solves them have kept thrust measurements as a secondary objective for ETEEV.

3.7.7 Additional instruments under consideration

There is a possibility that a Neutral Particle Flux probe will be added to the suite of Hall thruster diagnostics, courtesy of Alec Gallimore. It would need to be placed in the back-plane unless is could be miniaturized for the mid- or main plume.

An emissive probe may be a better choice to measure the plasma potential than the Langmuir probe. This decision will be made based on the ground tests of the Langmuir probes.

A magnetic spectrometer such as may be used on TechSat 21's diagnostics package would be a good alternative to the prohibitively large time-of-flight spectrometer. The significant development required to make such an instrument ready for a flight in a few years cannot be undertaken with the student resources currently available, however should a magnetic spectrometer become available through the course of TechSat 21's development, it would be given serious consideration.

Various camera combinations are under consideration for photographing the plume or analyzing the plume's optical emissions. Photos of the plume farfield shape would be correlated with models which may be available in-house at MIT in two years pending an AFOSR proposal. More study is required to determine the practicality of studying any emission lines of the plume, which may provide information on the composition of the plume in terms of Xe, Xe^{+} and Xe^{2+}. Regardless of whether any cameras are added to the ETEEV payload, full advantage will be taken of the Shuttle's onboard camera system whenever possible, including photos taken by the astronauts from the middeck.

3.8. ETEEV Diagnostics Package

Table 3.2. lists the instruments currently planned for ETEEV by the thruster for which they will be used. There will only be one background Langmuir probe which may be part of DIDM.

Table 3.2. ETEEV Diagnostics

Thruster	Instrument	Quan.	Location
Hall	Faraday	1	Arm, r = 25 cm, swept out to 60°
	Langmuir	1	
	RPA	3	Hard-mounted at θ = 30°, 45°, and 60°, r = 25 cm
	QCM	2-3	Pallet, θ = 70°-90°, r = 10, 20, 30 cm
	Witness plates	3-5	Collocated with QCM's and RPA's
	Thrust balance	1	Pallet

Table 3.2. ETEEV Diagnostics

Thruster	Instrument	Quan.	Location
Hall/PPT	DIDM[a]	1	Pallet, pointing away from thruster plumes, location TBD
	Spherical Langmuir[a]	1	
	QCM[a]	1	
	Cameras	?	Payload bay, middeck
PPT	Quadruple Langmuir or RPA	1	Arm, r = 10 cm
	Triple Langmuir	1	
	QCM	1-2	Pallet, 90°, r TBD
	Witness plates	?	?

a. for characterizing the Shuttle background environment, including contamination and floating potential

Below, desired measurements are matrixed with the instruments which may perform them. Those that may be a backup to another instrument are indicated, as is whether the measurement meets a primary or secondary objective. Shuttle background measurements are not included.

Table 3.3. Instrumentation Matrix[a]

Measurement / Instrument	Deposition	Erosion	Ion Density	Electron Temperature	Plasma Potential	Ion Energy	Current Density	Neutral flux	Shuttle background	Optical emissions	Farfield plume shape	Thrust	Operating mode
QCM	1								2				
Witness plates	2	1											
Langmuir probe			1	1	2				2				
Emissive probe					1								
RPA						1	2						
Faraday probe							1						
NPF								3					

Table 3.3. Instrumentation Matrix[a]

Measurement / Instrument	Deposition	Erosion	Ion Density	Electron Temperature	Plasma Potential	Ion Energy	Current Density	Neutral flux	Shuttle background	Optical emissions	Farfield plume shape	Thrust	Operating mode
DIDM									1				
CCD w/filter										3			
Shuttle cameras											3		
Thrust Balance												3	
Color video													3

a. Key: 1, primary objective; 2, backup measurement capability; 3, secondary objective.

The specifications which have been determined for the Hall thruster diagnostics are listed in the table below.

Table 3.4. Hall thruster diagnostic specifications

Instrument		Range	Resolution	Comments
RPA	j	0.3 to 0.05 mA/cm^2	0.005 mA/cm^2	Miniaturized
	E	1-600 V	1 V	
QCM	$\dot{\delta}$	0.7 to 7 Å/hr	0.5 Å	
Witness plates	δ	0 to 5 μm	0.05 μm	Erosion
Faraday probe	j	0.05-10 mA/cm^2	0.02 mA/cm^2	Reject 10 eV electrons
Triple LP	n	10^{14}-10^{16} m^{-3}		λ_d ~0.1-0.6 mm
	T_e	2-5 eV		
	ϕ	20 V		
Thrust balance	T	0-20 mN	0.1 mN	In-situ calibration
DIDM	n	0-2x10^{14} m^{-3}		Shuttle back-ground
	j	0-60 μA/cm^2	0.6 μA/cm^2	
	E	0-5 eV		

Detailed instrument specifications have not yet been determined for the PPT.

3.9. Configurations and budgets

The final configuration of ETEEV has not been determined since certain ground tests to characterize the thrusters are required to determine the best placement for some instruments. Two recent concepts as developed in ProEngineer by Andrew Suryali (WPI), the student researcher responsible for the mechanical design of ETEEV, are shown below.

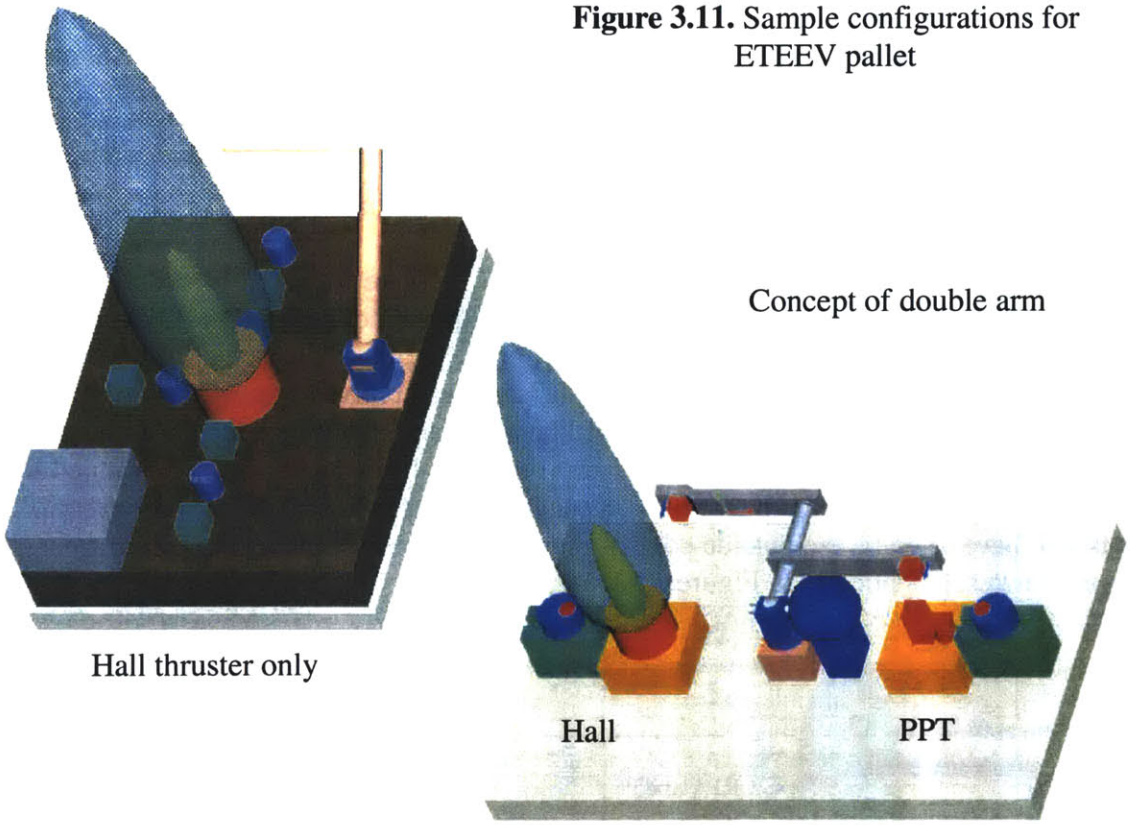

Figure 3.11. Sample configurations for ETEEV pallet

The idea of using a Hitchhiker canister with a motorized door was considered but quickly discounted. The thruster would have to be mounted at the top of the canister so the plume would not impinge on the canister walls and this leaves no room for the placement of diagnostics at any substantial distance from the exit plane. It was briefly considered that the Shuttle robot arm could be used to move diagnostics through a thruster mounted at the end of a canister, but apparently the arm has never previously been used for a Hitchhiker mission. Therefore it would not be feasible to use it for a small university payload. In addition, the positional accuracy of the arm is unlikely to meet the requirements of ETEEV. This leaves the possibility of a side plate or a single or double bay pallet. A side plate was considered but the required orientation of the thruster so that the plume travels away from the Shuttle and any other nearby experiments would be different depending on where the pallet was located in the payload bay, introducing unnecessary complexity. With the current

concept of two thrusters and their related diagnostics mounted together on one pallet, the logical choice is the double bay pallet for the cross-bay bridge, which is 33" wide and 55" long. Three-dimensionally, the height of the package mounted on the pallet is limited by the vertical distance to the bay doors.

In terms of mounting the diagnostics to the pallet, both translating, rotating, and fixed mounts have been considered. At issue is the mechanical robustness in terms of surviving launch and landing loads, and the risk of having any moving mechanism get stuck in one position, which would result in failure to get the full data matrix desired. The bearing on a rotating arm would be required to survive the applied loads without failure in all possible configurations. Instruments translating on tracks might be better in that regard. A fixed rake of instruments would be the simplest mechanically but the most complex in terms of the number of instruments to be constructed and the electronics needed to operate them all; it is also the most redundant. Instruments that have some capability for movement allow more of the plume volume to be covered with just one or two instruments. It may be possible to sweep at two different radii if an arm is used. Lastly, the plume must be swept with a current sensor to fully characterize the thruster performance (efficiency).

The current ETEEV configuration concept is a compromise between the rotating arm and hard-mounted instruments. The Hall suite will include hard-mounted RPA's, QCM's, and witness plates, and arm-mounted LP and Faraday probes. The PPT suite will put a triple Langmuir probe and either an RPA or quadruple Langmuir probe on the arm pending further tests, while the remaining diagnostics will be hard-mounted. Since the hard-mounted instruments will be at different angles and radial distances from the plume, but arranged so as not to block each other, there will be a "bleachers" effect on the pallet. These instruments will have to be on the outside edge of the pallet, outside of the sweep of the arm. This is shown schematically in Figure 3.12.

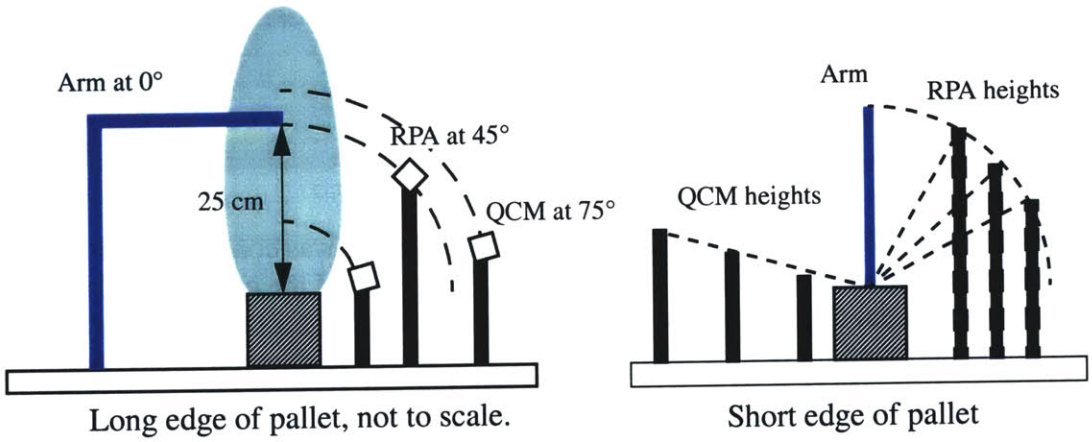

Figure 3.12. Representative spacing of hard-mounted instruments on pallet.

Besides the mechanical issues of moving parts, there are issues with placing essentially two different experiments on one pallet. The PPT and Hall thruster are very different as

outlined previously, and there is really no overlap in the measurements required for each. However if the experiments were on two different pallets they might be harder to manifest, and potentially one might fly and not the other. Therefore it was decided to keep the two thrusters together on one pallet and to share electronics and thermal hardware wherever possible to reduce overall weight and complexity. An arm has been developed which has two cross-pieces, one for each thruster, as shown in Figure 3.11. The cross-pieces are at different heights from the respective thrusters' exit planes. A barrier between the thrusters was considered but it could impinge the plume backflow and cause sputtering. Therefore contamination between the two thrusters will be managed operationally and possibly by using shutters on sensitive instruments like the witness plates. Any shutter will require a simple design and minimizing the number of times shutter must operate to reduce the failure risk.

The table below shows rough estimates of the masses of the ETEEV subsystems and diagnostics. Some subsystems have needed components listed even if there is no mass estimate available yet. The experiment will be well below the rated capacity of the pallet.

Table 3.5. Mass Estimates, lbs.

Subsystem	Component	Mass	Total
Hall thruster	Thruster	3	20
	PPU	10	
	Flow system	7	
PPT	Thruster	3	15
	PPU	12	
Computer	--	5	5
Arm	--	5	5
Thermal	Heaters	1	5
	Blankets	1	
	Heat pipes	1	
	Radiator	2	
Structural	--	5	5

Table 3.5. Mass Estimates, lbs.

Subsystem	Component	Mass	Total
Diagnostics	QCM's	1	20
	Langmuir's	1	
	Faraday's	1	
	Witness plates	1	
	RPA's	1	
	DIDM	5	
	Thrust balance	10	
Total			75

3.10. Operations

On any Shuttle mission, there are many constraints to be considered in the operations of the payloads. In the case of ETEEV there are many of these constraints, outlined below:

1. All experiments should take place as late in the Shuttle mission as possible for the lowest outgassing products contamination.
2. In general, ETEEV should be in the Shuttle wake for all data acquisition, although it might be instructive to operate the thrusters and some instruments in other Shuttle attitudes.
3. With no barrier between the two thrusters, possible interactions between them must be managed operationally. This will be accomplished by running the Hall thruster tests first, then the PPT tests second to keep teflon products from contaminating the instruments.
4. During thruster operation it will be important to avoid or at least track Shuttle water dumps and attitude control burns. Water could collect on the QCM's and witness plates, and Shuttle thruster firings and other disturbances will affect the thruster performance data.
5. ETEEV needs to be manifested with experiments that won't be affected by the thruster products, either experiments that run before ETEEV does or those in closed canisters. It should be noted that the plumes will be quite small, with an estimated distance of 0.5 m around the Hall thruster before plasma reaches Shuttle ambient levels.

Given these constraints, an important question to ask during the manifesting process is what is longest solid block of time ETEEV can have for undisturbed thruster operation? And, what is the total operating time each thruster can expect? Any start-up and shut-down time of the thrusters must be taken into consideration. For example, SPIRET expects to operate on the Shuttle in 6 one-hour segments. This means that the thruster must start up

and shut down six times. Any problems in start-up or shut-down could severely impact their overall operating time.

The main operational phases of ETEEV are outlined below.

1. Shuttle checkout phase: obtain control data on Shuttle background with LP, QCM, and DIDM before beginning thruster firings.
2. Unlock and calibrate the thrust balance.
3. Run the Hall performance test matrix, sweeping the arm several times for each setting. This test matrix should take at least two hours as the thruster must be allowed about 10 minutes to reach equilibrium before testing at each point.

Table 3.6. Hall thruster performance test matrix

	1	2	3	4	5	6
Main Flow (mg/s)	0.7	0.5	0.5	0.9	0.9	0.7
Power (W)	200	145	200	250	200	200
Discharge Voltage (V)	300	300	350	300	230	300
Discharge Current (A)	0.66	0.48	0.6	0.83	0.85	0.66
Magnet Current (I)	0.43	0.33	0.29	0.65	0.56	0.43

4. Stow the arm and lock the thrust balance. If necessary, unshutter the Hall contamination instruments, and begin the nominal Hall thruster operation phase. This phase should last as long as possible, preferably a day or more.
5. Shut down the Hall thruster and, if necessary, shutter the Hall contamination instruments.
6. Run the PPT performance matrix, which will include discharge energies of 5 - 20 J at an undetermined matrix. Sweep the arm several times at each setting. This test should lasts a couple hours.
7. Stow the arm, unshutter the PPT contamination instruments and begin the nominal PPT operation phase. This phase will last several hours but not a whole day.
8. Shutter the PPT contamination instruments, shut down the PPT, and perform any steps necessary to prepare for landing.

ETEEV will also include full pre- and post-flight testing. This testing will probably take place at the University of Michigan, which has very large vacuum facilities. This testing will duplicate the plasma diagnostic and witness plate measurements, although it may not

be possible to completely duplicate the QCM measurements as only a few QCM's are available, and they may need to be saved for the Shuttle flight. These duplicate measurements will help to pinpoint any differences between the space and ground data. Also, some measurements can be taken with facility mitigation techniques, such as collimators for the witness plates and Faraday cup, to help confirm their utility at mimicking true vacuum conditions.

Section 4.0. Ground Experiments

4.1. Introduction

This chapter will review the ground experiments planned in preparation for the shuttle flight. The new facility known as the Micropropulsion Lab is discussed. The instruments used, including a thrust balance, are described.

4.2. MicroPropulsion Lab

The MicroPropulsion Lab is the name given to the room containing two new vacuum chambers for propulsion research. One chamber (MiniVac) is very small, only 6" in diameter, and is designed for use with colloid thrusters. The second chamber (AstroVac II) is medium-sized, about 1.4 m in diameter, and is for use with Hall thrusters and other similar ion devices. This room was until recently used for a variety of small projects and significant overhaul of the room was required for easy and safe operation of the chambers, and to provide space for assembling mechanical and electrical components.

The following systems were required to operate the AstroVac facility:

1. Water manifold, valves, and lines to provide cooling water to the cryopumps and to the chamber
2. Nitrogen flow system for automatically purging the larger cryopump
3. Power supplies and rack to run the Busek thruster and cathode
4. Xenon flow system for the thruster, including a pressure regulator, two flowmeters, and the lines
5. Helium-based leak detector
6. Heat- and ion-removing louvered plate inside the chamber
7. Computer and input card to obtain instrument signals in LabView and control items like QCM's and a step motor for moving instruments using their own software

In addition, the lab had to be cleaned up to allow room for a soldering and shrink-tube station and a machining (primarily drilling) station. One lab bench had to be rewired for power.

An inverted-pendulum thrust balance is a permanent part of the facility. This balance was built for the use of Ph.D. candidate Vadim Khayms and used in an older vacuum tank. It is discussed in detail below (see "Thrust Balance" on page 84).

4.2.1 Vacuum chamber

The AstroVac chamber is a large cylinder 1.4 m in diameter and 1.6 m long, with two cryogenic pumps which produce a combined pumping speed of 7000 L/s of Xe. The

chamber is equipped with heaters so that it may be baked to 300°F to remove contaminants.

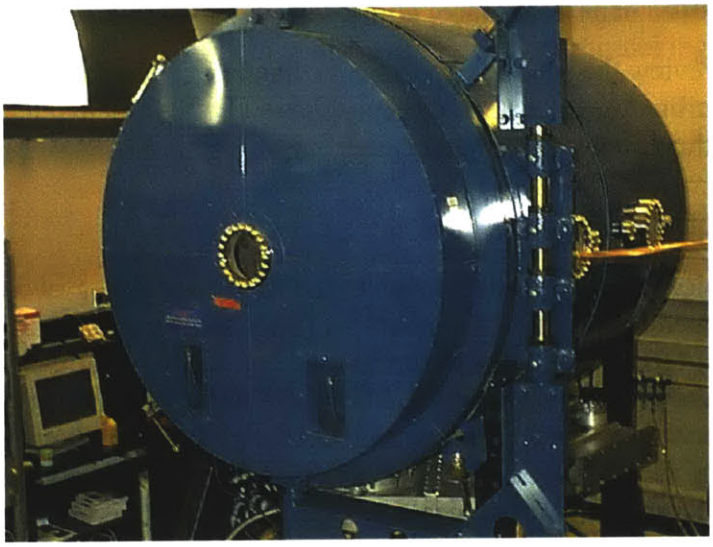

Figure 4.1. AstroVac II

The chamber is instrumented with a thermocouple for pressures in the range of 2 to $1x10^{-3}$ Torr and a cold cathode gage for pressures 10^{-3} to 10^{-8} Torr. The cold cathode gage is calibrated for nitrogen, so the measured chamber pressure must be converted to an equivalent pressure for Xenon when the thruster is running. This is done using a conversion factor. The factor most often used for Xenon, according to the manual from Varian, is 2.9.

$$P_{Xe} = \frac{P_{N2}}{2.9} = 0.35P_{N2} \tag{4.1}$$

When clean, the chamber roughs out to 50 mTorr with the mechanical pump in about 20 minutes and reaches a pressure of less than $1x10^{-6}$ Torr (N_2) in about 10 minutes of combined cryopump operation. This allows the chamber to be turned around rapidly should venting be required during an experiment. During regular thruster operation with 0.7 mg/s of main thruster flow the chamber is expected to achieve a minimum pressure of $2x10^{-5}$ Torr (Xe).

AstroVac has six windows, one door, 4 medium ports, and 8 small ports. Six of the small ports are required for water or Xenon flow, leaving the rest for instrumentation and power.

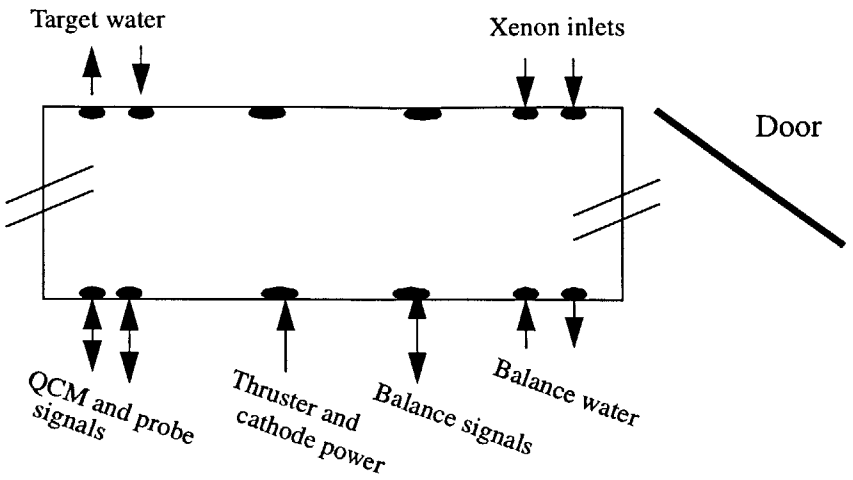

Figure 4.2. Schematic of vacuum chamber ports

4.2.2 Cooling Plate

When the vacuum chamber was designed, the heat load of the thrusters was not properly considered. Indeed, the chamber is well insulated to allow for baking it. Therefore, after the chamber was installed at MIT, an additional cooling mechanism was designed which can remove the heat load of the 200 W Hall thruster. This took the form of a cooling plate which also serves a second purpose: to catch the sputtered materials in the thruster plume and keep them from dirtying the chamber walls and windows.The plate, dubbed the "target" as the thruster plume will be aimed directly at it, was designed with louvers on the front and the cooling passages on the back (Figure 4.4. on page 80). This louver pattern is known as a "chevron". The resulting target is a meter in diameter and about 12 cm thick from the back plate to the chevron rim.

The target is made of aluminum to minimize cost and weight while achieving reasonable thermal conduction from the chevron to the cooling passages. Low weight was important to make the target manageable to work on and install. However the choice of aluminum as the construction material required that aluminum tubing be used for the cooling passages, as aluminum can only be welded to aluminum. The tubing then required careful stitch welding to the back plate, which was done by Atomic, Ltd. and leak tested to 100 psi.

The target was painted with black aerospace enamel donated by Busek. Busek found that this enamel holds up very well under the impingement of thruster plumes, and it prevents

sputtering of the target aluminum. It also has good thermal conduction to help transfer the plume heat to the aluminum chevron.

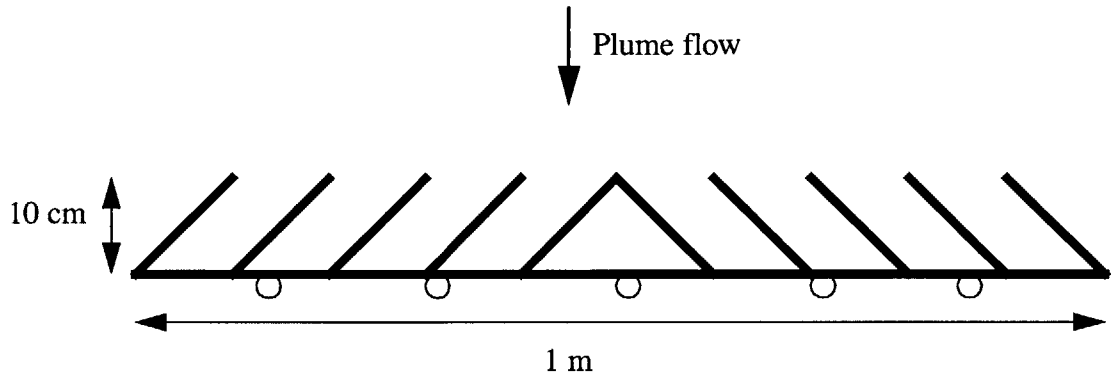

Figure 4.3. Chevron Design

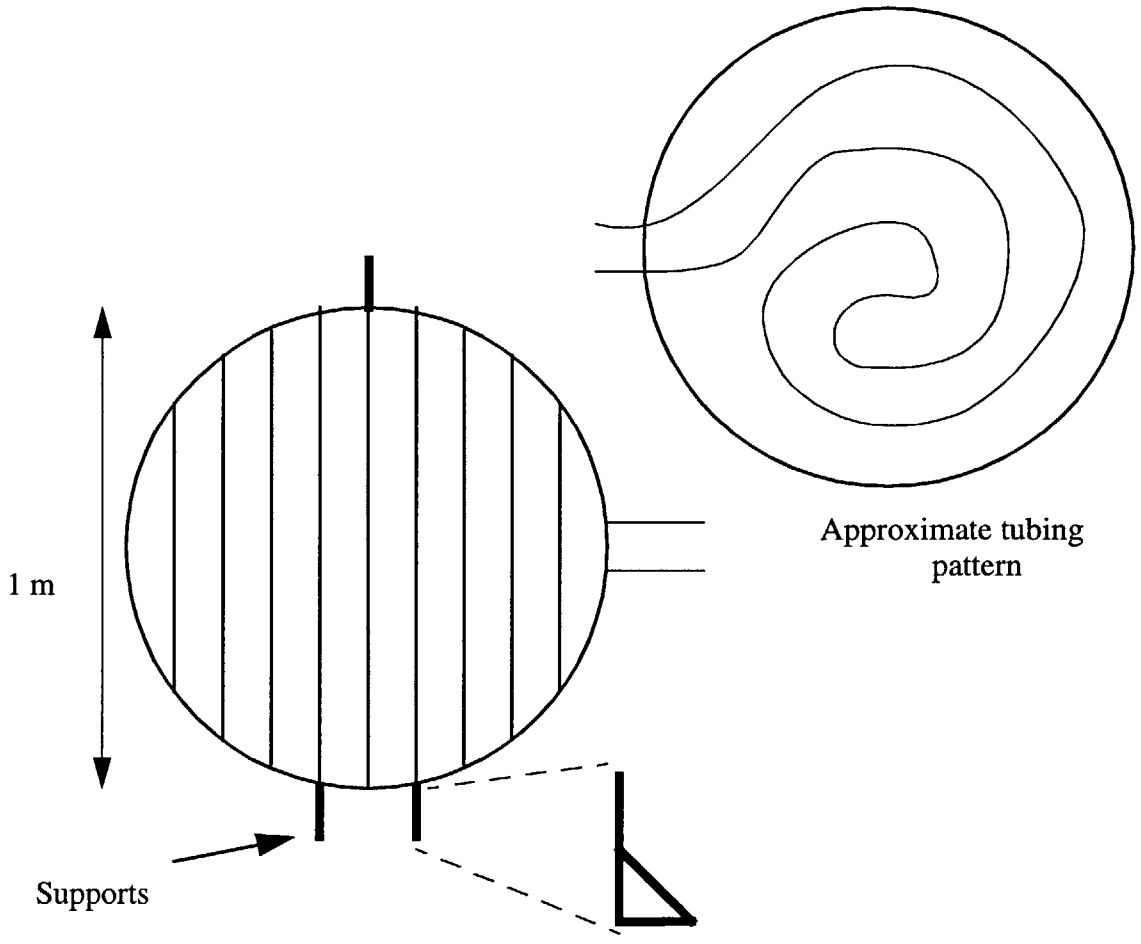

Figure 4.4. Chevron Front and Back Views

After the target was installed in the chamber, it was leak-tested by injecting helium into the cooling passages. The leak rate of helium into the chamber was found to be less than $1x10^{-8}$ cc/sec, which is acceptable.

4.2.3 Mechanical Arm

Some means is required to sample a large volume of the plume automatically. There are two ways to do this, either the thruster or the probes can be moved, and both are done in practice. It is not feasible to move the thruster in AstroVac since the chamber is not large enough to accommodate the plume for a variety of thruster angles. Stacked linear translators may be used to move probes, but they are very expensive and tend to have small travels as associated with optical alignments. Therefore it was decided to build a single degree-of-freedom swinging arm which can be manually adjusted to sweep the plume at different radii.

There are several constraints on the arm design. The arm must disrupt the plasma as little as possible, requiring a slim design and some radial spacing between the probes and the arm crosspiece supporting them. The motor must be able to operate reliably in vacuum. A high positional accuracy is desired so that the arm does not introduce unnecessary uncertainty to the plasma measurements. Vertical adjustment capability is necessary to line up the probes with the thruster exit. The pivot point of the arm must be aligned with the thruster exit plane, requiring the arm base to be located above or below the thruster. Specifications and a concept sketch are shown below..

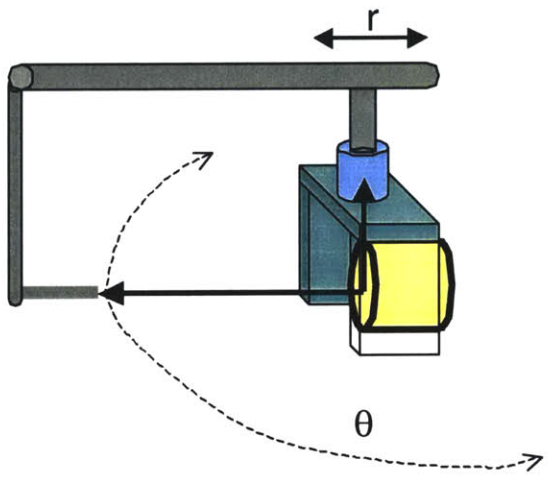

Figure 4.5. Mechanical arm concept

Table 4.1. Mechanical Arm Specifications

Angular accuracy	0.25°
Positional accuracy at 25 cm	1 mm
Vertical alignment	1 mm

Table 4.1. Mechanical Arm Specifications

Angular range	-90° to +90°
Radial range	10 to 50 cm

Stainless steel tubing was selected so that it would be easy to weld the joints. Tubing 1" in diameter and 1/16" thick, and 3/4" diameter and 1/16" thick, were selected for the arm and crosspiece.

Having determined that there will be no gears for the arm, the hardest part of the design is connection of the arm to the motor shaft. The connection must not create any errors in alignment. The arm will slide through this connection and be held in place with a set screw. Along with this connection a homing sensor is required to define zero. This sensor, possibly an optical encoder, should be in the middle of the travel so the arm goes through it often.

The motor selected is a 0.9 degree, 84 oz-in stepping motor from The Motion Group, Inc. with a controller which achieves quarter-step accuracy. The motor is model 5609M and the controller is a SID 2.0. The motor is commanded from a PC computer using a serial cable and QuickBasic.

The motor for the mechanical arm has been tested with the lab laptop. The motor successfully runs a self test when connected to the computer. Further plans for the arm include construction of the arm body and full tests of the arm in the lab but not under vacuum.

A motor of the same model with refurbished bearings more appropriate for use in vacuum has been ordered. These bearings will have powdered molybdenum-disulfide lubricant. Once the arm is completed and tested it will be attached to this refurbished motor for operation in the vacuum chamber.

4.2.4 Supporting Electronics

The Busek 200 W Hall thruster and cathode require four lab power supplies to operate. The circuit diagram is shown below. It is important that the supplies be isolated from ground and truly floating.

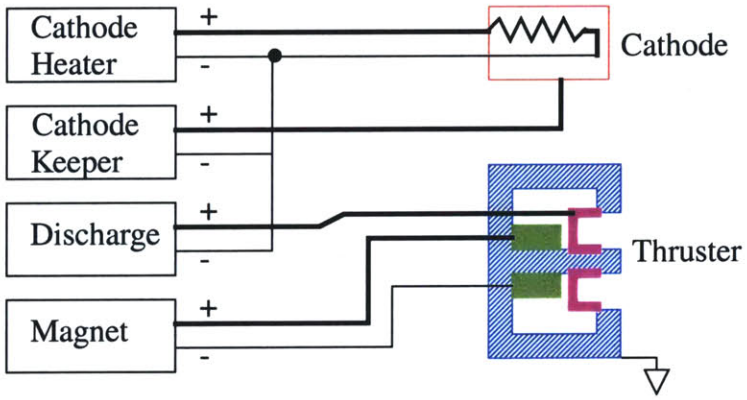

Figure 4.6. Thruster Electrical Circuit Diagram

The power supplies being used for each purpose are shown below.

Table 4.2. Thruster Electronics

Component	Brand	Specs
Cathode Heater	Anders Electronics, Inc.	25 V/10 A
Cathode Keeper	Sorensen	300 V/3.5 A
Main Discharge	Sorensen	600 V/1.7 A
Magnet	Kepco	10 V/10 A

4.2.5 Flow System

The 200 W Hall thruster and the cathode require very low Xenon flow rates, down to one standard cubic centimeter per minute (sccm), which is equal to about 0.1 mg/s. The Propulsion Lab was originally equipped with two Omega FMA1400 electronic mass flowmeters and a control box for them, but these meters are calibrated for Nitrogen and flow rates of 0-20 sccm and 0-200 sccm. One new low flow meter was purchased which was calibrated for Xenon, and after operating both types of meter a second new low flow meter has been ordered. There are many reasons to prefer a new meter: having the meters calibrated for Xenon is important because the accuracy is reduced from 1% of the full scale flow to 4% by the conversion from the Nitrogen calibrated reading to Xenon. The 1400 model meter sometimes cuts off the flow during adjustments, which is troublesome when the thruster is running. The 2400 model has proved easy to use during operation and displays

sccm directly, while the 1400 model displays a percentage of the full scale flow. The equation giving the flow in Xenon in this case, with an example for the 1400 0-200 sccm meter reading 2.5%, is given below.

$$Q = \frac{R}{100} \cdot K \cdot FS = \frac{2.5}{100} \cdot 1.4 \cdot 200 = 7 \text{ sccm (Xe)} \tag{4.2}$$

For now, the FMA 1400 0-200 sccm (N_2) and the FMA2400 0-10 sccm (Xe) meters have been used. A pressure regulator keeps the pressure to the meters at 30-50 psi and 1/4" copper tubing delivers the gases to the thruster and cathode. Valves are installed between the pressure regulator and the flowmeters and between the flowmeters and the vacuum chamber. The nominal thruster flow rate is 7.12 sccm Xe, or 0.7 mg/s, and the nominal cathode flow is 1 sccm Xe, or 0.1 mg/s.

Table 4.3. Flow Meter Specs

Use	Manufacturer	Meter and calibration	Equivalent flow rate of Xe
Cathode Flow	Omega	FMA2400, 0-10 sccm Xe	0-1 mg/s
Main Flow	Omega	FMA1400, 0-200 sccm N_2	0-28 mg/s
Unused - broken	Omega	FMA1400, 0-20 sccm N_2	0-2.8 mg/s
Expected - for Main	Omega	FMA2400, 0-10 sccm Xe	0-1 mg/s

The meters require rezeroing periodically, which requires disconnecting the flow and manually adjusting a potentiometer. The calibration of the meters can be checked using a simple method involving a graduated cylinder immersed in a beaker of water and a stopwatch. Timing the gas as it fills up the graduated cylinder gives an estimate of the full-scale flow for the meter. However, accurate recalibration of the full scale flow requires a measuring standard with 0.25% accuracy.

4.3. Thrust Balance

A previous graduate student, Vadim Khayms, used this thrust balance to test his experimental 50 W Hall thruster. The balance is an inverted-pendulum design of NASA Glenn heritage. This design is the current industry standard for measuring small thrusts. The pendulum consists of a platform supported by four flexures 0.01" thick and a large restraining spring. An LVDT measures the displacement of this platform, which is calibrated into a

thrust measurement. A set of known weights is used for this calibration. This balance will be a semi-permanent fixture in the AstroVac facility.

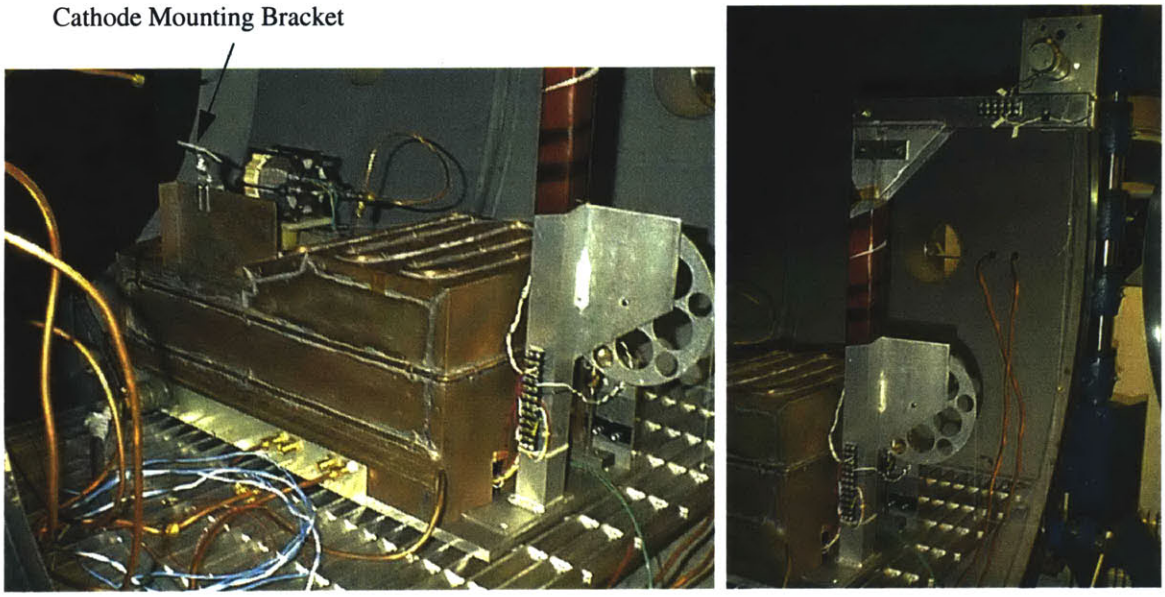

Figure 4.7. Thrust Balance

When AstroVac was delivered, the balance had not been used for over a year, so it was in a state of some disrepair, including missing a number of parts. The balance was revamped with some new plumbing, a new instrumentation and power cable and connections to the controller, a new fiberglass insulating platform, a cathode mounting system, and revised LabView software. Additional modifications are planned, including a set of ribbon cables and plexiglass deck for mounting them, and mounting the cathode directly on the thruster instead of on the balance cover. In the interest of time these final balance modifications were delayed indefinitely.

The balance is a challenging instrument to operate. Details which must be attended to include tuning the damping circuit, calibrating the LVDT and balance reliably, and fixing leaks in the water cooling lines. Also, since the vacuum chamber is not isolated from the lab floor the balance is sensitive to outside disturbances, so these need to be minimized during operation.

Documentation was developed to assist future students in using the balance. This documentation is in Appendix A.

The balance is quite large, taking up almost half the length of the vacuum chamber. This places the thruster near the middle of the chamber, when ideally it should be at one end so

the plume has the largest unimpeded volume possible. The configuration of the thrust balance in the chamber is shown in the pictures above and the schematic below.

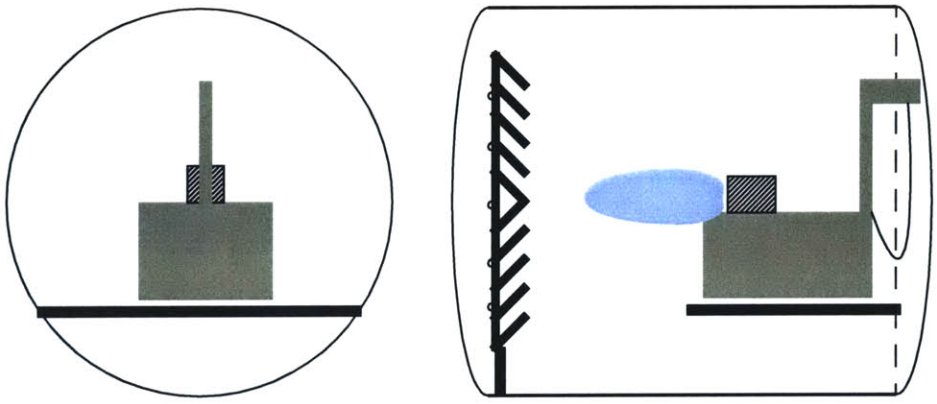

Figure 4.8. Schematic of chamber with thrust balance installed

4.4. Hall thruster operation and chamber checkout

The thruster has been operated successfully in the new chamber. Pressures of 1.97×10^{-5} Torr (corrected for Xe) have been achieved with the main flow at about 0.7 mg/s and a cathode flow of 0.1 mg/s. There are consistently no problems starting the thruster up. This shape, although discernible to the eye, does not show up in pictures taken with an inexpensive digital camera. However, the size of the plume is similar between the pictures and the naked eye. Pictures are shown below of the thruster operating in AstroVac. Plume color varies between purple, blue, and green depending on the voltage and magnetic field applied. These colors are not always true in photos.

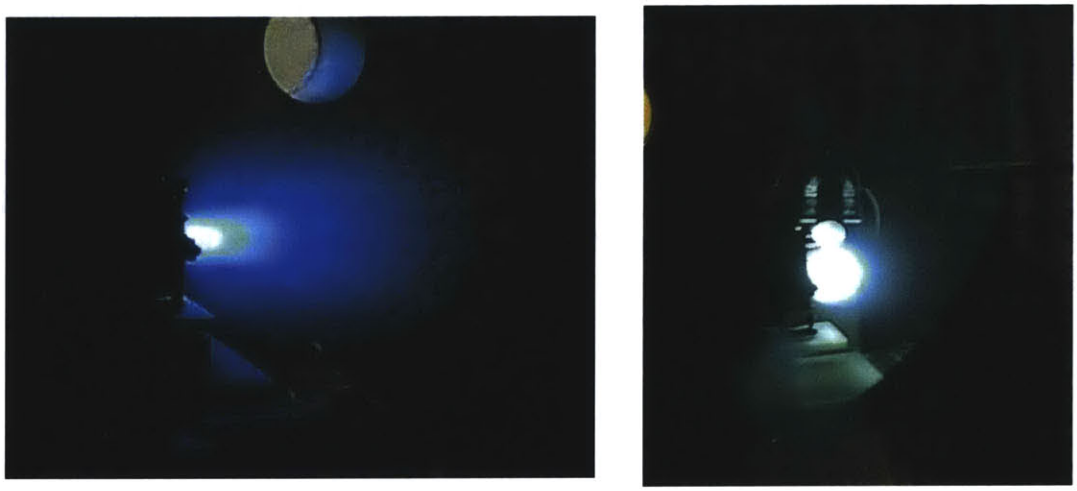

Figure 4.9. Busek 200 W Thruster operating in Astrovac II, low-voltage diffuse glow at right and high-voltage discharge at left.

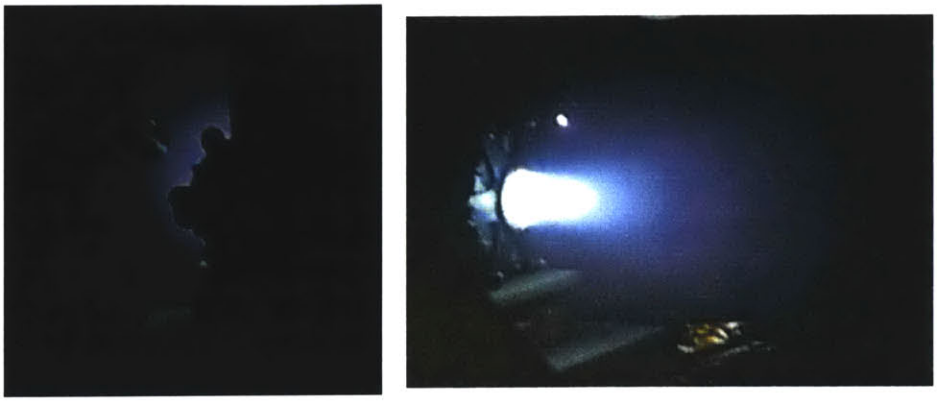

Figure 4.10. Plume size as viewed from behind and the side for a high-voltage discharge. Note that the thruster is ~10 cm in diameter.

Some sample operating conditions noted during operation are given below. Some trends to note are that after start-up the main discharge current tends to fall with time and the keeper voltage rises as this occurs. This is due to conditioning of the thruster surfaces from being exposed to atmospheric conditions for long periods of time. After an hour or two of operation, with appropriately low chamber pressure, the thruster conditions approach nominal as given by Busek. Another note is that the keeper condition of 0.7A is recommended for startup or standby while the 0.2A condition is for long-term operation. Eventually, the keeper can be shut off completely.

Table 4.4. Thruster Operating Conditions

	Main	Keeper	Magnet	Chamber Pressure (Xe)
1	95V/1.5A	13V/0.7A	0.65V/0.18A	3.5×10^{-5} Torr
2	201V/0.92A	15V/0.7A	0.95V/0.3A	3.1×10^{-5}
3	300V/0.7A	11V/0.7A	1.3V/0.37A	2.8×10^{-5}
4	201V/0.6A	17V/0.2A	1.48V/0.4A	2.5×10^{-5}
5	300V/0.48A	21V/0.2A	1.66V/0.4A	2.5×10^{-5}
Nominal	300V/0.65A	8.5V/0.2V	1.67V/0.39A	2.15×10^{-5}

The plume may take on different shapes depending on the chamber pressure. At moderate pressures the plume has a thin pencil-shaped jet, shown below. At low pressures, below 1×10^{-5} Torr, the jet spreads a few diameters downstream into a "swallowtail". Although it

is unlikely this mode can be achieved in Astrovac, this is the mode expected on the Shuttle. The different between these two modes is not believed to affect thruster performance.

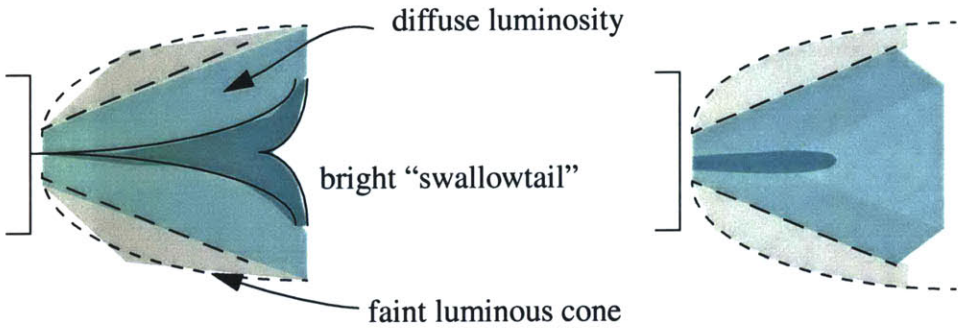

Figure 4.11. Swallowtail plume formation vs. pencil jet

4.5. Testing Plans

4.5.1 Thruster Performance

The goals of the thruster performance testing using the inverted pendulum thrust balance are to learn how to operate the thruster, identify any operating modes based on the background pressure or fine adjustments of the operating parameters, and compare the measured performance to that measured at Busek. Also, use of the balance will aid in finalizing an appropriate matrix of data to be taken during the Shuttle flight. The matrix for ground tests will include a flow range of 0.5-1 mg/s, discharge voltages between 200-400 V, and discharge power between 100 and 300 W. The anode efficiency and thrust will be calculated at each operating point.

The performance data for a similar model thruster as provided by Busek is plotted below. In general the magnet current is increased as much as possible at each point for maximum performance without instabilities.

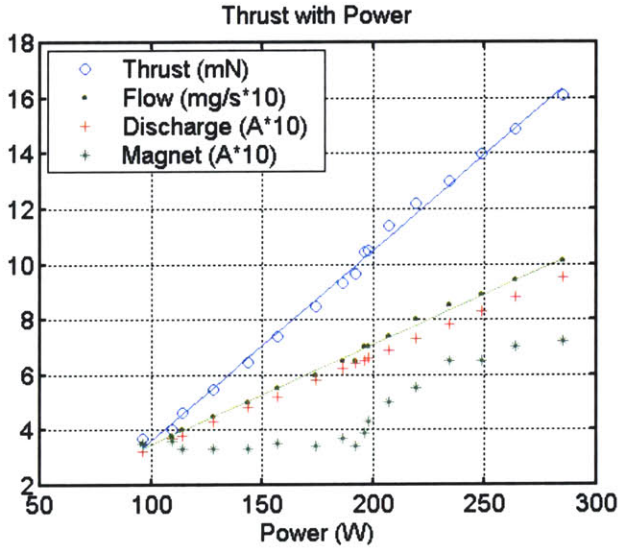

Figure 4.12. Thrust versus Power for Constant Voltage of 300 V

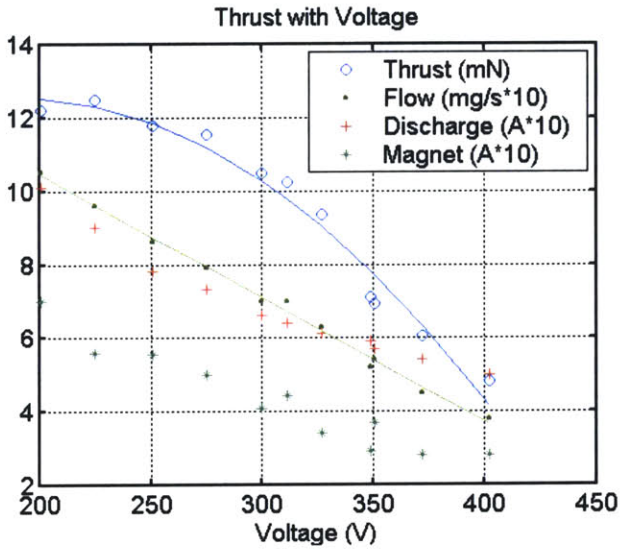

Figure 4.13. Thrust versus Voltage for Constant Power of 200 W

4.5.2 MK16 QCM's and M2000 Controller

Four MK16 flight-quality QCM's from QCM Research, plus their lab controller, are available for testing courtesy of the Air Force. The current ground test plan calls for one of these QCM's to be used for ground tests and while the remaining three are saved uncon-

taminated for the Shuttle flight. Software to run the controller is available on the QCM Research web site.

Each QCM requires 10 instrumentation wires to be passed from the controller through the chamber wall. This uses up an entire small port and may at some point be a strain on the chamber's instrumentation capability. This is an added reason to only use one QCM in the chamber at a time.

The QCM will be tested with a collimator in the backplane, between 70° and 90°. A primary objective of the tests is to rank the difficulty of interpreting the QCM data with the value of the data it provides. As mentioned in "QCM and Witness Plate Analysis" on page 60, the Shuttle background environment will include thruster firings, water dumps, and outgassed products in addition to the space background. A control QCM may be used to help identify and remove these effects from the data, but at the loss of a QCM which could be used to measure deposition at another position for the PPT or the Hall thruster.

Another primary objective of these tests will be to confirm the thruster firing time required for the minimum identifiable deposition. This time will be critical in planning the operation and manifesting of ETEEV.

Secondary objectives will be to test the thermogravimetric analysis capability of the QCM and to test the QCM with a positively biased grid. The first test selectively boils off constituents to allow them to be identified by their vapor pressure. The products of the thruster erosion, mostly boron, boron nitride, and molybdenum, might be very difficult to boil off. Vapor pressures for these materials must be found or estimated before this test can take place. Using a biased grid in front of the QCM would enable it to be an incoming deposition sensor instead of a net deposition sensor, and the QCM could be placed further into the main plume without degrading the crystal. Grids the same as those planned for the Retarding Potential Analyzers (RPA's) could be used.

4.5.3 Witness plates

The primary purpose of the witness plate testing will be to confirm the minimum time required for measurable erosion. A secondary purpose will be to develop contamination-avoidance procedures. Silver and quartz will be used as in Pencil's tests[30],[29]. If possible, chemical analysis will be performed on plates placed in the net deposition region in preparation for the post-flight analysis of plates from ETEEV.

4.5.4 Faraday cups

The goals of early Faraday probe testing are to establish typical current profiles for this thruster at different radial distances and to compare different probe configurations. Both flush and RPA-type current detectors are under consideration as discussed in "RPA Analysis" on page 66. Several materials such as stainless steel and tungsten will be used. These probes may be fixed-mounted in the chamber until the motorized arm is ready.

The Faraday cup circuit is challenging because the measurement is very small and the probe is isolated from ground. For this reason optically isolated opamps and precision resistors may be needed for the circuitry.

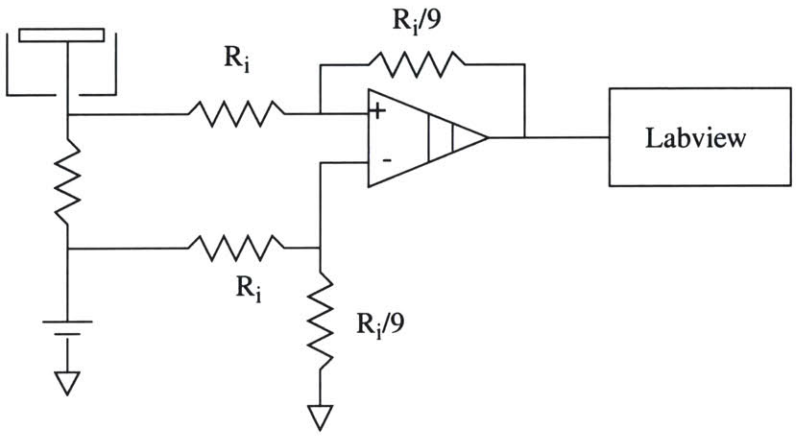

Figure 4.14. Faraday probe circuit with isolation op-amp

The probes will be constructed of Kimball Physics eV parts. Stainless steel or nickel wire will be spotwelded to stainless steel or tungsten plates. Stainless steel cylinders spot-welded to a backplate will be used for guard rings. Alumina tubes and teflon shrink tube will be used to shield the wire until it is connected with teflon-coated wire. Pins and sockets will be used to connect the stainless steel or nickel wire to the tin-plated copper wire. The support structure to mount the probes will be built of stainless steel and alumina parts which are spotwelded where necessary for structural rigidity.

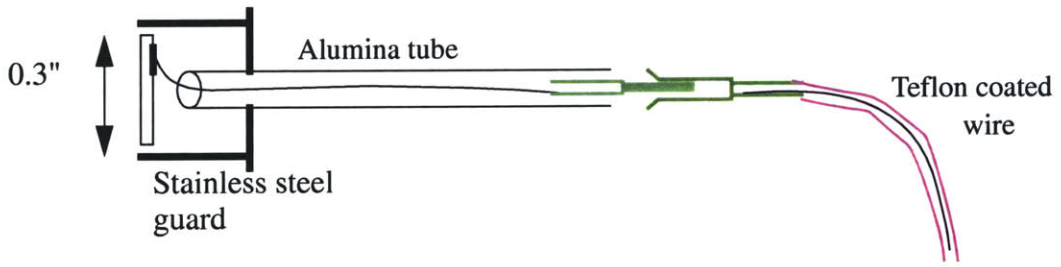

Figure 4.15. Planar Faraday probe construction

4.5.5 Langmuir probes

The main goal of this testing will be to compare probe configurations. This includes comparing swept single probes against triple probes for ease of use and data interpretation, and also verifying the appropriate interprobe spacing fro the triple probe.

Construction of a Langmuir probe requires spotwelding for high-temperature joints between tungsten and stainless wire. A pin is soldered to the stainless wire and a socket to

teflon-coated regular wire. Teflon shrink tube is used liberally to insulate joints between the protective alumina tubing and the teflon insulation in the signal wires.

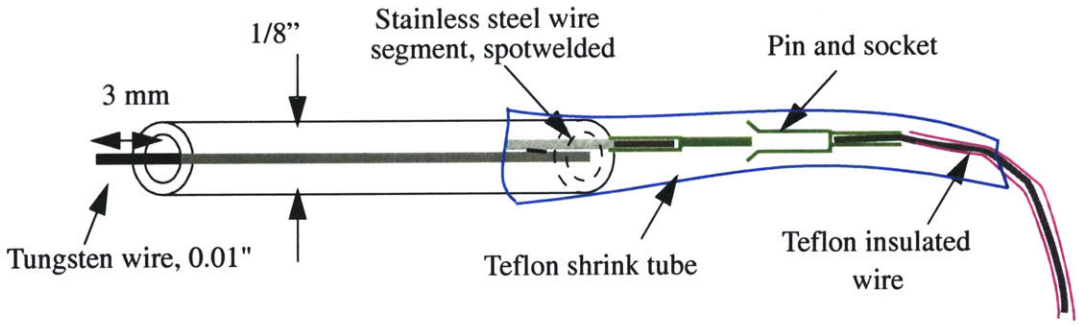

Figure 4.16. Langmuir Probe Construction

The circuitry for a single Langmuir probe requires a function generator for the voltage sweep. A circuit schematic is shown below.

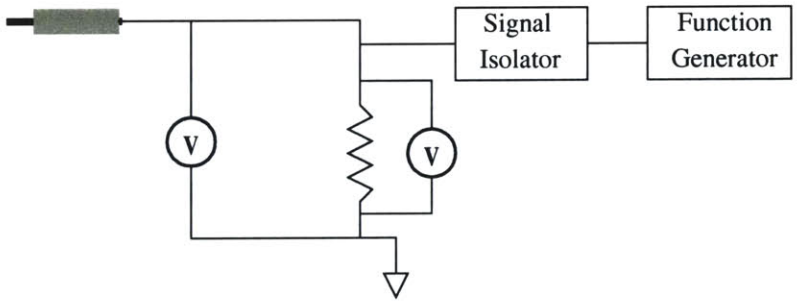

Figure 4.17. Single Langmuir Probe Circuit Schematic

The support structure for Langmuir probes will be made from stainless eV rods and plates similarly to the Faraday probe supports. The triple probes must robust to twisting, which may require some spotwelded assemblies. Ceramabond is available for bonding alumina tubes together or for bonding alumina to metal if needed.

References

[1] Abgaryan, V.; Kaufman, H.; Kim, V.; Ovsyanko, D.; Shkarban, I.; Semeov, A.; Sorokin, A.; Zhurin, V. *Calcuation Analysis of the Erosion of the Dicharge Chamner Walls and their Contamination during Prolonged SPT Operation.* AIAA/ ASME/SAE/ASEE 30th Joint Propulsion Conference and Exhibit, June 27-29, 1994. (AIAA 94-2859)

[2] Arrington, Lynn A.; Marrese, Colleen M.; Blandino, John J. *Pulsed Plasma Thruster Plume Study: Symmetry and Impact on Spacecraft Surfaces.* 36th AIAA/ASME/ SAE/ASEE Joint Propulsion Conference, July 17-19, 2000. (AIAA 2000-3262)

[3] Boyd, Iain D. *A Review of Hall Thruster Plume Modeling.* 38th Aerospace Sciences Meeting, January, 2000. (AIAA 2000-0466)

[4] Burton, R. L.; Turchi, P. J. *Pulsed Plasma Thruster.* Journal of Propulsion and Power, Vol. 14, N0. 5, Sept.-Oct. 1998, pp. 716-735.

[5] Capacci, M.; Matticari, G.; Noci, G.; Severi, A.; Borie, D. *An Electric Propulsion Diagnostic Package for the Characterization of the Plasma Thruster/Spacecraft Interactions on STENTOR Satellite*, 35th AIAA/ASME/SAE/ASEE Joint Propulsion Conference and Exhibit, June 20-24, 1999. (AIAA 99-2277)

[6] Cooke, David; Rich, Frederick; Wan, Li; Roth, Chris; Morgan, Al. *Introducing the Digital Ion Drift Meter.* Presented to the American Geophysical Union, Fall 1999.

[7] De Grys, K.H.; Tilley, D.L.; Aadland, R.S. *BPT Hall Thruster Plume Characteristics*, 35th AIAA/ASME/SAE/ASEE Joint Propulsion Conference and Exhibit, June 20-24, 1999 (AIAA 99-2283).

[8] Eckman, Robert; Byrne, Lawrence; Cameron, Edward; Gatsonis, Nikos A.; Pencil, Eric J. *Analysis of Triple Langmuir Probe Measurements in the Plume of a Pulsed Plasma Thruster.* 35th AIAA/ASME/SAE/ASEE Joint Propulsion Conference & Exhibit, June 20-24, 1999. (AIAA 99-2286)

[9] Eckman, R. *Pulsed Plasma Thruster Plume Diagnostics.* 36th Aerospace Sciences Meeting & Exhibit, January 12-15, 1998. (AIAA 98-0004)

[10] Fife, John Michael. *Hybrid-PIC Modeling and Electrostatic Probe Survey of Hall Thrusters.* Doctoral Thesis, MIT, September 1998.

[11] Gilchrist, B.; Davis, C.; Carlson, D.; Gallimore, A. *Electromagnetic Wave Scattering Experiments in HALL Thruster Plasma.* 34th AIAA/ASME/SAE/ASEE Joint Propulsion Conference and Exhibit, July 12-15, 1998 (AIAA-98-3642).

[12] Green, K. M.; Hayden, D. R.; Juliano, D. R.; Ruzic, D. N. *Determination of flux ionization fraction using a quartz crystal microbalance and a gridded energy analyzer in an ionized magnetron sputtering system.* Review of Scientific Instrumentation, Vol. 68, No. 12, Dec. 1997, pp. 4555-4560.

[13] Gulczinski, Frank S.; Hofer, Richard R.; Gallimore, Alec D. *Near-Field Ion Energy and Species Measurements of a 5 kW Laboratory Hall Thruster.* 35th AIAA/

ASME/SAE/ASEE Joint Propulsion Conference and Exhibit, June 20-24, 1999 (AIAA-99-2430).

[14] Hargus, W.; Fife, J. M.; Mason, L.; Jankovsky, R.; Haag, T.; Pinero, L.; Snyder, J.S. *Preliminary Performance Results of the High Performance Hall System SPT-140.* 36th Joint Propulsion Conference and Exhibit, July 17-19, 2000 (AIAA-2000-3250).

[15] Hruby, V.; Monheiser, J.; Pote, B.; Freeman, C.; Connolly, W. *Low Power Hall Thruster Propulsion System.* IEPC 99-092.

[16] Hutchinson, I. H. Principles of Plasma Diagnostics, Cambridge University Press, New York, 1987.

[17] King and Gallimore, *Gridded retarding pressure sensor for ion and neutral particle analysis in flowing plasmas*, Review of Scientific Instrumentation, 1997.

[18] King, Lyon B. and Gallimore, Alec D.. *Identifying CEX Collision Products within Ion-energy Distribution of Electrostatically Accelerated Plasmas.* Internal University of Michigan paper.

[19] King, Lyon B. and Gallimore, Alec D. *Ion Energy Diagnostics in the Plume of an SPT-100 from Thrust Axis to Backflow Region.* 34th AIAA/ASME/SAE/ASEE Joint Propulsion Conference and Exhibit, July 13-15, 1998 (AIAA-98-3641).

[20] King, Lyon B. and Gallimore, Alec D. *Propellant Ionization and Mass Spectral Measurements in the Plume of an SPT-100.* 34th AIAA/ASME/SAE/ASEE Joint Propulsion Conference and Exhibit, July 13-15, 1998 (AIAA-98-3657).

[21] King, Lyon B.; Gallimore, Alec D.; Marrese, Colleen M. *A Molecular Beam Mass Spectrometer for Hall Thruster Plume Studies: Preliminary Data.* 33rd AIAA/ ASME/SAE/ASEE Joint Propulsion Conference & Exhibit, July 6-9, 1997 (AIAA 97-3066).

[22] King, Lyon B.; Gallimore, Alec D.; Marrese, Colleen M. *Transport-Property Measurements in the Plume of an SPT-100 Hall Thruster.* Journal of Propulsion and Power, Vol. 13, No. 3, May-June 1998, pp. 327-335.

[23] Korsun, Borisov, et. al., *Comparison between Plasma Plume Theoretical Models and Experimental Data*, IEPC 99-221

[24] Manzella, David H. *Stationary Plasma Thruster Plume Emissions.* IEPC 93-097.

[25] Manzella, David H.; Sankovic, John M. *Hall Thruster Ion Beam Characterization.* 31st AIAA/ASME/SAE/ASEE Joint Propulsion Conference and Exhibit, July 10-12, 1995. (AIAA 95-2927)

[26] Marrese, Colleen M.; Gallimore, Alec D.; Haas, James; Foster, John; King, Brad; Kim, Sang Wook; Khartov, Sergei. *An Investigation of Stationary Plasma Thruster Performance with Krypton Propellant.* 31st AIAA/ASME/SAE/ASEE Joint Propulsion Conference and Exhibit, July 10-12, 1995 (AIAA 95-2932).

[27] Myers, R. M.; Arrington, L. A.; Pencil, E. J.; Carter, J.; Heminger, J.; Gatsonis, N. *Pulsed Plasma Thruster Contamination.* 32nd AIAA/ASME/SAE/ASEE Joint Propulsion Conference, July 1-3, 1996. (AIAA 96-2729)

[28] Myers, Roger M.; Manzella, David H. *Stationary Plasma Thruster Plume Characteristics.* IEPC 93-096.

[29] Pencil, Eric J.; Randolph, Thomas; Manzella, David H. *End-of-Life Stationary Plasma Thruster Far-field Plume Characterization.* 32nd AIAA/ASME/SAE/ ASEE Joint Propulsion Conference, July 1-3, 1996. (AIAA 96-2709)

[30] Pencil, Curran, Peterson. *Pulsed Plasma Thruster Technology Directions.* (AIAA 97-2926)

[31] Perot, C.; Gascon, N.; Bechi, S.; Lasgorciex, P.; Dudeck, M.; Garrigues, L.; Boeuf, J.P. *Characterization of a Laboratory Hall Thruster with Electrical Probes and Comparisaons with a 2D Hybrid PIC-MCC Model.* 35th AIAA/ASME/SAE/ ASEE Joint Propulsion Conference and Exhibit, June, 1999. (AIAA 99-2716)

[32] Randolph, T.; Pencil, E.; Manzella, D. *Far-field Plume Contamination and Sputtering of the Stationary Plasma Thruster.* 30th AIAA/ASME/SAE/ASEE Joint Propulsion Conference, June 27-29, 1994. (AIAA-94-2855)

[33] Samanta Roy, R. I.; Gatsonis, N. A.; Hastings, D. E. *A Review of Contamination from Electric Propulsion Thrusters.* 25th Plasmadynamics and Lasers Conference, June 1994. (AIAA 94-2469)

[34] Shuttle Small Payloads Project (SSPP) Capabilities brochure, "Carrier Capabilities 1999", http://sspp.gsfc.nasa.gov/documents/sspp_brochure20p.pdf

[35] Siebenforcher, A.; Schrittwieser, R. *A new simple emissive probe.* Rev. Sci. Instrum., 67 (3), March 1996.

[36] Spanjers, Schilling, Engleman, Bromaghim, Johnson. *Preliminary Analysis of Contamination Measurements from the ESEX 26 kW Ammonia Arcjet Flight Experiment.* 35th AIAA/ASME/SAE/ASSEE Joint Propulsion Conference & Exhibit, 20-23 June, 1999. (AIAA 99-2709)

[37] SPIRET Presentation from November, 2000, In-Space Plasma Diagnostics Conference at MIT.

[38] SSPP Customer Accommodations & Requirements Document (CARS), http:// sspp.gsfc.nasa.gov/documents, broken into sections for downloading.

[39] Tajmar, M. *SMART-1 Electric Propulsion Diagnostic Package and Simulation*, presented at the MIT-hosted In-Space Electric Propulsion Diagnostics Conference, Nov. 1999.

[40] Wang, J.; Brinza, D.; Goldstein, R.; Polk, J.; Henry, M.; Young, D.T.; Hanley, J. J.; Nordholt, J.; Lawrence, D.; Shappiro, M. *Deep Space One Investigations of Ion Propulsion Plasma Interactions: Overview and Initial Results,* 35th AIAA/ASME/ SAE/ASEE Joint Propulsion Conference and Exhibit, June 20-24, 1999 (AIAA 99-2971)

[41] Uy, O. Manuel; Cain, Russel P.; Carkhuff, Bliss G.; Cusick, Richard T.; Wood, Bob E. *Miniature Quartz Crystal Microbalance for Spacecraft and Missile Applications.* Johns Hopkins APL Technical Digest, Vol. 20, No. 2, 1999, pp. 199-211.

Appendix A. Thrust Balance Documentation

Thrust Balance Documentation

Author: Stephanie Thomas

Theory of Operation

The thrust stand is an inverted pendulum. There are two parameters which affect the stand's operation: the spring constant *k* and the platform mass *m*. These two parameters must be balanced for the thrust stand to work: the spring must be stiff enough to bring stability to a given mass *m*. The optimal sensitivity to extra thrust T occurs when F is zero or just positive. If F is very positive, such as when the spring is very stiff, the pendulum is very stable and not very sensitive to any extra forces, such as the thrust we are trying to measure. If a given spring is too stiff, the stand's sensitivity can be increased by adding mass to *m*.

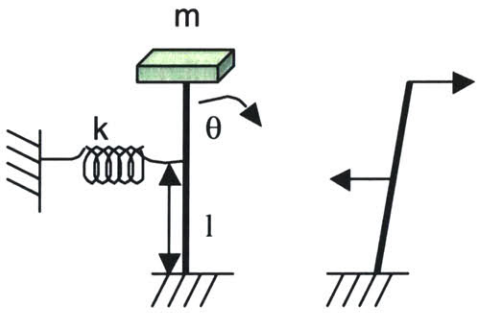

$$F_x \cong -mg\sin\theta + kl\sin\theta\,(-T)$$

Figure A.1. Thrust stand theory

Balance Hardware

Level

The level consists of a little black box on the bottom plate of the balance with eight wires visible. The level is adjusted with a motor on a drive screw near the balance arm.

This device levels the lower platform. It is an open loop which requires manual control. The upper platform is not exactly aligned with the lower platform, although the balance is not very sensitive to this. The object is to keep the level at about 0 on the scale displayed on the control box.

The level is important so that the balance has enough room to move forward when calibrating without hitting the front support. It is particularly critical for very sensitive applications such as the 200 W Hall thruster.

Damping Coil

The damping coil uses rate feedback from a circuit in the control box to damp out oscillations in the main balance. This coil is yellow. The position of the coil can be changed by altering the nuts and screw on the piston.

Sensing Coil (LVDT)

The sensing coil is located at the end of the upper platform towards the middle of the balance. As the balance moves forward due to force from the thrust, the metal rod at the edge changes position inside the coil, causing a change in the coil's output. The signal from the sensing coil is processed by the control box and sent to the computer. The position of the coil within its shell can be changed using a hex wrench on the set screw. It may be necessary to change this position to manually rezero the LVDT during calibration. See the LVDT controller manual for details.

Water Circuits

The water circuits cool the balance and case when the thruster is in operation. The water pipes on the balance are 1/8", those on the case are ¼".

Xenon connection

The balance has an inlet for the thruster gas. There is a place for a cathode gas connection as well, although the pipe is not installed.

Thruster Mount

There is a knob on the upper plate to which the fiberglass platform is attached after the cover is in place. The thruster rests on top of this platform. The thread with the calibration masses also attached to this platform.

Spring

The spring is a small strip of aluminum which has been bent into an s-shape. The stiffness of the spring, depending on the thickness of the strip and the height of the bends, may need to be changed depending on the magnitude of the thrust to be measured. The design of the spring is available as one of the parts drawings.

Calibration System

The calibration system consists of a motor, a spool of thread, a series of masses tied on the thread, and a wheel. The motor and spool are located on the tall arm at the back of the balance. The wheel is attached to the main balance. The thread goes down from the spool, loops up over the wheel, and attached to the thruster mount. (See Figure 5)

At one time a variable resistor was rigged to the spool to measure the position of the weights A wheatstone bridge in the control box was used to read the resistor. The position to the weights was then shown in LabView.

Case

The copper case provides EMI shielding and protects the balance from the thruster plasma. The case has its own cooling pipes.

Cathode Mount

A small set of brackets mounts the cathode to a heat shield on the copper case. The cathode can be manually adjusted to any position or angle required.

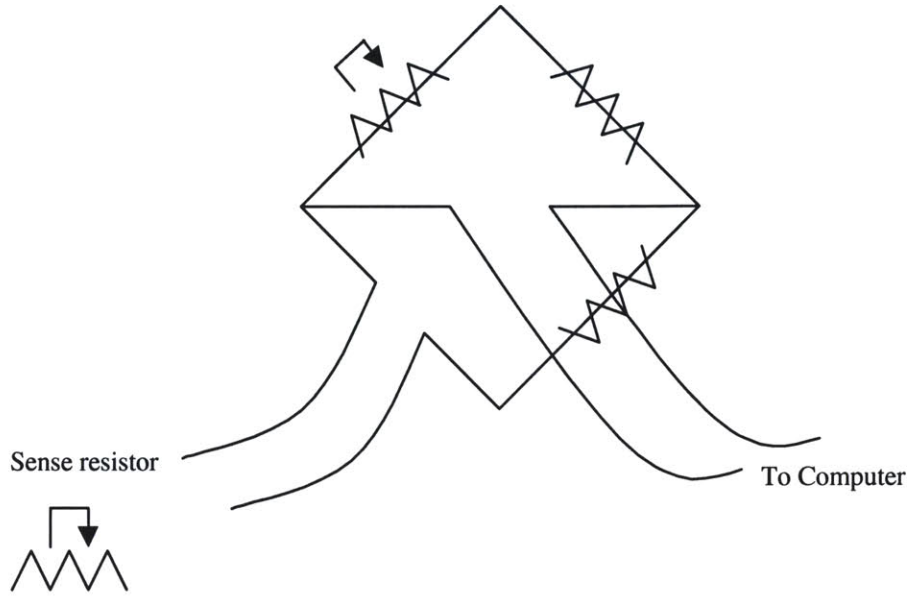

Figure A.2. Wheatstone Bridge

Cables

The balance has a cable that connects the balance to the chamber wall. This cables ends in pins that attach to spokes on the chamber port, in the configuration shown below. The control box has a cable that connects to the outside of the chamber wall.

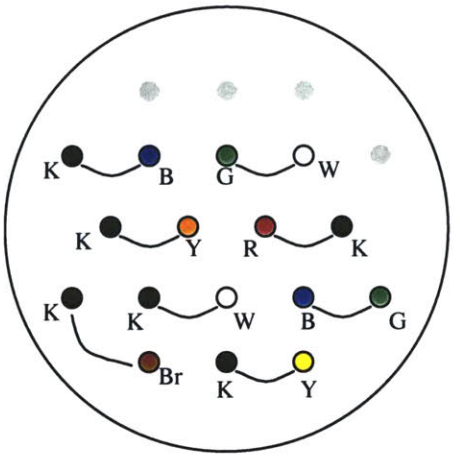

Key

B	Blue
Br	Brown
G	Green
K	Black
R	Red
W	White
Y	Yellow

Figure A.3. Pin Map for Vacuum Chamber Port

Control Box

The front of the control box has numerous switches and displays. They are described and pictured in the table and figure below.

Table 1. Control box components

Item	Function

Display at far left	LVDT display with controls
Knob 1	Gain for damping circuit
Knob 2	Offset for damping circuit
Switch 3	On/off for calibration motor.
Switch 4-1-0	Controls the calibration motor (up/down).
Digital display above knobs	Displays the level value. Unknown units, but 0 is zero. Maximum value is 12.5.
Dial (broken)	Displays the current through the damping coil
Switch at far right	Controls the level motor. Hold up to lift plate, hold down to drop plate. Automatically shuts off released.

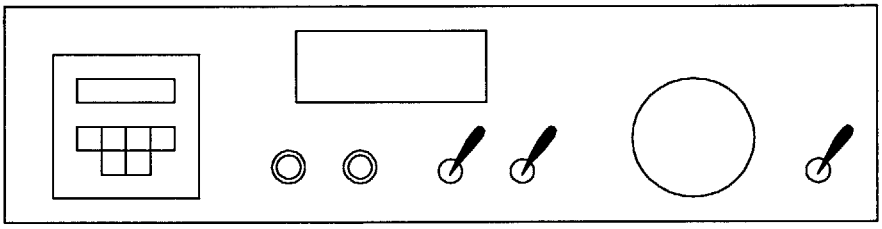

Figure A.4. Thrust balance control box

Inside the box, there are three power supplies, a breadboard circuit, and the display hardware and electronics. One power supply drives the damping circuit board and the calibration motor, one drives the LVDT, and one drives the level motor. An external power supply would be needed for the wheatstone bridge circuit.

The damping circuit filters the LVDT signal, takes a derivative, limits the derivative magnitude, and sends the result to the damping coil. The gain and offset of this circuit are adjustable using the knobs listed below. A complete circuit diagram is available along with the complete set of Busek part drawings in a large binder. The circuit is described in more detail below.

Thermal Control

The balance performs most accurately when all the flexures on the platform are the same temperature. This may require cooling of the balance and cover. The cooling circuits must be connected to a local water supply.

There are two sets of water pipes on the thrust balance: ¼" on outside of case, 1/8" on balance. There is some hardware required to set up the cooling circuits: connectors between 1/8" and ¼" sizes, rings and nuts to connect pipes at joints, the ports to connect pipes inside and outside the

vacuum chamber, and extra ¼" pipe. Currently, all connectors are brass Swagelock. These nuts may be used with Teflon or metal ferrules. Teflon has the advantage of being removable from the pipes and easily deforming to seal a joint.

Table 2. Hardware for Water Circuits

Hardware	Sizes	Number
Nuts	¼"	~8
Port	¼"	2
Connectors	¼" to 1/8"	2
Valve	¼"	1
Tubing	¼"	50 ft

There are two possibilities for the balance and case water circuits: they can run in parallel, requiring a split of the water coming into the tank, or they can run in series. Based on a simple thermal analysis, for the 200 W Hall thruster series connections should be adequate.

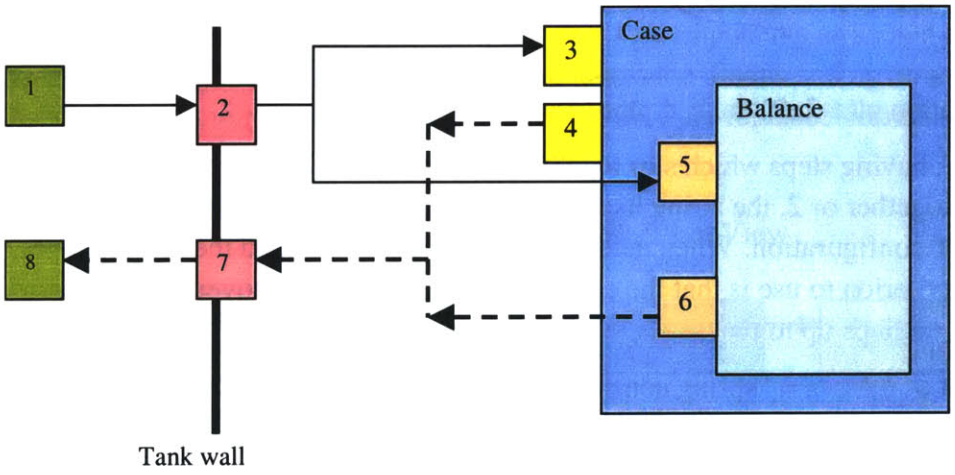

Figure A.5. Schematic diagram of parallel cooling circuits

Note that two T-connectors are needed to split and recombine the flow so that only one inlet and outlet pair is needed for the chamber wall.

Table 3. Description of components in circuit schematic

Component	Function
1	Connection to room water inlet
2	Inlet port through chamber wall

3	Connector to case pipe inlet
4	Connector to case outlet
5	¼" to 1/8" adapter connector to balance inlet
6	1/8" to ¼" adapter connector to balance outlet
7	Outlet port through chamber wall
8	Connection to room water outlet

Calibration

Calibration is required to determine the correlation between the balance output and the actual thrust. This is achieved with a series of weights of known mass on a string. The calibration motor can raise and lower these weights, producing a curve of balance output with time. Ideally there will be clear steps as each mass rounds the curve and is sensed by the balance.

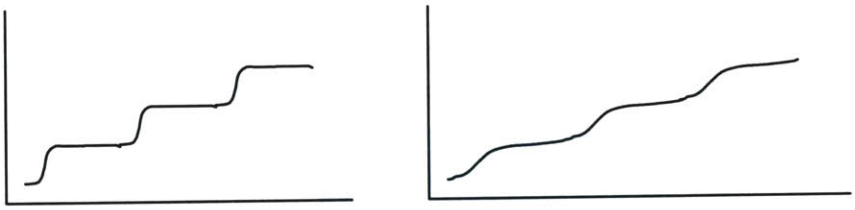

Figure A.6. Good calibration plot (left) vs. bad plot (right)

If the resulting plot is bad, having steps which slur together or no steps at all, it is either because 1. the masses are too close together or 2. the string itself is too heavy or 3. the masses are too small to be sensed by the LVDT configuration. When determining the mass to use and the distance between the masses, the criterion to use is that the calibration procedure must cover the whole range of expected thrust, perhaps up to two times the maximum thrust.

Volts from LVDT/Weight of masses = "spring constant", as calibrated by the LabView software

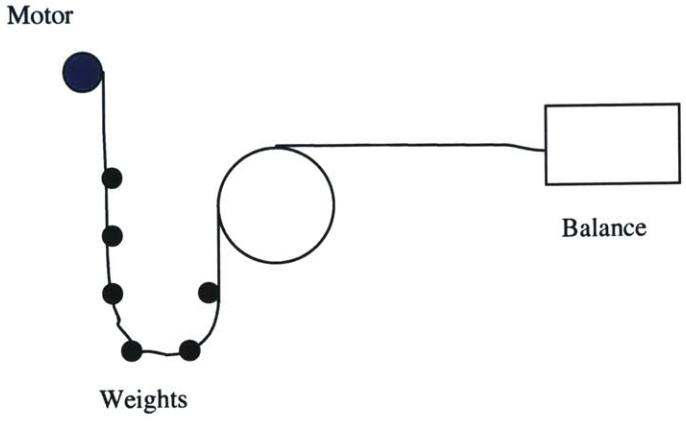

Figure A.7. Schematic of calibration setup

Once the balance is calibrated, it is ready to measure thrust. It may be necessary to recalibrate the balance from time to time during thruster operation.

Damping Circuit

The balance circuitry has two functions. The first is filtering the LVDT signal, which is then sent to the computer and used to calculate the thrust. The second is damping the balance oscillations. This circuit contains a derivative and drivers for the signal which is sent to the damping coil. The derivative has an adjustable gain and offset for fine-tuning the damping.

The damping is nonlinear. The most damping occurs at small displacements as are characteristic of thruster operation and not as are obtained by manually pushing the balance to test it. The diodes in the circuit limit the signal to the damping coil for very large oscillations.

If there are problems with the balance circuitry, there are several key troubleshooting steps:

1. Check all the connections for loose wires. This includes the circuit board and the power supplies.
2. Check the voltage coming from the power supply to the board and as supplied to the op amps and the power mosfets.
3. Use an oscilloscope to check the signal as it propagates through the parts of the circuit. Check the signal from the LVDT, the filtered signal going to the computer, and the signal before and after the derivative and driving components as shown on the circuit diagram.
4. Pending the results of (3), remove and test the diodes and op amps, paying careful attention to their orientation in the circuit so they are replaced correctly. Replace if needed.

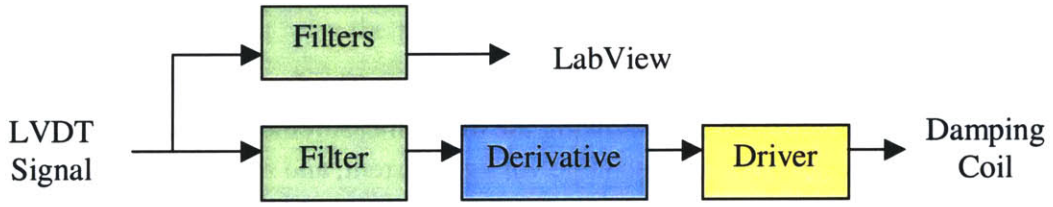

Figure A.8. Figure 6. Damping Circuit Block Diagram

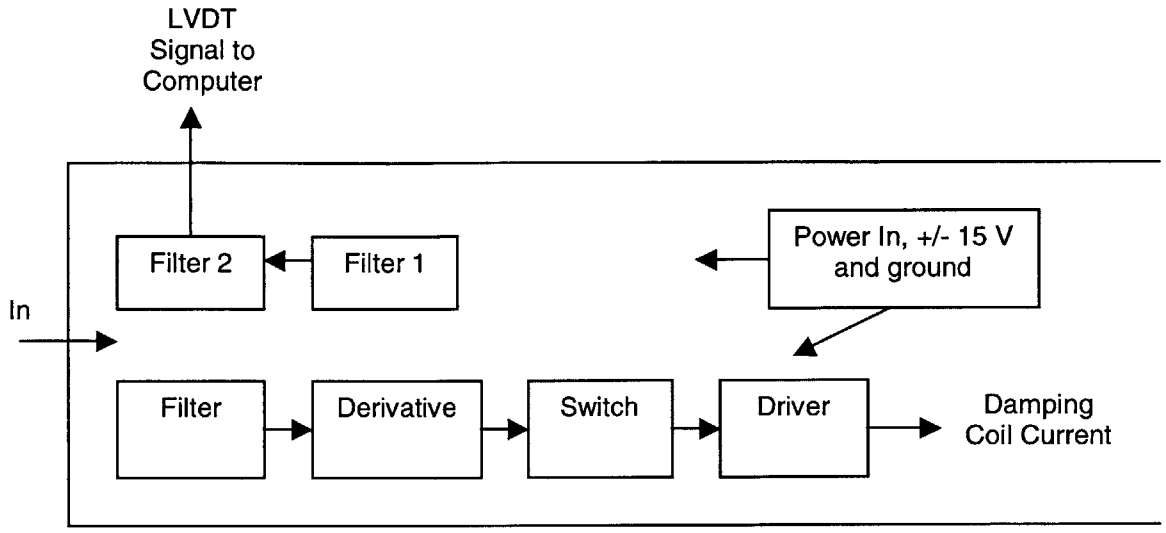

Figure A.9. Damping Circuit Board Layout

LabView Software

LabView gets data from the thrust balance, power supply, and flow controller through the GPIB card. Signals input to the connector block must be between +/- 10 V. Manuals are available for LabView, the GPIB card, and the connector block should problems arise.

LabView modules (virtual instruments):

- Thrust.vi
  This is the main instrument for operating the balance. The front panel includes an area for calibrating the balance, an area showing the thrust measurement on a graph, and an area showing the current values of discharge voltage, current, and mass flow and the calculated thrust and anode efficiency. Graphs showing the LVDT signal and the current to the damping coil are at the bottom of the VI for troubleshooting. The values for voltage, current, and mass flow may be read from the instruments if they are properly or connected or they may be set by hand.

  At one time, there was an indicator for the location of the calibration masses, which used a potentiometer and a wheatstone bridge. Copies of the old program are saved on the computer for reference.

  The calculations in the thrust module include scaling the outputs of the flowmeter and power supply to indicate mg/s, volts, and amperes; calculating the LVDT calibration slope; using the slope to convert the LVDT output to mN; and calculating the efficiency of the thruster.

Efficiency:

$$\eta = \frac{T^2}{IV}$$

- File.vi
  This sub-vi sends formatted data to a text file. A macro in Excel named "Process Lab Data" can then format the data. Data sets are appended to the chosen text file with each click of the "Store Data" button. Each data set appears as a row in Excel, notated with date and time.

Date			Time			LVDT	Voltage	Current	Mass Flow	Thrust	Efficiency
Month	Day	Year	Hour	Mins	Sec	Reading	V	A	mg/s	mN	
12	18	2000	17	4	30	45.649	300	0.5	0.5	5.49	9.595
12	18	2000	17	4	33	45.54	300	0.5	0.5	5.49	9.536
12	18	2000	17	4	35	45.64	300	0.5	0.5	5.49	9.733
12	18	2000	17	4	37	45.516	300	0.5	0.5	5.49	9.287
12	18	2000	17	28	9	-8.013	300	0.5	0.5	4.36	15.583
12	18	2000	17	28	11	-8.129	300	0.5	0.5	4.36	14.843
12	18	2000	17	28	37	-8.011	300	0.5	0.5	4.36	15.333
12	18	2000	17	41	9	-14.211	300	0.5	0.5	2.65	-11.939
12	18	2000	17	43	11	-19.39	300	0.5	0.5	2.85	0.293
12	18	2000	18	1	25	-21.459	300	0.5	0.5	2.43	10.203

Figure A.10. Sample Excel spreadsheet with data from operating thrust balance

- Voltage, current, mass flow.vi
  This sub-vi grabs data from the power supply and mass flow controller.

Procedures

Calibration

The balance requires careful calibration. If a new spring or calibration mass is used, practice the calibration procedure before operating the balance in vacuum.

1. With the thruster or equivalent weight on the balance and the cover off, loosen the set screw holding the LVDT and slide the coil until the LVDT readout is as close to zero as possible.
2. If ready, install the cover, platform, and thruster.
3. Raise the weights using switches 3 and 4.
4. If ready, pump down the vacuum chamber.
5. Use the offset knob to set the damping current to zero at a desired operating point. The damping coil input is indicated near the bottom of the vi panel.
6. Get a zero starting point by clicking the "Zero" button at the left of the Thrust.vi calibration area.
7. Begin lowering the weights. When the thrust signal levels off, stop the motor, allow the signal to settle, and grab the point by clicking "1" in the calibration area. Repeat for 2, 3,

and 4. Note the slope (g/V) in the indicator.

8. Raise the weights to the desired operating point.
9. Get a new zero before measuring thrust.

Operation

Operating the balance once it is successfully calibrated is simple. Just click the "Store Data" button to add a desired data point to the output file. Avoid unnecessary disturbances around the vacuum chamber while taking data. It is wise to check the calibration from time to time by shutting off the thruster, raising or lowering some weights, and checking the LVDT output against the calibration value for that mass level. If there is any noticeable drift, recalibrate the balance. It may be possible to rezero the LVDT if necessary by pushing the "Zero" button on its control panel.

Additional Work

Ideally, the cathode should be on the measurement platform with the thruster for a true measurement of the total thrust. However, this introduces three extra power lines which must be situated so that they don't interfere with the platform's motion. Poorly placed wires could affect the overall balance spring constant in an unpredictable way. To avoid this problem Busek has designed a "deck" which is designed to hold ribbon cables for the transmission of power to the thruster and cathode. The upper deck is attached to the thruster arm and the lower deck to the measurement platform. The ribbon cables spanning the decks have a very predictable effect on the balance spring constant which is accounted for in calibration.

Busek has donated an upper deck and a set of ribbon cables which could be used on this balance. However a lower deck is not available and must be manufactured for tis system to be implemented. In addition, several more parts are required to complete the change: a bracket to mount the cathode directly on the thruster, and a pipe set to bring the cathode gas through the balance in the same manner as the thruster gas.

This change to a ribbon cable deck is not trivial. Too avoid the time it will take to obtain and install all the parts, the cathode is mounted on the balance cover and the thruster power lines are wrapped around the balance pipes to minimize their effect on the platform.

Appendix B. Langmuir Probe Spreadsheet

Electrostatic probe analysis, following theory in Michael Fife's thesis.[10] Ion and electron current in a supersonic plasma for an electron-repelling probe bias:

$$I_e = e\frac{n_e\bar{c}}{4}\exp\left\{\frac{e(V-V_p)}{kT_e}\right\}S_e \tag{B.1}$$

$$I_i = en_e v_i S_i + I_{i,s} = en_e v_i S_i(1+f_s) \tag{B.2}$$

where S is the area of collection of electrons or ions. The ions arrive only from the front and see the projection of the probe on a plane perpendicular to the flow direction. The electrons arrive from all directions and see the total area of the probe. The extra term in the ion current equation accounts for the expansion of the sheath, where f_s is a first order estimate based on an empirically determined slope for the ion saturation region.

Ion and electron current for an electron-attracting probe bias:

$$I_e = e\frac{n_e\bar{c}}{4}(1+\frac{e(V-V_p)}{kT_e})S_e \tag{B.3}$$

$$I_i = en_e v_i S_i \tag{B.4}$$

This case is more complicated. If the ion density is unaffected by the positive probe bias, so that it is constant around the probe, then there are no potential barriers to the electrons. This is equivalent to an infinite sheath, or the orbit motion limit. In this case only the electrons' trajectory determines if they reach the probe. For a spherical geometry, the current is linear with potential, as given above.

Summary: in a supersonic plasma, both the electron saturation and ion saturation current regions are found experimentally to be linear with the probe bias. The exponential region in between remains as in a stationary plasma.

S_i changes with location since the probes are cylindrical. Since the exact ion beam vector is not known a priori these areas cannot be calculated with geometry but should be experimentally measured. Fife measured S_i by using a non-axial control probe and averages from his thesis were used in calculations.

For these calculations, a probe 3 mm long and 0.4 mm in diameter was assumed.

Parameters and intermediate calculations:

	Min	Max	
θ	45	10	deg
S_e	1.88E-06	1.88E-06	m^2
S_i	3.77E-07	1.20E-06	m^2
n	1.00E+15	1.00E+16	m^{-3}
V_p	1.50E+01	1.50E+01	V
V_d	3.00E+02	3.00E+02	V
η_e	4.20E-01	4.20E-01	--
Te	2.50E+00	2.50E+00	eV

Geometry, constants

l_{probe}	3	mm
r_{probe}	0.2	mm
r	25	cm
m_e	9.00E-31	kg
m_{Xe}	2.18E-25	kg
ε_0	8.85E-12	
e	1.60E-19	C

Calculations

λ_d	0.37	0.12	mm
v_i	13600	13600	m/s
V_f-V_p	-8.375	-8.2	V
M_s*λd	5.32E-02	1.68E-02	
V_f	6.625	6.8	V
$C_{bar}(e^-)$	1.06E+06	1.06E+06	m/s

Figure B.1: Calculated current values for electron repelling probe

Electron Repelling Probe									
	I_i/en_e				I_e/en_e	$I\,(Amps) = I_i - I_e$			
$V-V_p$	S_{min}		S_{max}			n_{min}		n_{max}	
	n_{min}	n_{max}	n_{min}	n_{max}					
	5.13E-03		1.63E-02		5.01E-01	1.60E-04		1.60E-03	
-1	5.40E-03	5.22E-03	1.72E-02	1.66E-02	4.20E-01	-6.64E-05	-6.45E-05	-6.64E-04	-6.46E-04
-2	5.68E-03	5.30E-03	1.80E-02	1.68E-02	2.82E-01	-4.42E-05	-4.22E-05	-4.42E-04	-4.24E-04
-3	5.95E-03	5.39E-03	1.89E-02	1.71E-02	1.89E-01	-2.93E-05	-2.72E-05	-2.94E-04	-2.75E-04
-4	6.22E-03	5.47E-03	1.98E-02	1.74E-02	1.27E-01	-1.93E-05	-1.71E-05	-1.94E-04	-1.75E-04
-5	6.49E-03	5.56E-03	2.06E-02	1.77E-02	8.49E-02	-1.25E-05	-1.03E-05	-1.27E-04	-1.07E-04
-6	6.77E-03	5.65E-03	2.15E-02	1.79E-02	5.69E-02	-8.02E-06	-5.66E-06	-8.20E-05	-6.23E-05
-7	7.04E-03	5.73E-03	2.24E-02	1.82E-02	3.81E-02	-4.97E-06	-2.52E-06	-5.18E-05	-3.19E-05
-8	7.31E-03	5.82E-03	2.32E-02	1.85E-02	2.56E-02	-2.92E-06	-3.71E-07	-3.16E-05	-1.13E-05
-9	7.59E-03	5.91E-03	2.41E-02	1.88E-02	1.71E-02	-1.53E-06	1.12E-06	-1.80E-05	2.61E-06
-10	7.86E-03	5.99E-03	2.50E-02	1.90E-02	1.15E-02	-5.80E-07	2.16E-06	-8.79E-06	1.21E-05
-11	8.13E-03	6.08E-03	2.58E-02	1.93E-02	7.70E-03	6.95E-08	2.90E-06	-2.59E-06	1.86E-05
-12	8.40E-03	6.16E-03	2.67E-02	1.96E-02	5.16E-03	5.19E-07	3.45E-06	1.61E-06	2.31E-05
-13	8.68E-03	6.25E-03	2.76E-02	1.99E-02	3.46E-03	8.35E-07	3.86E-06	4.47E-06	2.62E-05
-14	8.95E-03	6.34E-03	2.84E-02	2.01E-02	2.32E-03	1.06E-06	4.18E-06	6.43E-06	2.85E-05
-15	9.22E-03	6.42E-03	2.93E-02	2.04E-02	1.55E-03	1.23E-06	4.44E-06	7.79E-06	3.02E-05
-16	9.50E-03	6.51E-03	3.02E-02	2.07E-02	1.04E-03	1.35E-06	4.66E-06	8.75E-06	3.14E-05
-17	9.77E-03	6.60E-03	3.10E-02	2.10E-02	6.98E-04	1.45E-06	4.85E-06	9.43E-06	3.24E-05

Probe characteristics for V>Vp				
	I			
$V-V_p$	n_{min}		n_{max}	
16	-5.93E-04	-5.91E-04	-5.93E-03	-5.91E-03
15	-5.61E-04	-5.59E-04	-5.61E-03	-5.59E-03
14	-5.29E-04	-5.27E-04	-5.29E-03	-5.27E-03
13	-4.96E-04	-4.95E-04	-4.96E-03	-4.95E-03
12	-4.64E-04	-4.63E-04	-4.64E-03	-4.63E-03
11	-4.32E-04	-4.30E-04	-4.32E-03	-4.30E-03
10	-4.00E-04	-3.98E-04	-4.00E-03	-3.98E-03
9	-3.68E-04	-3.66E-04	-3.68E-03	-3.66E-03
8	-3.36E-04	-3.34E-04	-3.36E-03	-3.34E-03
7	-3.04E-04	-3.02E-04	-3.04E-03	-3.02E-03
6	-2.72E-04	-2.70E-04	-2.72E-03	-2.70E-03
5	-2.40E-04	-2.38E-04	-2.40E-03	-2.38E-03
4	-2.08E-04	-2.06E-04	-2.08E-03	-2.06E-03
3	-1.76E-04	-1.74E-04	-1.76E-03	-1.74E-03
2	-1.44E-04	-1.42E-04	-1.44E-03	-1.42E-03
1	-1.11E-04	-1.10E-04	-1.11E-03	-1.10E-03
0	-7.94E-05	-7.76E-05	-7.94E-04	-7.76E-04
-1	-6.64E-05	-6.45E-05	-6.64E-04	-6.46E-04
-2	-4.42E-05	-4.22E-05	-4.42E-04	-4.24E-04
-3	-2.93E-05	-2.72E-05	-2.94E-04	-2.75E-04
-4	-1.93E-05	-1.71E-05	-1.94E-04	-1.75E-04
-5	-1.25E-05	-1.03E-05	-1.27E-04	-1.07E-04
-6	-8.02E-06	-5.66E-06	-8.20E-05	-6.23E-05
-7	-4.97E-06	-2.52E-06	-5.18E-05	-3.19E-05
-8	-2.92E-06	-3.71E-07	-3.16E-05	-1.13E-05
-9	-1.53E-06	1.12E-06	-1.80E-05	2.61E-06
-10	-5.80E-07	2.16E-06	-8.79E-06	1.21E-05
-11	6.95E-08	2.90E-06	-2.59E-06	1.86E-05
-12	5.19E-07	3.45E-06	1.61E-06	2.31E-05
-13	8.35E-07	3.86E-06	4.47E-06	2.62E-05
-14	1.06E-06	4.18E-06	6.43E-06	2.85E-05
-15	1.23E-06	4.44E-06	7.79E-06	3.02E-05
-16	1.35E-06	4.66E-06	8.75E-06	3.14E-05

Figure B.2: Calculated current values for electron attracting probe

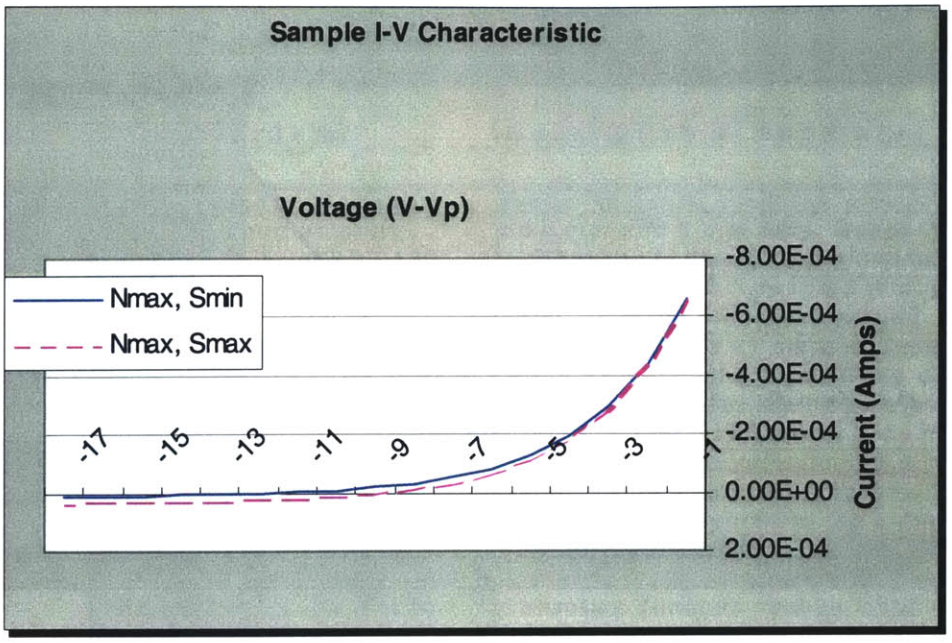

Figure B.3: Sample I-V Characteristic for Low Density Plume Plasma

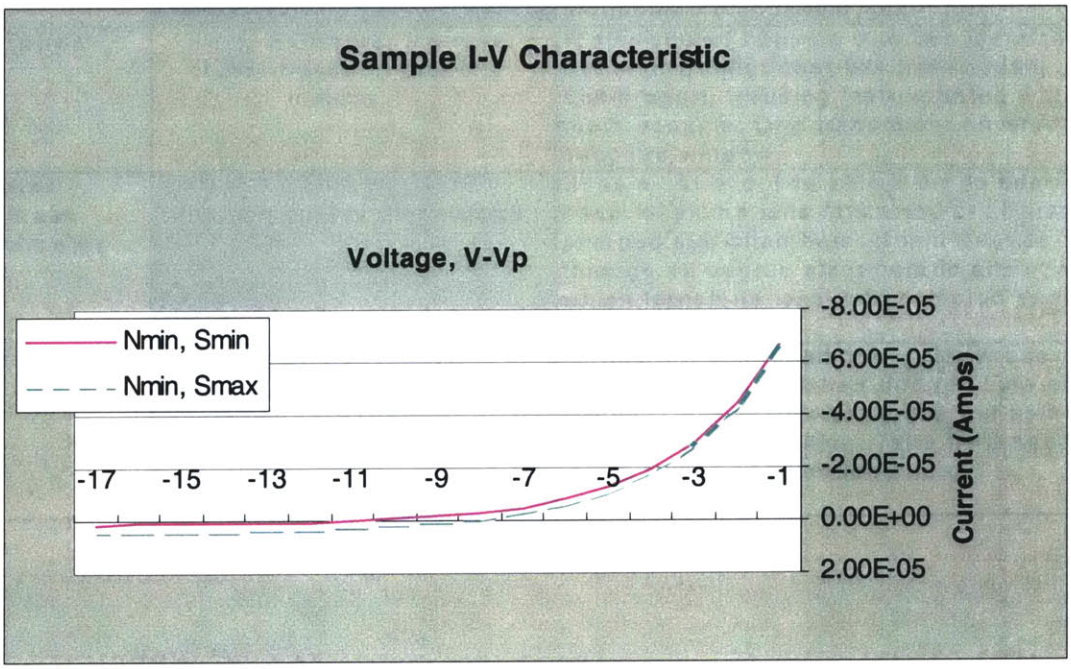

Figure B.4: Sample Characteristic for High Density Plume Plasma

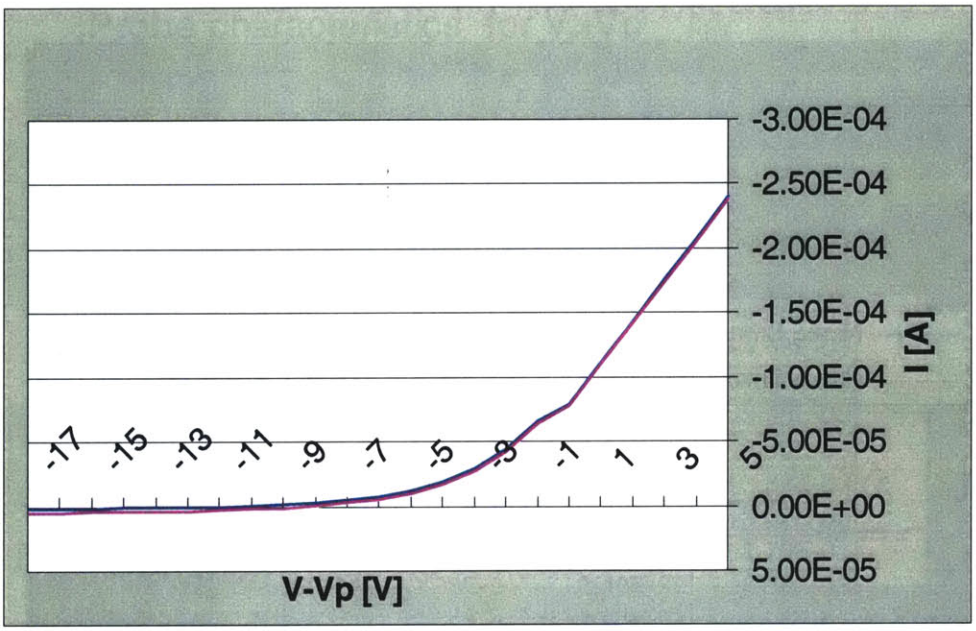

Figure B.5: Characteristic including electron-attracting region

Appendix C. Hall and PPT Research Overview Spreadsheets

Hall Thrusters		
Instrument	**Paper/Thruster**	**Description of Apparatus**
Emissive probe	King, Gallimore, Marrese, 1998: transport-property measurements of SPT-100	Probe filaments: tungsten wires 0.05 mm in diameter and 6 mm long. Copper support wires were insulated with alumina tubing. Emission current measured through 1 kOhm shunt between probe and ground.
Faraday Cup	Myers and Manzella, SPT Plume Characteristics (SPT-100)	Cup aperture of 3.81 cm and depth of 7.6 cm, probe diameter of 5.1 cm. Base of cup molybdenum, walls stainless steel. Outer surface of cup insulated with dielectric tape.
Faraday cup with negative collimator	BPT-4000 Hall thruster characteristics, by Grys, Tilley, and Aadland from Primex	Standard JPL-designed/built 0.9 in diam. Faraday cup with guard ring which is electrically connected to the stainless steel collimator. Faraday cup coated with tungsten to minimize secondary electron emission. Collection surfaces always focused at thruster centerline.
Faraday probe (Planar)	King, Gallimore, Marrese, 1998: transport-property meas.	2.3 cm diam planar disk spray-coated with Tungsten, mounted flush at end of stainless-steel cylindrical body
	Myers and Manzella, SPT Plume Characteristics (SPT-100)	5.1 cm diameter molybdenum disk mounted 3 mm below 3.81 cm inner diameter grounded molybdenum guard ring.
Heat probes	King, Gallimore, Marrese, 1998: transport-property meas.	Water-cooled housing with two identical Schmidt-Boelter heat-flux transducers placed 5 mm apart. Housing instrumented with a thermocouple. One transducer covered with a sapphire window.
Molecular Beam Mass Spectrometer	King and Gallimore, 1997; 1998: Ion energy diagnostics (SPT-100)	Uses a set of orifice skimmers to admit a beam of plume ions into array of differentially-pumped sub-chambers. Beam passes through 45-degree electrostatic analyzer which transmits ions with selected energy to detector.
	King and Gallimore, 1997; 1998: Mass spectral measurements (SPT-100)	Instrument described above; Ion mass detection accomplished through time-of-flight method. Ions of different mass but same E/q have different velocities. Take time spectra for varied values of selection energy.

Conditions	Measurement, location in plume	Range
	Plasma potential, 0* to -60* at 0.5 and 1 m	Between 7.2 and 5.4 V with respect to tank ground
Collector **and** walls biased up to -100 V. Walls to repel secondary e-'s.	Ion current density, 0* to 52.5* at 2 m and 4 m	0.2 to 0.02 mA/cm^2 at 2 m
Collimator mitigates facility charge-exchange ions	Beam ion current density, Semicircle at 60 cm	Collimated: 0.001 to 10 mA/cm^2 Uncollimated: 0.01 to 10 mA/cm^2
Collector **and** body biased negative (-30 V) to collect only ions	Ion-current density, -60* to 60* at 0.5 and 1 m	5 mA/cm^2 to 1.6 mA/cm^2, centerline at 0.5 and 1 m respectively
Collector biased up to -60 V relative to tank wall	Ion current density, 0* to 52.5* at 2 m and 4 m	0.2 to 0.02 mA/cm^2 at 2 m
	Total and radiant heat flux, -60* to 60* at 0.5 and 1 m	From 0.05 to 1.2 W/cm^2
Distance traveled: 2.35 m	Current at detector, 360* sweep at 0.5 m, 260* at 1 m	40x10^{-15} to 1x10^{-18} Amps for voltage from 0 to 600 V wrt plasma
	Ionization fraction of propellant; species-dependent analysis of ion energy distribution	Same currents as above for times from 0 to 140 μs, corresponding to m/q of 0 to 200.

Neutral particle flux probe	King, Gallimore, Marrese, 1998: transport-property meas.	Off-the-shelf MKS Instruments hot cathode ionization gauge with a set of four grids at the inlet. First grid grounded, second at -40V, third variable from 0 to 500 V, fourth grid grounded.
Retarding Potential Analyzer	King, Gallimore, Marrese, 1998: transport-property meas.	Three grids in front of a current collector. Outer grid floating, second grid biased at constant negative potential, third grid variable positive potential.
	Myers and Manzella, SPT Plume Characteristics	4 equally spaced tungsten grids and a molybdenum ion collector. Outer grid and guard ring grounded, second grid biased negative to repel electrons, third grid variable, inner grid negative to repel secondary electrons. Probe aperture 3.8 cm.
Solar cell cover slides with collimators	BPT-4000 Hall thruster characteristics, by Grys, Tilley, and Aadland from Primex	Small samples with tantalum-foil masks mounted at base of 5.1 cm diam, 15 cm long tantalum-foil lined stainless steel tube. Samples of polished quartz, coated-CMX, and AR-coated CMX. Some samples mounted without collimators
Optical Emission Spectroscopy	Manzella, SPT Plume Emissions (SPT-100)	Scanning monochromator with grating 1200 grooves/mm. Photodetector a photomultiplier tube biased to 1000 V. Measurements taken thru chamber window.
Cylindrical LP	Myers and Manzella, SPT Plume Characteristics	1.57 cm long, 0.051 cm diam. tungsten wire extending from 1 mm diam. alumina insulator.
Spherical LP	Myers and Manzella, SPT Plume Characteristics	0.95 cm radius stainless steel sphere mounted with 20 cm length of alumina tubing

Overpressure protect set point at 0.8 Pa; Must be calibrated for a specific material (here, Xe)	Neutral pressure, -60* to 0* at 0.5 and 1 m	0.001 to 0.8 Pa
Variable grid from 0 to 500 V	Collected ion current for various retarding voltages -60* to 60* at 0.5 and 1 m	Tens of μA near centerline to hundreds of nA far off centerline, up to 60 degrees.
Swept with a 700 V sawtooth at 0.15 Hz	Ion flux as a function of energy , at 15* and 4 m	Peak energy of 270 V
Length of test: 200 hr.	Erosion/deposition rate, Optical properties, Infrared reflectance, Surface resistance, 1 m at +/- 90* sweep and incidence angles from 0 to 75*	Deposition: $1.2x10^{-4}$ to $8.7x10^{-4}$ A/s Erosion: $2.8x10^{-4}$ to $1.2x10^{-1}$ A/s Mass: -32.48 mg to +0.05 mg Infrared: no measurable change Reflectance: -1 to 3 % change Absorptance: -4 to 8 % change Transmittance: -8 to 2 % change
In-situ intensity calibration with tungsten lamp	Emission spectra of plume between 3000 and 9000 A	Over 270 atomic and ionic transitions identified Majority of emission in blue (4200-5000 A). Clear evidence of ionized ingested facility gasses (N2). Total radiated optical power about 250 mW.
Driven with 1 kHz triangular wave	Near-field electron temperature and density, +/- 50* at 31 cm	n_e from $2x10^{17}$ to $1x10^{16}$ m^{-3} Te from 2 to 4 eV
Minimum r/λ_d ratio of 10	Far-field electron temperature and density, at 2 and 4 m and 0-83*	n_e from $1.3x10^{15}$ to $1x10^{14}$ m^{-3} Te from 1.5 to 3.5 eV Plasma potential of 12 V

PPT's		
Instrument	**Experiment**	**Description**
Cylindrical LP	Contamination of LES 8/9 PPT by Pencil, Gatsonis et al.	0.32 cm diam x 1 cm lng, aligned along plume centerline perpendicluar to plasma flow at 10 cm intervals
Fast Ionization Gauges	Eckman 1998.	Measure pressure by ionizing gas near gauge, then collecting ions and measuring current. Gauge head wrapped in negatively biased copper screen to repel electrons. --Beam Dynamics FIG-1
Faraday Cup (Planar LP)	Contamination of LES 8/9 PPT by Pencil, Gatsonis et al.	2.1 cm diam of copper w/ guard rings for 1-D sheath approximation
Quartz sensors	Contamination of LES 8/9 PPT by Pencil, Gatsonis et al.	Near Field: 2x2 cm quartz samples placed at rear of 2.5 cm diam x 2.5 cm long collimators on rakes Far field: samples at rear of 5.1 cm diam, 15 cm long collimators lined with tantalum
Residual Gas Analyzer	Eckman 1998, using LES 8/9	Molecules are ionized, passed through a mass filter, and collected. Only ions of one mass reach the collector at a time. --Dycor Quadrupole Gas Analyzer
Single LP	Eckman 1998.	0.1625 cm copper wire exposed to plasma, connected to coax cable.
Triple LP	NASA Lerc Model PPT by Gatsonis and Pencil et al., 1999	Three identical probes of 0.25 mm diam x 9 mm long tungsten wire. The first probe floats in plasma, fixed voltage V applied between other 2. Hall effect current probe also used.

Conditions	Measurement	Range
	time-of-flight based ion velocity	Arrival times of 6e-6 to 1.5 e-5 s, velocity of 42 km/s
Must calibrate gauge against nitrogen. Must estimate plume components.	Neutral pressure	Gauge capability: 10^{-8} to 10^{-2} Torr. Volatge from -15 to 15 V giving neutral densities from 1e17 to 5e20 m^{-3}
Biased at -40 V	Ion current densities	500 to 50000 A/m2 from -75 to +75 degrees from axis
$2x10^5$ pulses	deposition/erosion, transmittance: samples characterized by weight, transmittance, and deposited film properties	deposition: 0.0025 to -0.005 $\mu g/cm^2$-pulse transmittance: 70 to 95, out to 120 degrees from centerline
Not calibrated so mole ratios unknown. Single trace takes many seconds.	ratio of mass-to-electric charge in a molecule	Gauge capability: 1 to 200 amu. Main peaks seen at 31, 50, and 69 amu corresponding to CF, CF2, CF3
Biased at -40 V	Ion velocity by comparing ion current measurements from two LP's	Voltage from -0.6 to 0.8 V over times from 0 to 1e-4 s, giving velocities of 0 to 60 km/s
Discharge levels of 5, 20, and 40 J. Utilized glow discharge cleaning.	Electron temp and density, from voltage difference and collected current	5 J: 10e19 to 2x10e20 m^{-3} 20 J: 6x10e20 to 10e21 40 J: 2x10e20 to 1.4x10e21 Temps: 1 to 3 eV